ISSN 1000-9620

Marine Science Bulletin

海洋通报

Volume 12 • Number 1 2010

ISSN 1000-9620

NATIONAL MARINE DATA AND
INFORMATION SERVICE OF CHINA

MARINE SCIENCE BULLETIN

Vol. 12 No. 1 May 2010

CONTENTS

Relationship between East China Sea Kuroshio and Climatic Elements in East China ····· WU Zhi-yan et al. (01)

Simulation of Pacific Ocean Circulations Based on Global Warming from 1960 to 1999 ····· CAI Yi et al. (10)

Numerical Study of the Donghai Dam Impact on the Hydrodynamic Environment of Zhaniang Bay ····· LI Xi-bin et al. (16)

Diagnostic Calculation of the Oceanic Circulation ····· YANG Yang et al. (30)

Analysis of a Wenzhou-Hitting Exceptionally Strong Rainstorm Associated with a Typhoon Inverted Trough in September, 1999 ·····ZHENG Feng (39)

Horizontal Distribution and Annual Variations of Fecal Coliform Bacteria in Luoyuan Bay ····· CAI Lei-ming (48)

Three 5'-flanking Regions of *crtO* Encoding β-carotene Oxygenase in *Haematococcus pluvialis* ····· GAO Zheng-quan et al. (59)

Genetic Analysis of Five *Porphyra* Species by Isozyme Markers·····SHENG Song-dong et al. (65)

Phylogenetic Relationships between Pruple and Tea-green Individuals of the Blue Swimming Crab *Portunus trituberculatus* by PCR-SSCP Analysis ····· CHI Da-li et al. (79)

Constructing Marine Ecological Civilization of Qingdao·····SUN Yun-tan et al. (89)

Relationship between East China Sea Kuroshio and Climatic Elements in East China

LIBRARY
MAR 07 2011
LIBRARY
Pacific Islands Fisheries Science Cente
NOAA Fisheries
Honolulu, Hawai'i
National Oceanic and Atmospheric Administration
U.S. Dept. of Commerce

WU Zhi-yan[1]*, CHEN Hong-xia [2, 3], LIU Na [2, 3]

1. *Weihai Meteorological Bureau, Weihai* 264200, *Shandong Province, China;*

2. *Key Lab of Marine Science and Numerical Modeling, First Institute of Oceanography, SOA, Qingdao* 266061, *Shandong Province, China;*

3. *The First Institute of Oceanography, SOA, Qingdao* 266061, *Shandong Province, China*

Abstract: Using long term observation data in the main part of East China Sea Kuroshio, variations of Kuroshio upper layer temperature and salinity, their relationships with surface temperature and precipitation in east China are studied. Results reveal that the Kuroshio upper layer temperature experienced slight rise while salinity decreased in the past 50 years. In winter, Kuroshio upper layer temperature is closely related to the surface temperature in east China, and large area in east China shows positive correlation to the Kuroshio upper layer temperature, which might be related to the mass temperature reduction as a result of the cold air activities in winter. In summer, the increase of the precipitation causes the increase of diluted Yangtze River water into the shelf sea, thereby results in the salinity decrease of Kuroshio in the upper layer.

Keywords: Kuroshio; East China Sea; climatic elements

Kuroshio originates from the north branch of NEC east of Philippine; it is as famous as the Gulf Stream, both are west boundary currents, and have the characteristics of faster flowing speed, large flow, high-temperature and high-salinity. It flows from the east of Taiwan Island to East China Sea then turns northeastward, and flows out of East China Sea via Tokara channel. It transfers enormous energy from the low latitudes to the mid-high latitudes and releases huge heat flux to the atmosphere above [1].

As China is near to Kuroshio area, researches reveal that SST of Kuroshio is closely related to the climate in mainland China. In summer, the positive SSTA in Kuroshio region corresponds to the precipitation increase over lower reach of the Yangtze River Valley [2-4], while the heat transport in previous winter is negatively correlated to the summer precipitation in Huanghuai Plain and North China[5, 6]. Xu [7] pointed out that the increase (decrease) of the previous January Kuroshio SSTA is beneficial to summer flood (drought) over South China. On how Kuroshio affects the precipitation in mainland China, Li [8] proposed that Kuroshio affects the Western Pacific subtropical high and the Asian summer monsoon by means of the blocking highs, and thereby affects the precipitation in mid-lower reaches of the Yangtze River.

The results of the above are not the same, and the data used are mainly reanalysis data of low

Received on April 24, 2009

*Corresponding author: wuzhy@live.cn

resolution, in addition, the regions selected are not absolutely Kuroshio region (120-130°E, 25-35°N) as well. Although the observation data of PN section in year 1954-1990 are used [5], heat transport of Kuroshio and its impact on climate in Huanghuai Plain are studied only.

Based on the characteristics of high-temperature and high-salinity of Kuroshio, with observation data of temperature and salinity in the Main Part of Kuroshio in East China Sea, it is possible to study variations of temperature and salinity in the upper layer of Kuroshio in East China Sea and their interrelationships with climate in China.

Distinct from previous studies, this article not only uses the longest observation data available at the PN section, but also analyses the interrelationships between Kuroshio in East China Sea and climate in mainland China, and makes further effort to propose some explanation of possible mechanisms.

1 Source of data

Monthly mean precipitation and surface temperature data at 160 national meteorological observation stations from Jan 1951 to Dec 2004, compiled by the China Meteorological Administration (CMA), as well as data of temperature and salinity of Kuroshio in East China Sea at PN section during the period of 1955-2001, obtained from JODC (Japanese Oceanographic Data Center), are used in this paper.

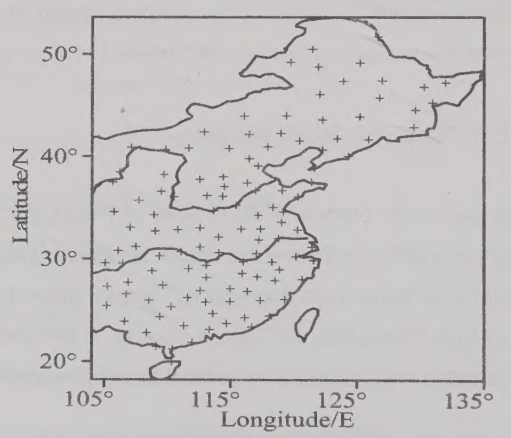

Fig. 1 Distribution of 120 stations in the East China

Fig. 1 shows the distribution of the selected observation stations in China (Fig. 1). As the stations are concentrated in the east, less in the northeast and sparse in the west, this paper chooses the 120 stations in the east of 105°E representing the area in the east of China.

G-PN section, situated in the main part of Kuroshio in East China Sea, has been systematically investigated. Temperature and salinity data at G-PN section (126.5-127.5°E) are used in this paper, further more, depth of above 100 m (Fig. 2) is chosen as the upper layer, therefore the average of sea temperature and salinity within which are averaged as those in the upper layer . As shown in Fig. 2 b, in the late stage, the sample points are much more concentrated than those in the earlier stage (Fig. 2 a).

This article focuses on the discussions in summer and winter season, for seasons that: a) Most of investigations concerning G-PN section were taken in summer and winter, especially before the year 1978, seen from the time range of 47 years, data in summer and winter are notably more than those in spring and autumn; b) Winter and summer are the typical seasons for the change of the Kuroshio temperature and salinity, while spring and winter are the transient seasons.

Correspondently, all monthly data used are averaged to seasonal mean data.

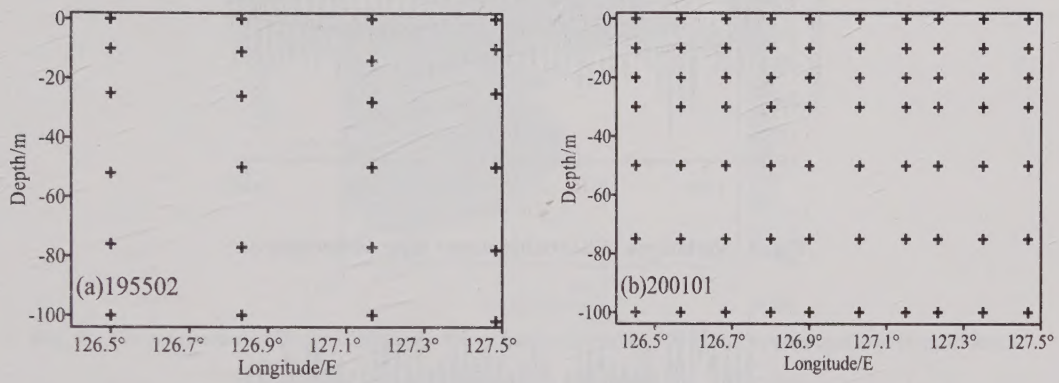

Fig. 2 Distribution of sample points in the upper layer of Kuroshio in East China Sea

2 Variations of upper layer temperature and salinity of Kuroshio in East China Sea

Fig. 3 shows the variations of Kuroshio upper layer temperature. It can be seen that seasonal variation is significant: temperature reaches the lowest in winter and highest in summer, while spring and summer are the transient seasons.

Fourier Transform of annual mean temperature reveals that Kuroshio temperature underwent an inter-annual variation with a period of 5-6 years (5.0%) and a decadal variation (1.7%), besides seasonal variation (with an energetic contribution ratio of 82.9%). Variations in a longer pattern are shown in Fig.3: Kuroshio underwent a temperature reduction during the period from 1955 to 1960, then a rise in the year between 1961 and 1966, followed by a reduction during the year 1966 and 1972, and then rise again from 1973-1979. The period from 1980-2001 corresponds to a variation in a longer pattern.

In the view of long-range variations, in the year between 1955 and 2001, the increasing rate in the upper layer is 0.026 °C /year; from the year 1978, the rate is 0.012 °C /year and from 1988 is 0.064 °C /year, and all the above are significantly greater than that of global increasing rate[9] (0.006 °C/100 year) respectively.

Variations of Kuroshio upper layer salinity are shown in Fig. 4. Similar to those of temperature, the most significant variation of salinity is still seasonal variation, while it reaches the highest in winter and lowest in summer, spring and winter are still transient seasons.

Seen from Fourier Transform, besides seasonal variation, inter-annual variations with a period of 5-6

years and a decadal variation still exist, and the energetic contribution ratio rise to 84.9%, 5.9% and 1.8% separately. It can be seen that as a conservative quantity, the upper layer salinity better reflect the seasonal and inter-annual variation of Kuroshio than temperature. Furthermore, it is noteworthy that Kuroshio salinity in the upper layer exhibits a yearly decreasing rate of 0.034/year from the year 1993, compared with that of 0.003/year since 1955.

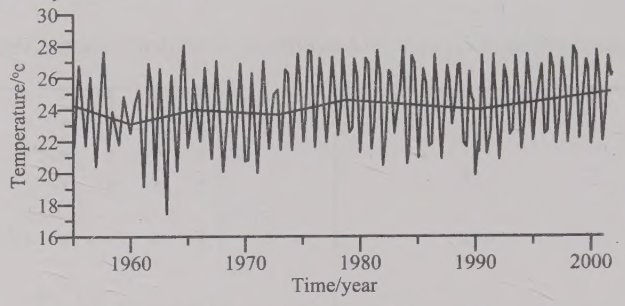

Fig. 3 Variations of Kuroshio upper layer temperature

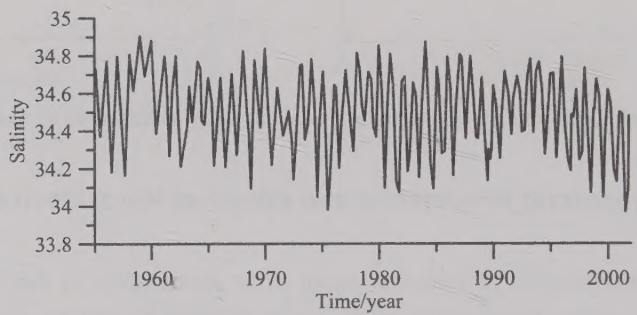

Fig. 4 Variations of Kuroshio upper layer salinity

On the whole, temperature of Kuroshio experienced slight rise while salinity tended to decrease during the past 50 years.

3 Relationship between winter Kuroshio temperature and winter surface temperature in East China

Fig. 5 shows the correlation coefficients between winter Kuroshio temperature and the corresponding surface temperature in east China during 1955-2001, and areas with a significance level higher than 0.05 are shaded. In winter, large areas of significant positive correlations are located in East China. Previous researches found that winter surface temperature in east China (110°E east) is closely related to the corresponding temperature in Kuroshio area[10], but the spatial mode was not given. As shown in figure 5, areas of high correlation (0.146, passing a 0.05 significance level) are located mainly in east and north China, showing notable consistency of temperature variation in east China and Kuroshio.

The first EOF mode of winter surface temperature in east China is shown in Fig. 6a, with a variance contribution of 60.25%. Seen from the first mode, winter surface temperature in east China shows a

consistent negative variation and the correlation coefficients decrease from south to north, and the negative center is located in the Inner Mongolia. Seen from the corresponding time series (Fig. 6b, the real line indicates a 9-year smooth average), it rises notably from the year 1975, and decreases from the year 1985.

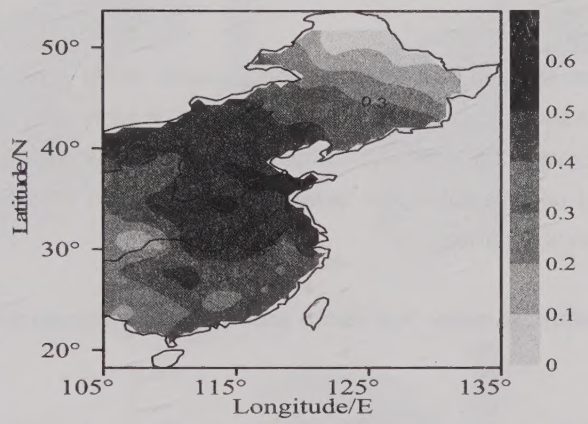

Fig. 5 Correlation distribution of upper layer temperature of PN section and surface temperature of 120 stations in winter

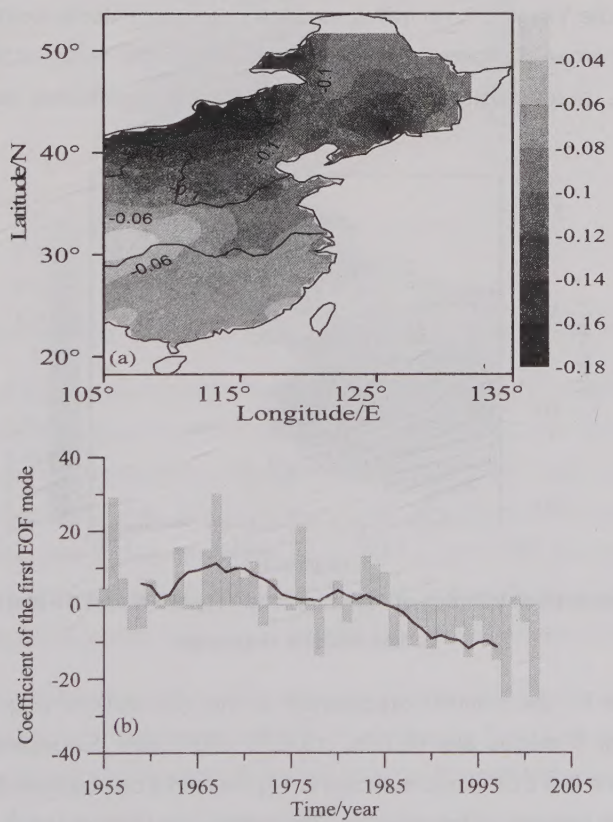

Fig. 6 Spatial distribution (a) and time series (b) of the first EOF mode of winter surface temperature in the east of China

From Fig. 6a and 6b, it can be seen that the surface temperature in east China shows a decreasing trend from 1975 to 1985 and an increasing trend after 1985. The correlation coefficient between the time series of the first EOF mode and the corresponding Kuroshio upper layer temperature at PN section is -0.438, passing a 0.05 significance level, showing a consistent temperature variation trend of Kuroshio and east China.

From the above we can see that in winter, the Kuroshio upper layer temperature and surface temperature in east China show a significant positive correlation. In winter, large area including east China and Kuroshio experience mass temperature reduction resulting from the cold air; this may be the primary reason for the significant positive correlation between them. While in summer, the relationship is not evident and the discussion is not given.

4 Relationship between summer Kuroshio salinity and summer surface temperature in east China

Correlation coefficients between summer Kuroshio salinity and the corresponding precipitation in east China (Fig.7) exhibit great spatial variation: areas of negative correlation located mainly in the south and the lower reach of the Yangtze River valley, and the negative center is located in Lake Poyang and Bay of Hangzhou, while areas of positive correlation are located in the center of Inner Mongolia, Shaanxi, Shanxi and Hebei Pro., areas near the positive center pass a significance level of 0.005(correlation coefficient of 0.407).

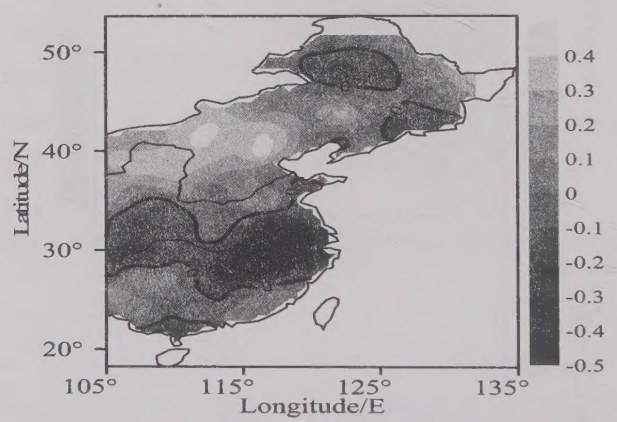

Fig. 7 Correlation distribution of upper layer salinity of PN section and precipitation of 120 stations in summer

The EOF analysis for the summer precipitation of the 120 stations (Fig. 8) shows the variance contributions of the first 3 modes are 16.79%, 13.22% and 7.55% respectively, and the cumulative contribution is 37.6%. The first EOF mode is shown in Fig. 8a, and it can be seen that the positive center is located in the mid-lower reaches of the Yangtze River valley, and the negative center is located in the south China. The correlation coefficient of time series of the 1st mode and the corresponding Kuroshio salinity is 0.01, failed to pass the significance level of 0.005. The second mode is shown in Fig. 8b, the

correlation coefficient of its time series and Kuroshio salinity is 0.316, passing a 0.005 significance level, whereas its spatial distribution is not similar to Fig. 9.

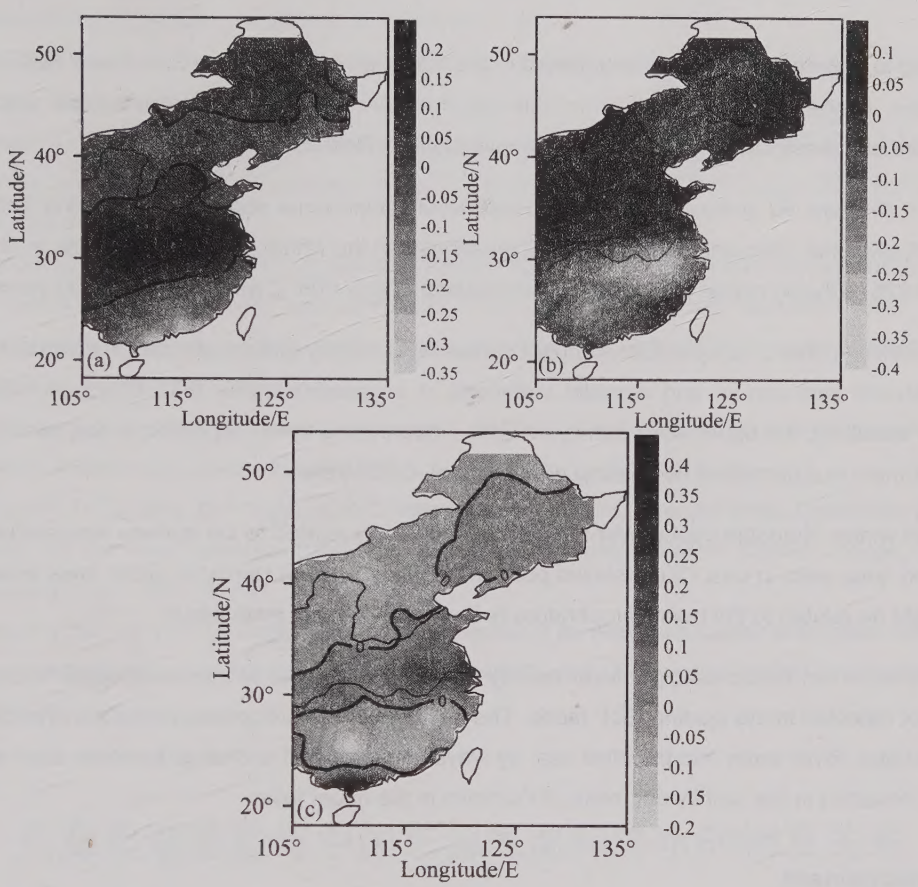

Fig. 8 Spatial distribution of the first 3 EOF modes of summer precipitation in the east of China

The 3rd EOF mode is shown in Fig. 8c, it exhibits a 'negative-positive- negative-positive' pattern from south to north, with a positive center located in the mid-lower reaches of the Yangtze River valley around 30°N, and the distribution resembles the correlation distribution of upper layer salinity of PN section and precipitation of 120 stations in summer. The correlation coefficient of its time series and Kuroshio salinity is -0.321, passing a 0.005 significance level, indicating that in summer, Kuroshio salinity is positively correlated to the precipitation in east China, and the increase of precipitation in the mid-lower reaches of the Yangtze River valley corresponds to the decline of the upper layer salinity in PN section.

Nevertheless, this relationship is not reflected in the leading EOF mode. It is conceivable that the increase of the precipitation in the mid-lower reaches of the Yangtze River valley results in the increase of the runoff into lakes and rivers, consequently abundant Yangtze Diluted Water flows into the sea, results in the salinity decreasing of continental shelf water. Thereby the mixing and exchange of Kuroshio and the shelf water lead to the salinity decreasing of Kuroshio in the upper layer, and the Kuroshio salinity reaches the minimum in summer. While in winter, the relationship is not evident and the discussion is not given.

5 Discussions and summaries

Using long term hydrologic data collected in the main part of Kuroshio in East China Sea, variations of Kuroshio temperature and salinity in the upper layer and their interrelationships with surface temperature and precipitation in east China are investigated. Results reveal that:

(a) In the past 50 years, the Kuroshio upper layer temperature shows an increasing trend, and it underwent seasonal, inter-annual and decadal variations. On the whole, the increasing rate in the past 50 years is 0.026 °C/year, higher than the global increasing rate (0.006 °C/year) in recent 100 years.

(b) Similar to that of temperature, Kuroshio upper layer salinity underwent seasonal variation as well, and underwent inter-annual and decadal variations in a greater degree than those of temperature. Generally speaking, the upper layer salinity exhibits a decreasing trend, especially in the period after the year 1993 there is a persistent decreasing with a rate of -0.034/year.

(c) In winter, Kuroshio upper layer temperature is closely related to the surface temperature in east China, and large area in east China shows positive correlation to the Kuroshio upper layer temperature, which might be related to the mass temperature reduction of the cold air in winter.

(d) In summer, Kuroshio upper layer salinity is negatively related to the precipitation in east China, but it is not reflected in the leading EOF mode. The increase of the precipitation results in the increase of diluted Yangtze River water into the shelf sea; by ways of mixing and exchange between shelf water and Kuroshio, resulting in the salinity decrease of Kuroshio in the upper layer.

Acknowledgement

This work was supported by National Natural Science Foundation Project 'Multi-core Structure of Antarctic Circumpolar Current and a Dynamic View of Its Spatial-temporal Variation' (No. 40506011). The key project of the National Natural Science Foundation of China 'Diagnostic Analysis and Numerical Simulation of the Inter-decadal Variations of East Asian Summer Monsoon and Summer Precipitation in East of China' (No. 40331010). The key project of the Major Natural Fundamental Researches of Universities in Jiangsu Province 'Research of development and prediction theory of Drought and Flood in the mid-lower reaches of Yangtze River' (No. 05KJA17002)

Reference

[1] Hsiung J. Estimates of global oceanic meridional heat transport [J]. J Phys Oceanogr, 1985, 15 (11): 1 405 - 1 413.

[2] Ni D H, Sun Z B, Chen H S, et al. Spatial/temporal features of summer SSTA in the Kuroshio Current region and its relation to summer precipitation in China [J]. Journal of Nanjing Institute of Meteorology, 2004, 27(3): 310 -

316.

[3] Li Y F, Ding Y H. Sea surface temperature, land surface temperature and the summer rainfall anomalies over eastern China [J]. Climatic and Environmental Research, 2002, 7(1): 87 - 101.

[4] Chen W, Kang L H, Wang D. The coupling relationship between summer rainfall in China and global Sea Surface Temperature [J]. Climatic and Environmental Research, 2006, 11(3): 56 - 269.

[5] Weng X C, Zhang Q L, YangG Y L, et al. The Kuroshio heat transport in the East China Sea and its relationship with the precipitation in the rainy season in the Huanghuai plain area [J]. Oceanologia Et Limnologia Sinica, 1996, 27(3): 237 - 245.

[6] Zhang Q L, Weng XC, Cheng M H. Relationship between the precipitation in the rainy season in north China and the tropical western Pacific warm pool and Kuroshio. Plateau Meteorology, 1999, 18(4): 575 - 583.

[7] Xu H M. Relationship between South China summer precipitation and global SST [J]. Journal of Nanjing Institute of Meteorology, 1997, 20(3):392 - 399.

[8] Li Z X, Sun Z B. Relation between January Kuroshio SSTA and Summer Rainfall in China [J]. Journal of Nanjing Institute of Meteorology, 2004, 27(3):374 - 380.

[9] Houghton J T, Y. Ding, D J Griggs, et al. Climate Change 2001, The Scientific Basis, Contribution of Working Group I to the Third Assessment Report of the Intergovernmental panel on Climate Change, Cambridge University Press , 2001 , 99-181.

[10] Chen P Y, Ni Y Q, Yin Y H. Diagnostic study on the impact of the global sea surface temperature anomalies on the winter temperature anomalies in eastern China in past 50 years [J]. Journal of Tropical Oceanography, 2001, 17 (4): 371 - 380.

东海黑潮温盐与中国东部气温和降水的相互关系

吴志彦[1]，陈红霞[2,3]，刘 娜[2,3]

（1. 威海市气象局，山东 威海 264200；2. 国家海洋局 第一海洋研究所，山东 青岛 266061；
3. 海洋环境科学和数值模拟国家海洋局重点实验室，山东 青岛 266061）

摘 要：采用东海黑潮主流段长时间序列的实测温盐资料，研究了东海黑潮上层温度、上层盐度的变化及其与中国东部降水和地面气温的关系。结果表明，在过去 50 年内，东海黑潮上层海温呈上升趋势，而上层盐度略呈下降趋势。东海黑潮上层海温和我国东部地面气温的关系在冬季十分密切，呈现出大面积显著的正相关，这与冬季南下冷空气的整体降温作用有关。夏季，长江中下游江水的增多致使大量长江冲淡水入海，导致黑潮上层水盐度下降，此时东海黑潮上层盐度与我国大陆东部降水呈负相关。

关键字：东海；黑潮；气候；中国东部

Simulation of Pacific Ocean Circulations Based on Global Warming from 1960 to 1999

CAI Yi *, WANG Zhang-gui

National Marine Environmental Forecast Center, Beijing 100081, *China*

Abstract: The Pacific Ocean circulations were simulated based on the global warming from 1960 to 1999 by using the Non-Boussinesq POP model and the data of wind stress and temperature at 1 000 hPa from the NCEP. The results show that the circulation in the tropical Pacific Ocean was weakening during the past 40 years. The heat transported to the tropical western Pacific Ocean coast by the north equatorial current and the heat transported to middle and high latitudes in the southern hemisphere by the south equatorial current decreased with time due to the global warming, while the heat transported to middle and high latitudes in the northern hemisphere by the north equatorial current increased with time due to the global warming.

Keyword: global warming; Pacific Ocean circulation; Non-Boussinesq model

1 Introduction

The changes of the global environmental system due to global warming have been researched in the past decades [1-4]. It is of interest to study ocean circulation changes caused by this, and it has been found that ocean circulations are changing due to global warming. IPCC's[5] report shows that the thermohaline circulation in the Northern Hemisphere decreased in strength in the 20th century[6], causing the heat transport to middle and high latitudes in the upper layer of the oceans to decrease. For example, the Atlantic thermohaline circulation weakened in the past years. It was also found that the Pacific Ocean circulation, which is formed by cool water in the subtropical area at 100 - 1 000 m depths flowing to the equator and upwelling there and turning back to the subtropical zone at the surface, was weakening too. Bogi Hansen [7] found that the water from the subtropical to the equator had decreased by about 25% in volume in the past 30 years. The heat transport from the tropical to middle and high latitudes changed accordingly due to these circulation changes, eventually affecting the global climate. A great many researchers [8-10] have focused on the changes of the Atlantic thermohaline circulation due to global warming, but less is known concerning the Pacific Ocean circulations. Therefore, we have simulated the Pacific circulations in the past 40 years using the Non-Boussinesq POP model improved by Greatbatch et al.[11] Many numerical models have been used in the simulation of global warming in the past years, but the results of numerical models are quite different from each other. One of the reasons is that in the models the Boussinesq approximation is used, which means that they are built on the basis of the conservation of volume, instead of mass in the ocean, hence are not able to give sea level expansion due

Received on April 27, 2009

*Corresponding author: caiyi@nmefc.gov.cn

to global warming accurately. Greatbatch, Youyu and Cai Yi relaxed the Boussinesq approximation in the POP ocean model in 2000. The Non-Boussinesq POP ocean model can calculate accurately sea level expansion caused by global warming. Cai Yi et al discussed the difference between the results of the Boussinesq and Non-Boussinesq models based on global warming. It is found [12] that the results are significantly improved by using the Non-Boussinesq POP. Having been convinced of the improvement in the simulation results of temperature, heat content and sea level in the Pacific Ocean over the past four decades by using this model,[13,14] we now turn to discuss the simulation of Pacific Ocean circulations.

2 Data processing and grid scheme

The simulation domain is from 67.5°S to 67.5°N and from 97.5°E to 86.25°W. There are 12 levels in the vertical direction, which are at 25.5, 85.0, 169.0, 295.5, 483.0, 754.5, 1130.5, 1622.5, 2228.5, 2935.0, 3721.0 and 4565.5 meters. The resolution of the model is 4.5° (lat) × 3.75° (lon). The topography is extracted from U.S. Navy Bathymetry data. The surface heat flux circulation is based on the air temperature at 1 000 mb. Both 1000mb temperature and wind stress data are from the reanalysis data of the NECP, USA. The sea surface salinity data is from IGOSS. The restoring time is 30 days. The initial horizontal temperature and salinity fields are supposed to be uniform and are interpolated in the vertical direction according to Levitus' profiles. Initially the ocean is at rest. The Non-Boussinesq POP model is first run based on the wind stress and air temperature in January to December 1960. The thermodynamic time step increases with depth. The time steps for these levels are 1.000, 3.245, 6.434, 11.187, 18.264, 28.509, 42.698, 61.264, 84.123, 110.792, 140.453 and 172.321 hr respectively. The dynamic time step is 1 hr. The time steps are set to be constant at all levels after the 550th year. The model spin-up is 1 180 years. The difference between the annual mean temperatures of two successive years for the entire domain (6.53×10^8 km^3) is 0.000 03 °C. Then the model is run using data from January 1960 through December 1999. The simulated circulation of the Pacific Ocean is discussed belows.

3 The results

First of all, we compare the measured and simulated sea surface temperatures in the Pacific Ocean. Fig. 1 shows the sea surface temperatures obtained from this simulation and the observation by Scripps. We found that they are almost the same. Comparisons were also made for simulated and observed temperatures and for other quantities at the sea surface and 169 m depth; positive results were obtained (figures omitted). [13] We conclude that the results we obtained are valid.

Secondly, we discuss the changes of heat fluxes with time along each latitude and longitude based on global warming. We have calculated the zonal and meridianal heat fluxes every 3.75 degrees longitude and every 4.5 degrees latitude. The heat fluxes increase in some areas with time due to global warming is shown in Fig. 2. Fig. 2a shows the mean zonal heat flux in the western Pacific Ocean (for 105 - 127.5ºE along meridioal sections from 0 to 754.5 m in the vertical direction), Fig. 2b shows the mean meridional

heat flux in the South Pacific Ocean (for 40.5 - 27°S along zonal sections from 0 to 754.5 m in the vertical direction), and Fig. 3c shows the mean meridional heat flux in the Tropic North Pacific Ocean (for 4.5 - 9.0°N along zonal sections from 0 to 754.5 m in the vertical direction). All these results imply that global warming causes the heat fluxes to increase in these areas. The mean zonal heat flux in the Western Pacific Ocean is caused mainly by the north equatorial current. It means that the heat transport to the Equatorial Western Pacific Ocean coast decreases with time. The change of the heat flux is about 0.1PW during the past 40 years. The mean meridional heat flux in the South Pacific Ocean, which signifies heat transported to the southern hemisphere by the south equatorial current, decreases with time as shown in Fig. 2b. The change of the heat flux is about 0.1PW also. We have analyzed [5] the changes of the heat content and found that the heat content in the southern Pacific Ocean increased during the past 40 years. It means that the heat content increases in the southern Pacific Ocean and does not come from the tropical Pacific Ocean transported by the south equatorial current. The mean meridianal heat, transported to middle and high latitudes by the north equatorial current in the tropic North Pacific Ocean, increases with time as shown in Fig. 2c.The change of the heat flux is about 0.2PW during the past 40 years. It means that the heat content, which has increased in the northern Pacific Ocean, comes from the Tropical Pacific Ocean and is transported by the north equatorial current.

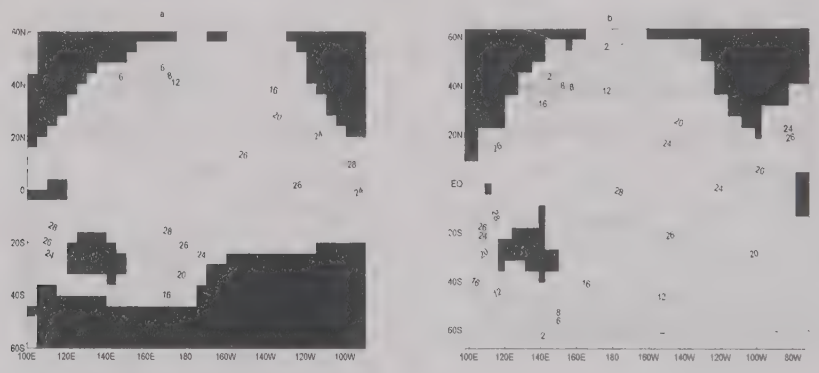

Fig. 1 Sea surface temperatures obtained from the simulation (b) and observation by Scripps (a)

Thirdly, we discuss the zonal overturning anomaly in the tropical Pacific Ocean using EOF analysis. Fig. 3 shows the first and second modes of the mean zonal overturning from 4.5°S to 4.5°N, which account for 62.1% and 26.1% of the total, respectively. The time coefficients all increase with time in Fig. 3c and Fig. 3d. They both represent the modes of the global warming. The first pattern in Fig. 3a is a clockwise circulation and opposite to the Walker circulation, which means that the Walker circulation in the Tropical Pacific Ocean decreases with time. The second pattern in Fig. 3b shows a clockwise circulation in the western Pacific Ocean and a counterclockwise circulation in the eastern Pacific Ocean. Combining the two modes, we can see that the Walker circulation in the western Pacific Ocean is weaker than that in the eastern Pacific Ocean due to global warming.

It has been reported [6] that the meridional circulation in the Tropical Pacific Ocean and the Subtropical Pacific Ocean weakened in the past 40 years. Here we examine the behavior of the

meridional overturning. Fig. 4 shows the simulated climatic meridional overturning mean from 168.75°E to 112.5°W and its annual change, which is the meridional overturning in 1990 to 1999 minus that in 1969 to 1960 and divided by 20, representing the annual change of the mean meridional overturning. We can see that the meridional overturning in Fig. 4a is opposite to that in Fig. 4b. It is found that the meridional overturning between 20°S to 20°N weakened in the past 40 years. The mean maximum value of the decrease is about 0.4Sv annually. Therefore we can conclude that the meridional overturning is significantly decreasing in the Tropical Pacific Ocean and is similar to that in the Atlantic due to global warming.

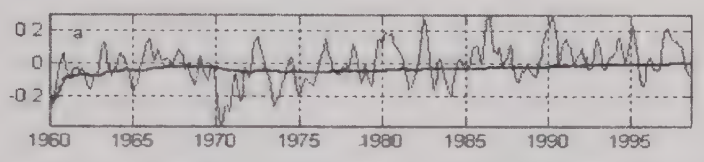

Fig. 2a The change of the mean zonal heat flux in the West Pacific Ocean with time

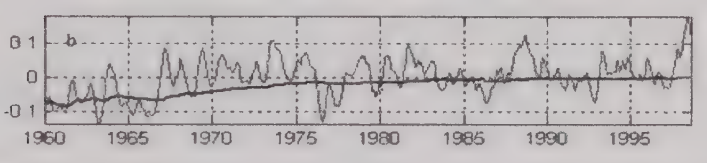

Fig. 2b The change of the mean meridianal heat flux in the South Pacific Ocean with time

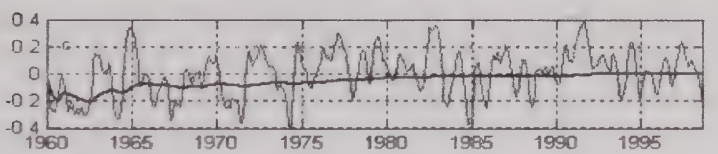

Fig. 2c The change of the mean meridianal heat flux in the Tropic North Pacific Ocean with time

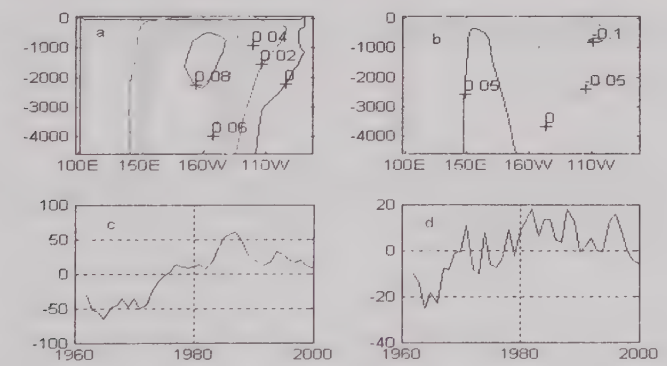

Fig. 3 First and second EOF modes for the zonal overturning anomaly in the tropical Pacific Ocean

4 Conclusions

In this paper we simulated and discussed the circulations in the Pacific Ocean from 1960 to 1999. The most important results are as follows:

a) The circulations in the Tropical Pacific Ocean became weaker due to global warming.

b) The heat fluxes in three areas increased with time due to global warming. They are the mean zonal heat flux for105 - 127.5°E along meridioal sections from 0 to 754.5 m in the vertical direction, the mean meridional heat flux for 40.5 - 27°S along zonal sections from 0 to 754.5 m in the vertical direction and the mean meridional heat flux for 4.5 - 9.0°N along zonal sections from 0 to 754.5 m in the vertical direction.

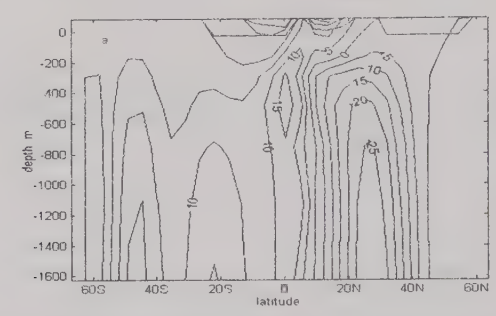

Fig. 4a Simulated climatic meridianal overturning mean from 168.75°E to 112.5°W

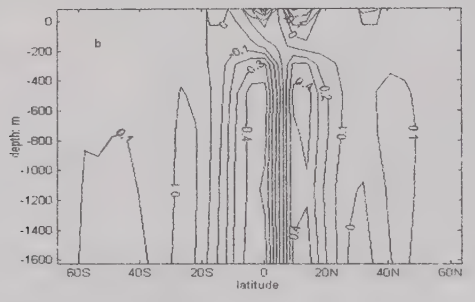

Fig. 4b Mean meridianal overturning from 1990 to 1999 minus that from 1969 to 1960 and divided by 20

Acknowledgement

This paper was supported by Natural Science Foundation of China (No. 40976015) and National Science Foundation for Youth (No. 40906014).

Reference

[1] Timmermann A, Ohberhuber J. Increased El Nino Frequency in a Climate Model Forced by Future Greenhouse Warming [J]. Nature, 1999, 398: 694 - 696.

[2] Hansen D. Forcings and Chaos in Interannual to Decadal Climate Change [J]. J Geophys Res, 1997, 102: 25 679 - 25 720.

[3] Munk W. From the Cover: Twentieth century sea level: An enigma [J]. *Proc Natl Acad Sci U. S. A.* 2002, 99: 6 550 - 6 555.

[4] Cai Yi. The analysis of air and sea temperature and sea level in Pacific Ocean based on global warming [J]. Atmospheric Science Research and Application, 2004: 26(1): 42-48.

[5] IPCC Third Assessment Report: Climate Change 2001 A contribution of Working Groups I, II and III to the Third Assessment Report of the Intergovernmental Panel on Climate Change, Watson, R.T. and the Core Writing Team (Eds.), Contains the Synthesis Report itself, the Summaries for Policymakers and Technical Summaries of the three Working Group volumes, and supporting Annexes. Cambridge University Press, UK. pp 398, Available from Cambridge University Press. The Edinburgh Building Shaftesbury Road, Cambridge CB2 2RU England.

[6] Hansen B, Turrell W R, Østerhus S. Decreasing overflow from the Nordic seas into the Atlantic Ocean through the Faroe Bank channel since 1950 [J]. Nature, 2001, 411: 927 - 930.

[7] Michael J, McPhaden, Zhang Dongxiao. Slowdown of the meridional overturning circulation in the upper Pacific Ocean [J]. Nature, 2002, 415: 603 - 608.

[8] Schmidt M W, Spero H J, Lea D W, et al. Lea Links between salinity variation in the Caribbean and North Atlantic thermohaline circulation [J]. Nature, 2004, 428: 160 - 163.

[9] Rahmstorf S. Risk of sea-change in the Atlantic [J]. Nature, 1997, 388: 825 - 826.

[10] Rühlemann C, Mulitza S, Müller P J, et al. Warming of the tropical Atlantic Ocean and slowdown of thermohaline circulation during the last deglaciation [J]. Nature, 1999, 402: 511 – 514.

[11] Greatbatch R J, Lu Y, Cai Y. Relaxing the Boussinesq approximation in ocean circulation models. J. Atmos. Ocean [J]. Tech, 2001, 18(11): 191 - 19 23.

[12] Cai Yi. The study of the error about Boussinesq's approximation in ocean model [J]. Advances in Marine Science， 2005, 23(2): 121 - 126.

[13] Cai Yi. The simulation of the sea temperature in Pacific Ocean based on global warming from 1960 to 1999 [J]. Acta Oceanologica Sinica, 2008, 37(6).

[14] Cai Yi. The simulation of the sea level and heat content in Pacific Ocean based on global warming from 1960 to 1999 [J]. Journal of Tropical Oceanography, 2006, 25(4): 14 - 19.

[15] Monterey G I, Levitus S. Climatological cycle of mixed layer depth in the world ocean. U.S. Gov Printing Office, NOAA NESDIS, 1997, 5pp.

全球变暖背景下对太平洋环流（1960 — 1999）的模拟

蔡 怡，王彰贵

（国家海洋环境预报中心， 北京 100081）

摘 要：我们用 Non-Boussinesq POP 海洋模式和 NECP 1 000 hPa 的风应力和气温场资料，模拟了 1960 — 1999 年太平洋环流，结果显示：在过去的 40 年，热带太平洋环流变弱了，另外，由于全球变暖，由北赤道流产生的向热带西太平洋沿岸的热输送和由南赤道流产生的向南太平洋中高纬度的热输送随着时间是减弱的，而在北半球，由北赤道流产生的向中高纬度的热输送是增加的。

关键词：全球变暖；太平洋环流；Non-Boussinesq POP 模式

Numerical Study of the Donghai Dam Impact on the Hydrodynamic Environment of Zhanjiang Bay

LI Xi-bin [1], SUN Xiao-yan [2], YU Hua-ming [3], BAO xian-wen [3]

1. *Tianjin Marine Environmental Monitoring Central Station, State Oceanic Association (SOA), Tianjin* 300451, *China;*

2. *National Marine Data and Information Service, Tianjin* 300171, *China;*

3. *College of Physical and Environmental Oceanography, Ocean University of China, Qingdao* 266100, *Shandong Province, China*

Abstract: In this paper, the Finite Volume Coastal Ocean Model (FVCOM) was employed and configured for 3 dimensional numerical simulations of tide and tidal current based on the field observations in Zhanjiang Bay. The model's results agree well with the field observed data. Based on the well validated model, the hydrodynamic fields of zhanjiang bay area were calculated both before the Donghai Dam constructing and after that. Compared the tidal level, current field, tidal capacity and water exchange ratio before the construction of Dohai dam with those after construction of the dam, we analyzed and get some conclusions of effects of Donghai Dam on Hydrodynamic environment of the Zhanjiang Bay.

Keywords: Zhanjiang bay; Donghai dam; numerical model; hydrodynamic environment

Zhanjiang City is the most southern city in the mainland China. Donghai Island lies to the south of Zhanjiang City. It is the biggest island with area about 286 km^2 in Guangdong province and the fifth biggest island among islands all over the China. Donghai Dam which connects Donghai Island and Zhanjiang City started to be built in September, 1958 and was constructed in February, 1961. Its total length is 6.82 km [1] (see Fig. 1). In history, Donghai Dam has ever played a positive role in the local economic development, culture communion and traffic improvement between Zhanjiang and Donghai Island [2]. However, part of the bay was obstructed and water exchange between Leizhou bay and Zhanjiang Bay was blocked and decreased as a result of the dam, which inevitably effected local marine environment [3-6]. In this paper, a 3-D unstructured-grid, free-surface, primitive equation, Finite-Volume Coastal Ocean circulation Model (FVCOM) was employed to simulate and calculate tidal capacity, current field, tidal level, water exchange ratio and other hydrodynamic characteristics of Zhanjiang Bay between pre- and post-construction of Donghai Dam. Then we analyzed the Donghai Dam's Environmental effects on local hydrodynamic environment, ports and sea-routes.

Received on July 7, 2009

*Corresponding author: lixb_tj@yahoo.com.cn

1 Model description

The water depth in Zhanjiang Bay differs from a few meters to 40 meters, with deep water in sea-routes and shallow water in the other areas. Large intertidal zone also appears in Zhanjiang Bay. In order to simulate the active boundary and configure a high resolution grid in the concerned area, a 3-D unstructured-grid, free-surface, primitive equation, Finite-Volume Coastal Ocean circulation Model (FVCOM) was employed to simulate hydrodynamic fields of Zhanjiang Bay.

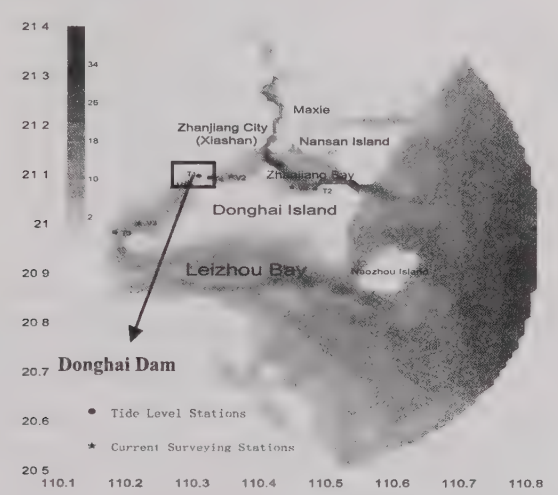

Fig. 1 Locations and depth filed of Zhanjiang Bay and the observation stations

In comparison to the differential form used in finite-difference and finite-element models, FVCOM discretizes the integral form of the governing equations. Since these integral equations can be solved numerically by flux calculation (like those used in the finite difference method) over an arbitrarily-sized triangular mesh (like those used in the finite element method), the finite-volume approach guarantees mass conservation both in the individual control element and in the entire model domain. From a technical point of view, FVCOM combines the advantages of finite-difference methods for simple discrete coding and computational efficiency and finite-element methods for geometric flexibility [7]. Thus, it is a better choice to use FVCOM for solving the difficulty on fitting the irregularly coastal lines, barrier island complexes for numerical simulation in Zhanjiang Bay. It is possible to simulate the tidal current on smaller scale near the coast and islands, and the resolution can be higher in the concerned area. In addition, a new wet/dry point method has been developed for FVCOM to provide an accurate simulation of the water transport that floods onto and drains out of the inter-tidal zone, and it can solve the numerical simulation difficulty on large intertidal marsh in Zhanjiang Bay. This method has been validated in a series of tidal simulations using an idealized semi-enclosed estuary with an inter-tidal zone. The rule used for validation is mass conservation, which is a prerequisite condition for an objective evaluation of the wet/dry point treatment technique in estuaries bay. Thus, the model can assure the mass conservation both in whole

model domain and in the local domain, especially in the intertidal domain. The FVCOM code has been parallelized using a Single Processor Multiple Data (SPMD) approach. So the parallel calculation ability assures the calculation's efficiency for the fine grid system. From above discussion we can say that, FVCOM is a suitable model for the numerical realizations in Zhanjiang Bay.

This paper mainly focuses on the barotropic tide simulation. The control equations are listed bellow. The σ-coordinate transformation is used in vertical in order to obtain a smooth representation of irregular bottom depth in FVCOM. The σ-coordinate transformation is defined as:

$$\sigma = \frac{z - \zeta}{H + \zeta} = \frac{z - \zeta}{D} \tag{1}$$

In σ-coordinate transformation, governing equations are given as:

$$\frac{\partial \zeta}{\partial t} + \frac{\partial Du}{\partial x} + \frac{\partial Dv}{\partial y} + \frac{\partial \omega}{\partial \sigma} = 0 \tag{2}$$

$$\begin{aligned} &\frac{\partial D}{\partial t} + \frac{\partial u^2 D}{\partial x} + \frac{\partial uvD}{\partial y} + \frac{\partial u\omega}{\partial \sigma} - fvD \\ &= -gD\frac{\partial \zeta}{\partial x} - \frac{gD}{\rho_0}\left[\frac{\partial}{\partial x}\left(D\int_{\sigma}^{0}\rho d\sigma'\right) + \sigma\rho\frac{\partial D}{\partial x}\right] + \frac{1}{D}\frac{\partial}{\partial \sigma}\left(K_m\frac{\partial u}{\partial \sigma}\right) + DF_x \end{aligned} \tag{3}$$

$$\begin{aligned} &\frac{\partial vD}{\partial t} + \frac{\partial uvD}{\partial x} + \frac{\partial v^2 D}{\partial y} + \frac{\partial v\omega}{\partial \sigma} + fuD \\ &= -gD\frac{\partial \zeta}{\partial y} - \frac{gD}{\rho_0}\left[\frac{\partial}{\partial y}\left(D\int_{\sigma}^{0}\rho d\sigma'\right) + \sigma\rho\frac{\partial D}{\partial y}\right] + \frac{1}{D}\frac{\partial}{\partial \sigma}\left(K_m\frac{\partial v}{\partial \sigma}\right) + DF_y \end{aligned} \tag{4}$$

In the σ-coordinate system, DF_x and DF_y are the horizontal diffusion terms.

Literal boundary: $$u\cos\alpha + v\cos\beta = 0 \tag{5}$$

Surface boundary: $$(\partial u/\partial\sigma, \partial v/\partial\sigma) = 0, \quad \omega = 0 \tag{6}$$

Bottom boundary: $$(\partial u/\partial\sigma, \partial v/\partial\sigma) = D/\rho_0 K_m(\tau_{bx}, \tau_{by}), \quad \omega = 0 \tag{7}$$

Open boundary: $$\zeta = \zeta' \tag{8}$$

where

$$t = 0, \quad \vec{v} = \vec{v}_0, \quad \zeta = \zeta_0 \tag{9}$$

2 Field data analysis for both sides of the dam

In order to study the water exchange of Zhanjiang Bay between pre- and post-construction of

Donghai dam, Tidal level observations of four particular stations (T1-T4) and successive tidal current observations of four particular stations (V1-V4) for 26 hours from both sides of the dam were carried on. T1、T2、V1、V3 iocated at west side of the dam in Leizhou Bay, and T3、T4、V2、V4 located at east side of the dam in Zhanjiang Bay. Locations of observation stations can be seen in Fig.1.

Fig. 2 showed comparison of tidal level observations of T1 and T4 stations which located at both sides of Donghai Dam during spring tide. The real line showed tidal level changing of T1 station (west side of the dam in Leizhou bay), and the broken line showed tidal level changing of T4 station (east side of the dam in Zhanjiang bay). From the figure we can see that tidal amplitude of T1 was larger than that of T4 with the maximum difference about 0.6 m during spring tide. The tidal phase changing of T1 lagged behind T4 for about 2 hours. That`s because channel between Leizhou bay and Zhanjiang bay was obstructed artificially because of the Donghai dam, water transmission distance to T1 was father than T4 as a result of topography influence. Tidal water from both sides of the dam was concentrated to the location, as a result tidal phase was influenced.

From the analysis of data from tidal current observations, we conclude that in the Zhanjiang bay, the type of tidal current is the irregular semi-diurnal tides, and the flood-ebb tidal orientation is basically SW-NE and the tidal current is mainly the alternating current. During flood tide, water flowed from inlet to interior of the bay, and during ebb tide, water flowed reversely. Flow velocity increased from bottom to surface with the maximum value at the surface. Velocity is faster during spring tide than neap tide, while flood average time is longer tide than ebb tide. The maximum velocity appears at V3 station which located at the west inlet of Donghai Island had the value about 100 cm/s during spring tide. While the minimum velocity appears at V1 and V2 stations which located near the dam had only about 40 cm/s during spring tide.

Fig. 3 showed comparison of actual tidal current measurements of observation stations V1 (located in Leizhou bay to the west of the dam, broken line) and V2 (located in Zhanjiang bay to the east of the dam, real line) during spring tide. We can see that velocity and direction changing of tidal current for V1 station lagged behind V2 station for about 2 hours, which agreed well with relevant tidal measurements. Similarly, tidal current which passed through Zhanjiang Bay could not transmit to Leizhou bay because of the existence of the dam. So the transmit distance from V1 station was farther than V2 station, accordingly tidal current in Leizhou bay lagged behind Zhanjiang bay.

3 Model configuration

The calculation domain includes Zhanjiang Bay and Leizhou Bay as shown in Fig. 4 with the maximum distance about 91 km from the south to the north and 69 km from the east to the west. The large model domain avoids the open boundary conditions' effect. The model depth is derived from the digitized dataset from the new chart published by the China National Maritime Affairs Administration. In this model unstructured triangular grids were used to divide the concerned field. The grids in the model interior of

Zhanjiang Bay, especially those in the inlets, around the island and irregular boundary and concerned areas, are much more refined. In order to reduce boundary effects, open boundary is extended to the open ocean far away from the inlet of Zhanjiang Bay. There were totally 28258 grid nodes and 53609 triangular grid elements with a minimum grid resolution of 100 m and a maximum grid resolution of 2 000 m (see Fig. 4). And 6 σ-layers were set in vertical direction and the time step used was 5 seconds. From the Fig. 4 we can see triangular grids could fit coastal lines and topography characters quite well.

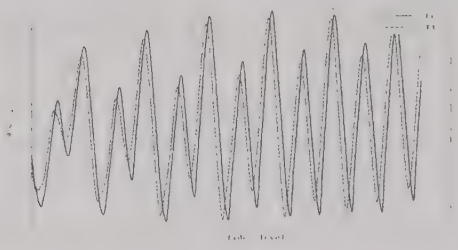

Fig. 2 Comparison of actual tidal level measurement from both sides of the dam

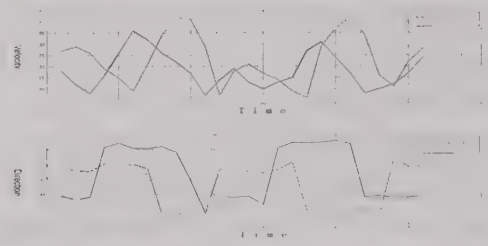

Fig. 3 Comparison of actual tidal current measurement from both sides of the dam

4 Model validation

In this paper, field tidal level measurement data of T1 - T4 stations was used for tidal level validation, and the actual tidal current measurement data of V1 - V4 stations were used for tidal current validation. Locations of these stations can be seen in Fig. 1, and validation results can be seen in Fig. 5 and Fig. 6. The error of tidal level and tidal current can be neglected. The simulated tidal level was consistent well with the measured values with maximal error less than 20 cm which can be accepted. The simulated flood-ebb tidal current field also matches well with the topography and frame of Zhanjiang bay. Therefore the model in this paper is reliable, and the simulated results can basically reflect hydrodynamic field characters of our study area. The simulated results from this model can be used to analyze hydrodynamic characters around Zhanjiang bay, and we can also predict hydrodynamic fields pre-construction of the dam from simulation.

5 Discussion on hydrodynamic field for pre- and post- construction of the dam

5.1 Analyses of present tidal elevation and tidal current

Fig. 7 showed the simulated surface tidal current field of the entire Zhanjiang sea area at flood and

ebb time during spring tide respectively. During flood time, seawater flowed in through the east boundary. Seawater flowed into Zhanjiang Bay through the east inlet of Donghai Island and spread westward and northward. At the same time, seawater from south of Donghai Island rounded the island and spread westward, then seawater spread from west inlet of Donghai island and flowed into Leizhou Bay at west of the dam with maximum current velocity about 160 cm/s at west inlet of Donghai island. During ebb-tide, seawater in Zhanjiang bay at east of the dam flooded from east inlet of Donghai island and spread eastward to the open ocean. Seawater in Leizhou bay at west side of the dam flooded through west inlet of Donghai Island, rounded Donghai Island and spread eastward to the open ocean. Similarly, maximum current velocity which amounted to 180cm/s appeared at west inlet of Donghai island.

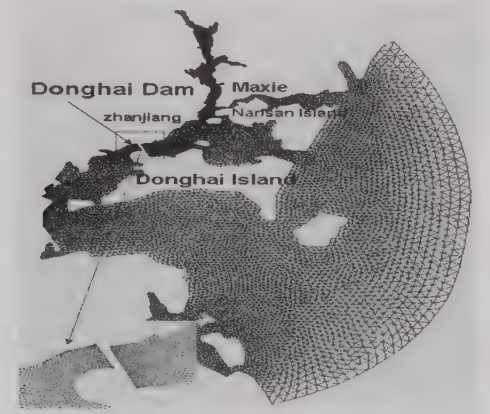

Fig. 4 Model gridding figure

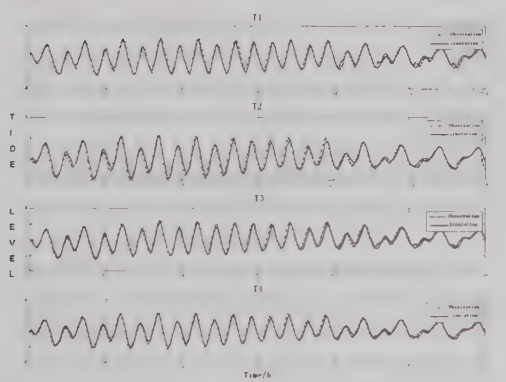

Fig. 5 Tidal level validation

Simulated tidal current fields for both sides of the dam at flood tide time and ebb-tide time were given respectively by Fig. 8, which showed actual simulated current fields at flood and ebb time respectively. we can see that the current field had a characteristic of lower velocity alongshore and higher velocity in deep water with the minimum velocity near the dam location. The type of tidal current is the irregular semi-diurnal tides, and the flood-ebb tidal orientation is basically SW-NE and the tidal current is mainly the alternating current. During flood tide, seawater in Zhanjiang bay flowed into the bay through Longteng

water route between Nansan Island and Donghai island. After entering into the bay, water cross-section broadened, the current velocity declined. Seawater in Zhanjiang bay passed through Dongtoushan Island, then branched into northward and westward current along the deep trough. Current velocity reduced near Donghai dam. In Zhanjiang bay, current direction was westward, while in Leizhou bay, the current direction near the dam was northeast and reversed at ebb time. The difference was that seawater current velocity during neap tide was distinctly lower than that during spring tide.

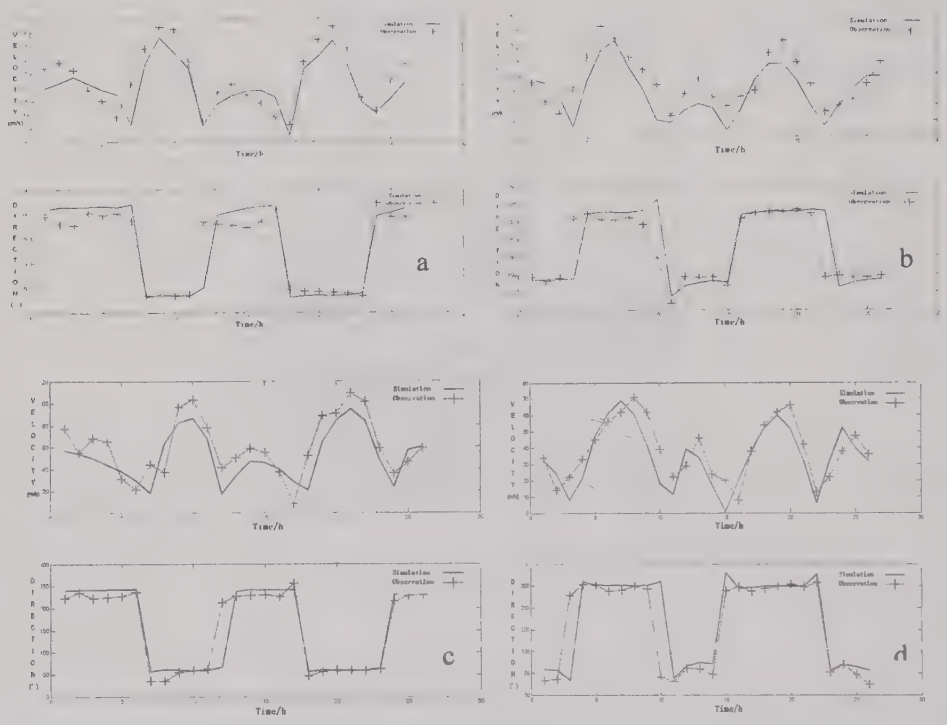

Fig. 6 tidal current validation (a for V1station, b for V2 station, c for V3 station，d for V4 station)

Fig. 7 Actual current field of Zhanjiang sea area

(the former was flood time and the latter was ebb time)

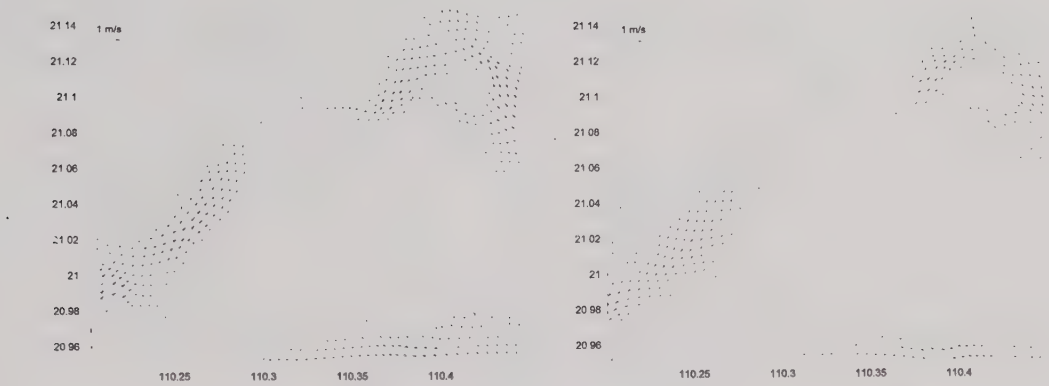

Fig. 8 Actual current field during spring tide from both sides of the dam

(the former was flood time and the latter was ebb time)

5.2 Current field analysis before construction of the dam

In order to reconstruct the hydrodynamic condition of Zhanjiang Bay and Leizhou Bay before Donghai Dam constructed, we change the topography in our model by wiping off the Donghai Dam and redid numerical simulation. Tidal current field distribution around the area where the Dam was built differed due to the alterant coastlines. In order to analyze the pre-construction current field, two typical tidal times of spring tide were selected to do numerical simulation. From Fig. 9 we can see pre-construction current distribution at flood time and ebb time during spring tide.

As Zhanjiang Bay and Leizhou Bay were connected before the dam was constructed, hydrodynamic environment near Donghai Dam was heavily influenced by tidal current from the two Bays. Current field changed a lot by comparison with present status, current velocity changed obviously, and current directions were basically opposite under the two conditions. Seawater flow pattern during neap tide was similar to that during spring tide, except that velocity dicreased.Before the construction of the dam, seawater in Zhanjiang Bay passed through the original dam section and swarmed into Leizhou Bay during flood tide, which with sea water of Leizou Bay both converged to area around Tongming sea (about from 21°N to 21.03°N). During ebb tide, part of seawater in Leizhou Bay passed through the dam section and swarmed into Zhanjiang Bay. It was equivalent to that water from north of Tongming Sea to the dam section which belonged to Leizhou Bay was brought into Zhanjiang Bay, that increased tide capacity of Zhanjiang Bay.

5.3 Analysis of tidal change between pre- and post-construction of the dam

In order to evaluate the effects Donghai Dam conducted on tidal characters of Zhanjiang and Leizhou Bays, this paper analyzed the simulated tidal level of T1 and T4 stations which located at both sides of the dam for pre- and post- construction of the dam respectively. Fig.10 showed comparison of a tidal level cycle of T1 and T4 stations for pre- and post- construction of the dam respectively. The light

broken line was tidal level changing curve pre-construction, and the dark real line was tidal level changing curve at present. After the dam was built, tidal level of T4 station changed slightly. But tidal level of T1 station post-construction lagged about 2h compared to pre-construction, and amplitude increased as well.

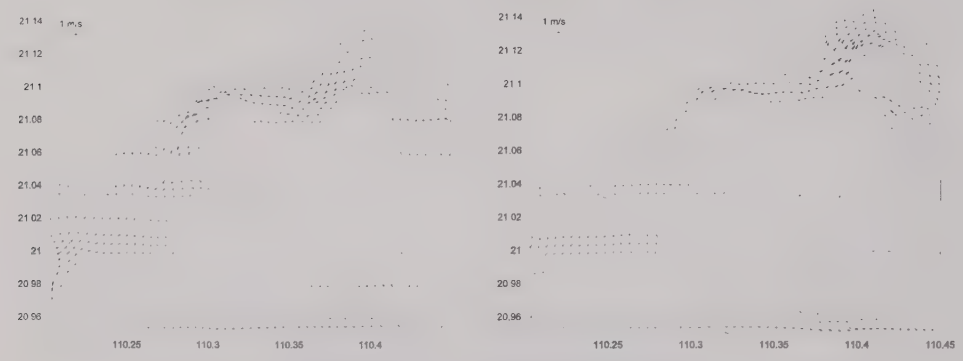

Fig. 9 Pre-construction current field distribution during spring tide

(the left was flood time and the right was ebb time)

Tab. 1 showed major tidal constituents change of T1 and T4 stations for pre- and post-construction of the dam respectively. After the dam was constructed, tidal amplitude and phase of the major tidal constituents of T1 station increased. Amplitude of M_2 tidal constituent increased by 8.44 cm, phase increased by 20.1°. Adlittoral tidal constituent M_4 and MS_4 also changed obviously, and increase of phase caused tidal level changing of T1 station delayed. Major tidal constituents of T4 station changed slightly. So it is obviously that, Donghai dam influenced the tidal system of T4 station at east side of the dam slightly, but influenced heavily on tidal system of T1 station with tide postponed and amplitude increased.

5.4 Analysis of tidal current change between pre- and post- construction of the dam

Donghai Dam had large effects on tidal system at both sides of the dam. Fig. 11 showed comparison of simulated current velocity and direction of V1 and V2 stations during spring tide for pre- and post-construction of the dam(real line stands for pre-construction, broken line stands for post-construction). We can see that after the dam was constructed, current direction of V2 station at east side of the dam differed slightly,while current velocity decreased. And current direction of V1 station at west side of the dam basically reversed, while current velocity also decreased. Time for water spreading to V1 station from Zhanjiang Bay was less than that from Leizhou Bay, and seawater in Zhanjiang Bay flowed to the location of the dam and continued to spread to V1 station, which converged at about 21°N in Leizhou Bay with seawater which spread to Leizhou Bay. During flood tide, seawater from Zhanjiang Bay could pass through the original Donghai Dam section and flowed into Leizhou Bay. While during ebb tide, seawater could pass through the dam section from Leizhou Bay to Zhanjiang Bay. So the current passed by V1 and V2 stations had the same characters, which was basically opposite to current passed by V1 station after the dam was constructed. Moreover, the dam obstructed sea water spreading, which severely influenced water circulation at both sides of the dam, and seawater velocity slowed down at the dam location.

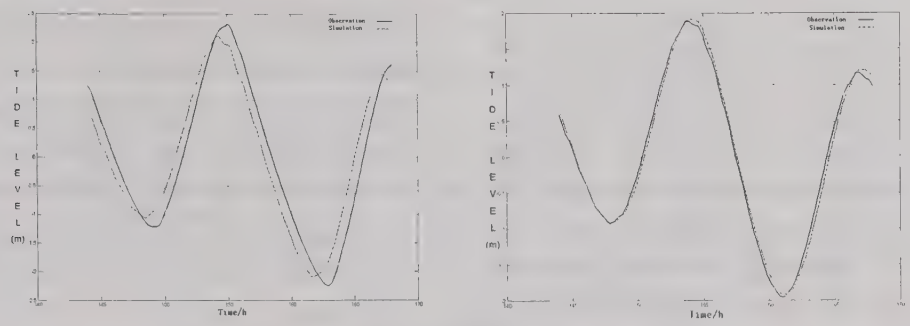

Fig. 10 Comparison of tide level between pre- and post-construction of the dam

(The left was T1 station and the right was T4 station)

Tab. 1 Major tidal constituents change of T1 and T4 stations for pre- and post-construction of Donghai Dam

	T1 (pre-)	T1 (post-)	T1 variety	T4 (pre-)	T4 (post-)	T4 variety
K_1 amplitude / cm	41.21	42.78	1.57	39.93	39.70	-0.23
K1 phase (°)	319.74	326.76	7.02	314.14	312.23	-1.91
O_1 amplitude (cm)	45.34	47.79	2.45	43.51	43.11	-0.4
O_1 phase (°)	218.43	225.22	6.79	213.28	211.54	-1.74
M_2 amplitude (cm)	107.35	115.79	8.44	102.98	101.55	-1.43
M_2 phase (°)	321.13	341.23	20.1	320.78	318.57	-2.21
S_2 amplitude (cm)	54.57	59.22	4.65	49.60	48.97	-0.63
S_2 phase (°)	359.13	15.62	16.49	345.78	342.90	-2.88
M_4 amplitude (cm)	6.63	9.49	2.86	2.62	2.03	-0.59
M_4 phase (°)	118.05	150.6	32.55	110.74	79.75	-30.99
MS_4 amplitude (cm)	6.88	9.11	2.23	2.64	1.87	-0.77
MS_4 phase (°)	218.01	252.98	34.97	217.53	193.27	-24.26

5.5 Comparison of tidal capacity between pre- and post- construction of the dam

Tidal capacity is an important proxy for vitality of half-closed bay, whose change was general reflection of tidal current character of the bay, which will directly influence sand transport capacity, water exchange ability, and even environmental capability.

This paper caculated tidal capacity by caculating flux which passed through the section, and the formula used was

$$Q = \int_{t1}^{t2} (Q_u + Q_v) dt \qquad \text{in which, } Q_u = \sum_{n=1}^{n} uhl_v \text{ , } Q_u = \sum_{n=1}^{n} vhl_v$$

Among which, n was number of grid nodes on the section, u and v was transmeridional and meridional velocity of seawater for one certain grid at one certain time, h was depths of corresponding time and grid, l_u and l_v were transmeridional and meridional widths of grids respectively, Q_u and Q_v were transmeridional and meridional water flux which passed through the section for a unit time respectively, t1 and t2 were the beginning time of flood tide and the ending time of ebb tide respectively. The gained Q was water flux which passed through one section for one flood tide or ebb tide cycle.

Tab. 2 compared flux which passed through the main section in Zhanjiang sea area for pre- and post-construction of the dam, and analyzed tidal capacity change in Zhanjiang Bay caused by construction

of Donghai Dam. The results showed: There was large difference in current flux passed through the sections of the whole sea area between pre- and post-construction of the dam. About 7.302 million m^3 sea water inflowed to Leizhou Bay from Zhanjiang Bay by passing through the section where the dam located during flood tide, while seawater inflowed to Zhanjiang Bay from Leizhou Bay during ebb tide. Part of Leizhou Bay area at west side of the dam was brought into tidal capacity area of Zhanjiang Bay. This played an important role in water exchange of Zhanjiang Bay, which can effectively reduced discharge of contamination, quicken discharge rate of contamination to opean ocean, improved water exchange quantity in bay with the open ocean and water self-purification ability, then improved water quality of Zhanjiang Bay. This was advantageous to environmental protection of Zhanjiang Bay and meaningful to continuable development of Zhanjiang.

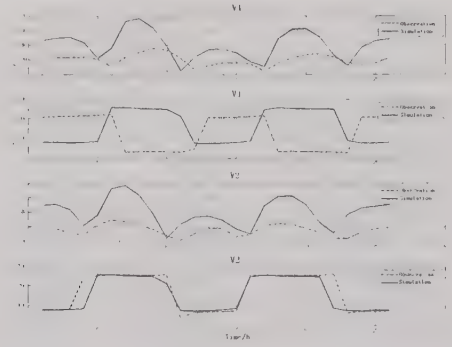

Fig. 11 Comparison of tidal current of V1 and V4 station at pre- and post- construction of the dam

At the same time, because tidal capacity of tidal passage in Zhanjiang Bay increased, tidal energy strengthened ulteriorly. Erosion effect on watercourse caused by tidal current intensified, which made it deepen and broaden to overcome blockage of coastal suspended sands caused by waves from the open ocean. All of these made the inlet of Zhanjiang Harbor—Longteng watercourse flowing and stable. Moreover, one more watercourse between Zhanjiang Bay and the open ocean played significant roles to the development of Donghai Island and Zhanjiang.

Tab. 2 Comparison of water flux which passed through the major sections

Section / spring tide	present status / $10^6 m^3$	Pre-construction / $10^6 m^3$
Inlet west of Donghai Island	249.06	153.55
Inlet east of Donghai Island	721.20	788.36
Inlet north of Nansan Island	107.86	113.99
Section of the dam	–	73.02

5.6 Changes of ratio of water exchange between the pre- and post-construction of the dam

Numerical simulation was conducted to study the impact of Donghai Dam on water exchange ability of Zhanjiang Bay. At the initial simulated time, concentration of the contamination on grid nodes in entire Zhanjiang Bay was given as value 1, and grid nodes out of the Bay were given as value 0 [8, 9]. Numerical simulation of contamination diffusion was conducted for 30 days under the same hydrodynamic conditions refered above. Average residual concentration of contamination and water exchange ratio inside the bay

was caculated for 10 days, 20 days and 30 days respectively. The results showed in Tab. 3, Fig.13 and Fig. 14.

Tab. 3 Results of water exchange rate

state	post-construction Contamination concentration	post-construction water exchange rate	pre-construction Contamination concentration	pre-construction water exchange rate	Increased percentage of pre-construction water exchange rate
10 days	0.8566	14.34%	0.7403	25.97%	11.61%
20 days	0.8022	19.78%	0.6419	35.81%	16.03%
30 days	0.7501	27.99%	0.5331	46.69%	18.7%

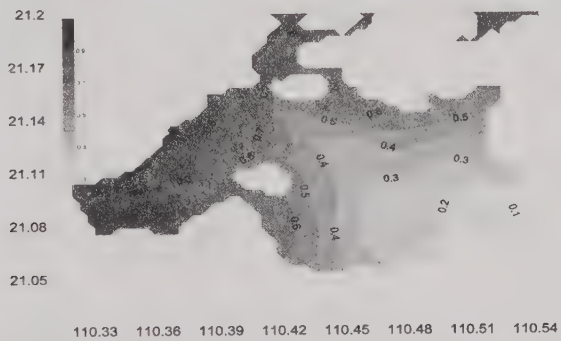

Fig. 12 Contamination concentration inside the bay after 30 days for present status

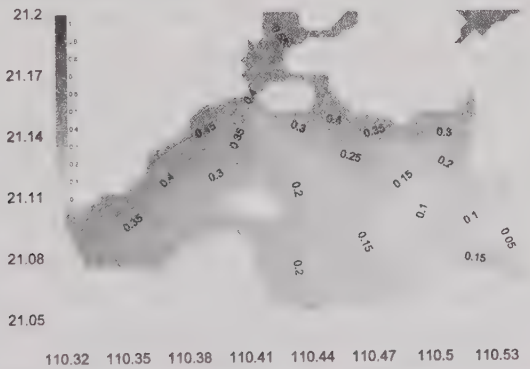

Fig. 13 Contamination concentration inside the bay after 30 days before the dam was constructed

According to diffusion conditions of the contamination, sea area inside the bay can be divided into 3 parts: 1. area north of Techeng Island; 2. area between east of the dam and west of Dongtoushan Island; 3. area between south of Techeng Island and east of Dongtoushan Island. Tab. 4 showed simulated results of average contamination concentration and water exchange ratio of the above areas after 30 days. From the table, we can see area part 2 was just in exchange with water at its east side because of its shallower water, lower current velocity and closed status. Water exchange ability of this area was quite weak at present status. While before the dam was constructed, this area was not closed, water exchange could operate between Zhanjiang Bay and Leizhou Bay. Water exchange ability could be improved notably, with increase above 50% compared with present status. The simulated water exchange ratio of area part 1 was only 6.6% because of the narrow water channel. And before the dam was constructed,

water exchange ratio could reach 15.85% which was much higher than that at peresent status. Similarly, seawater exchange ratio of area part 3 near Zhanjiang Bay inlet improved greatly as getting rid of the dam block. The simulated results revealed that water exchange ratio could reach 68.46%, higher than the present status 44.98%. It is obvious that construction of Donghai Dam influenced the water circulation in Zhanjiang Bay, especially it made large negative effect on water exchange of area part 2.

Tab. 4 Results of water exchange rate from different sea areas in the Bay

area	Present contamination concentration in the Bay	Present water exchange rate	Pre-construction contamination concentration	Pre-construction Water exchange rate	Increased percentage of pre-construction water exchange rate
North of Techeng Island	0.9339	6.61%	0.8415	15.85%	9.24%
West of Dongtoushan Island	0.8851	11.49%	0.3567	64.33%	52.84%
East of Dongtoushan Island	0.5502	44.98%	0.3154	68.46%	23.48%

6 Conclusion

The Donghai Dam which was built in 1958 played an important role in the traffic improvement, economic development and culture intercommunion between Zhanjiang and Donghai Island. This paper simulated and predicted hydrodynamic fields of the sea area around Zhanjiang for pre- and post-construction of the Donghai Dam by using numerical simulation method, and analyzed the possible effects of the dam. The results showed that hydrodynamic environment of Zhangjiang Bay without the dam was better than that with the dam. Tidal capacity and water exchange ratio of Zhanjiang Bay were larger without the Dam than with the Dam. Construction of Donghai Dam blocked the water exchange between Zhanjiang Bay and the open ocean, which reduced decontaminative abilities of sea water in Bay. Construction of Donghai Dam played a negative role in water quality improvement in our numerical study area. However, hydrodynamic field changes of Zhanjiang Bay arisen by Dam construction were not calculated due to conditions restricted when the dam was under building.

Reference

[1] China Bay records editing committee. China Bay Records the tenth fascicle (Bay at west of Guangdong province) [Z]. Beijing: China Ocean Press. 1999, 187 - 248.

[2] Ying Zhifu, Wang Hongshou. The relationship between fill-block engineering and tidal inlet system response in zhanjiang bay [J]. Acta Scientlarum Naturalium Universitatis Sunyatseni, 1996, 35(6): 101 - 105.

[3] Chen Dasen, Yan Jinhui. A characteristic and impact on Water Enviromnent Current in the Gulf Sea Area of Zhanjiang [J]. Science Technology and Engineering, 2006, 14(6): 2 100 - 2 103.

[4] He Songlin, Ding Pingxing. Prediction of effects of coastal engineerings on erosion and sedimentation in Zhanjiang Bay: I. dynamical physiognomy analysis [J]. Acta Oceanologica Sinica, 1997, 19 (1): 55 - 63.

[5] Ding Pingxing, He Songlin, Zhang guoan. Prediction of effects of coastal engineerings on erosion and

sedimentation in Zhanjiang Bay: Ⅱ. Numerical caculation of erosion and sedimentation [J]. Acta Oceanologica Sinica, 1997, 19 (1): 64 - 72.

[6] Xia Huayong, Lin Diyang, Niu Zhiwang. Prediction of effects of reclamation engineering on hydrodynamic conditions in the Zhanjiang Bay [J]. Marine Science Bulletin, 2006, 25(6): 47 - 54.

[7] Chen Changsheng, Beardsley R C, Cowles G. An unstructured grid, finite-volume coastal ocean model fvcom user mannual. second edition. Draft July 2006.

[8] Sun Yinglan, Zhang Yuemei. A numericai model of pollutant transport and seawater exhange in dingzi bay [J]. Journal of Ocean University of China, 2003, 33(1): 001 - 006.

[9] Wei Hao, Tian Tian, Zhou Feng, et al. Numerical study on the water exchange of the bohai sea: simulation of the half-life time by dispersion model [J]. Journal of Ocean University of China, 2002, 32(4): 519 - 525.

东海大堤对湛江湾水动力环境影响的研究

李希彬[1]，孙晓燕[2]，于华明[3]，鲍献文[3]

（1. 国家海洋局 天津海洋环境检测中心站，天津 300451；2. 国家海洋信息中心，天津 300171；
3. 中国海洋大学 海洋环境学院，山东 青岛 266100）

摘 要：在湛江附近海域建立了三维动边界水动力模型，通过验证，结果与观测数据符合良好，并在此模型基础上分别模拟计算了湛江东海岛填海大堤现状以及 1958 年大堤修建之前湛江海域的水动力场，通过两种情况下的流场、潮位、纳潮量以及水交换率的比较，分析了东海岛大堤的存在对湛江湾水动力环境的影响。

关键词：湛江湾；东海岛大堤；数值模型；水动力环境

Diagnostic Calculation of the Oceanic Circulation

YANG Yang[1*], ZHOU Wei-dong[2], DONG Dan-peng[2]

1. *South China Sea Marine Engineering Surveying Center, State Oceanic Administration, Guangzhou* 510300, *Guangdong Province, China;*

2. *South China Sea Institute of Oceanology, Chinese Academy of Science, Guangzhou* 510301, *Guangdong Province, China*

Abstract: A 2-dimensional global free surface diagnostic model, combined with dynamic calculation, is used to investigate the world ocean circulation; the model has a horizontal resolution of 1/4°×1/4°. The simulated results agree well with the results of other modesl and observations. The distribution of Stream Function suggests that the main circulation systems in the world ocean have been represented, including oceanic currents strengthened in the oceanic western. Be close to the observed results, the net mass transport of the Kuroshio axes is estimated about 54Sv; The distribution of the horizontal circulation in each layer shows that the main circulation systems in the world ocean are well simulated, for example, the Kuroshio and the Antarctic Circumpolar Current can go down to the bottom layer, but the Gulf Stream cannot, and its direction reverses at the depths of 1 000 to 2 000 m.

Keywords: diagnostic model; stream function; dynamic calculation; oceanic circulation

Like the forecast model, the diagnostic model is also a significant tool for researching the oceanic circulation. Diagnostic model, exploiting density field, is an economical, traditional and dynamic completed method of diagnostic calculation of oceanic dynamic factors, such as current field and sea level elevation. It not only possesses the dynamical categoricalness as the forecast model, but also maintains the trait of the diagnostic method which ascertains the current field according to the density field. The current field structure shown by the diagnostic model is a complete and actual answer to the density stratification on dyn, which can't be reached by other diagnostic models, and can't be replaced by the forecast model. Compared to forecast model, diagnostic model can reduce the uncertainty due to the "Prediction Algorithm", which enables the circulation field to become more objective. More importantly, spin up integration time for reaching stable state of the forecast model is too long. Fujio [1] indicates that it takes 1000a integration time to reach stable state for upper layer circulation, while the spin up time for the deep ocean circulation up to 10000a, which brings a drastically calculative cost. At this stage, forecast model can only reach a meta-stable state, but it only takes 30~40d for the diagnostic model to reach the stable state even in the global sea area. Obviously, on the price of calculation, diagnostic model is far less than value forecast model.

Sarkisyan [2] from former USSR is the representative of the valuing and promoting on international

Received on April 21, 2009

*Corresponding author: yyang0213@sina.com

study and application of diagnostic model. Owing to the disorganization of the USSR and the complexity of the model making, diagnostic model didn't get the international value it should have in the recent years. Fujio etc[3-5] work is the most systemic, but has a low resolution of 2°×2°and its Levitus climate data is 1°×1°. So the result of Fujio et al. [3-5] losses some useful information, such as it can't imitate the Chinese offing circulation and details of other circulation (like Mindanao cold eddy). In contrast, Chinese scholar attach importance to the diagnostic model, and extensive use it in marginal sea [6]. Wei etc [7] and Wei zexun et al. [8] took advantage of global ocean circulation diagnostic model (Robust diagnostic model), which based on the MOM model, to research global ocean circulation. Their outcome has a great improvement than Fujio etc [3-5], although the model resolution is not high enough (1°×1°). Some current systems still can't be reflected well. For example, the position of Kuroshio has a little eastward move. The above-mentioned global ocean circulation diagnostic model are all rigid-lid model, while in this paper, free-surface model is adopted. Despite the 2-dimensional model, we can obtain the three-dimensional result approximately by the simulation results combining dynamic calculation. The reliability of this method has been particular analyzed and validated [9] during the previous study. The purpose of this paper is to estimate the global ocean circulation through this method.

1 Model and data

Here is a brief introduction to the model. This is a 2-dimensional global linearity diagnostic model with a horizontal resolution of 1/4°×1/4°, which bases on TOM [10, 11] free surface forecast model. And the forecast model is a free surface model under the Bossiness Approximation, Hydrostatic Approximation and Z-coordinate conditions (detailed description: http://www.scsio.ac.cn/TOM/TOM.htm). The model range is 0 - 360°E，65°S - 65°N, and NS-trending and EW-trending use the solid boundary condition and periodic boundary condition respectively.

The model output is a whole layer barotropic velocity $\overline{U}$ integrating from sea surface to seafloor. In order to get the vertical velocity distribution, the relative velocity $U'(z)$ is derived by dynamical calculation, and reference speed U_0 is obtained by the processing as follows:

Let $U(z)$ be absolute velocity, then $U(z)=U_0+U'(z)$

After the vertical integration, $\overline{U}=U_0+\frac{1}{H}\int_0^H U'(z)dz$, where H is the depth from the sea surface to the seafloor.

From the equation above, we can get the undetermined reference velocity: $U_0=\overline{U}-\frac{1}{H}\int_0^H U'(z)dz$

The reliability of the above velocity calculation of three-dimensional structure has been inspected by Zhou et al. [10]

The data of temperature and salinity used by this model is Levitus climatology monthly average temperature and salinity data, with the resolution of 1/4°×1/4°. There is no seasonal variation deeper than

1 500 m among this data. While depth is divided into non-isometric 33 layers along the perpendicular direction from sea surface to seafloor. 10 layers are above 200 m, and it is segmented into 19 layers above 1 000 m, which can incarnate the thermo cline structure better. The sea surface is driven by the COADS monthly average climatology wind stress.

Fig. 1 Global annual mean stream function(unit:Sv)

2 Outcomes and discussion

2.1 Stream function

By using our simulation, the distribution of global ocean circulation is shown in Fig. 1. The outcome is well agreed with that of Fujio et al. [4] and Wei et al. [7] However, thanks to the improvement of the resolution, there are some little eddy in fig.1 which can not be simulated by Fujio et al. [4] and Wei et al. [7] And it is also similar to the global ocean circulation simulated by diagnostic model of Wei Zexu et al. [8] which is based on MOM model. But there are some discrepancies in Equatorial Pacific, reflecting at the discrete and weak little eddies on the simulated outcome. It is because the resolution of our model (1/4°×1/4°) is higher than that of Wei Zexun et al. [8] The main features of the annual average stream function diagram during this imitation are: a 0 isoclines traversing the North Pacific around the 12°N in the Pacific. To the north of this line is a prominent subtropics current cycle; to the south is equator reverse current. Similar to the simulative outcome of Wei Zexu[8], we simulate the Mindanao Cold Eddy to the east of Mindanao Island. And the stream function of the west boundary current of the North Pacific (Kuroshio) in the model reaches 40 - 50*Sv*, which is very close to the actual measurement. Especially at the ASUKU cross section, the current rates of the simulative spindle of Kuroshio and ASUKU cross section are 54*Sv*

and 48*Sv* respectively, while the actual measurement is 57*Sv* and 42*Sv* [12] respectively. On the 17°S of the South Pacific, 0 isoclines extends to the west from the extreme south coastline of Peruvian. Even though the stretch zone is quite winding, 0 isoclines of the north Pacific links the NW angle of the New Guinea Island. In the famous gulf stream area of the northern Atlantic, the stream function is 20 - 30*Sv*. And the gulf stream Sverdrup transport value is 30*Sv*, driven by the wind stress by Godfrey. [13] And gulf stream simulative value is 50*Sv* and 40 - 50*Sv* by Fujio et al. [4] and Wei zexun et al. [8] respectively. In the southern hemisphere, stream function value gets extremely large near the Antarctica, and it gets larger when closer to the Antarctica land. Moreover, as the isoclines is so thick that the big grads of the stream function constitute the driving Antarctica flow around. Except for the Antarctica circumpolar current area, most stream function in other area is negative value. There're two maximum negative value centers, which locate at 30°S - 45°S sea area of the southeast area of Africa and 30°S - 40°S to the east of South America. And the homologous transport of sea volume is mainly clockwise. According to the density state of the isoclines of the stream function, isoclines of the ocean west boundary is particular thick, while eastern one is sparse, which just match along with the phenomenon of the westward intensification of the ocean circumfluent, such as the famous Kuroshio and the gulf stream etc. In addition, there are high value isoclines surrounding the Antarctica, which distribute especially thick. And here is just the place where the Antarctica circumpolar current locate.

2.2 Horizontal flow field

Global annual mean vector diagram of horizontal flow field in upper layer (0 - 200 m), middle layer (200 - 1 000 m), lower layer (1 000 - 2 000 m) and bottom layer (>2 000 m) is shown in Fig. 2, Fig. 3, Fig. 4 and Fig. 5 respectively.

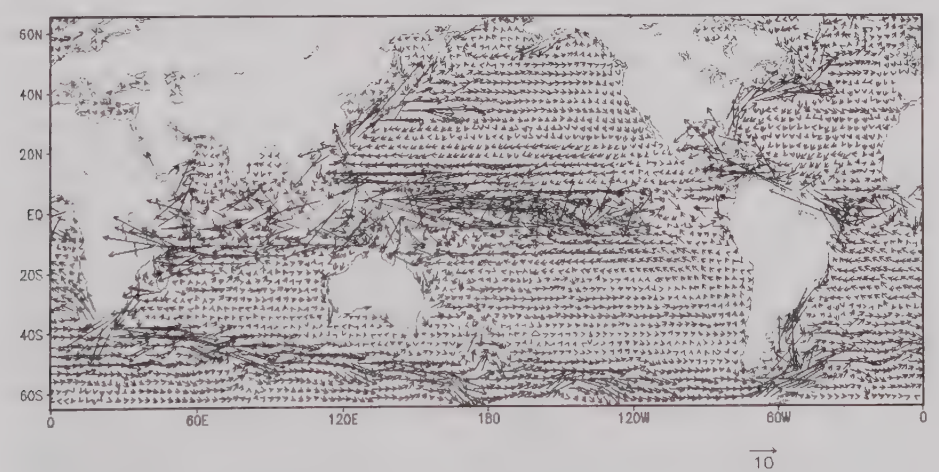

Fig. 2 Upper layer (0 - 200 m) global annual mean circulation (unit: cm/s)

2.2.1 Pacific

As shown in Fig. 2, the main character of upper layer circulation of North Pacific is: there is a current

known as "north equator current" which flows from the east coast of Pacific to the west coast between 10° - 20°N, and this current divides into two west boundary currents when it reaches the west coast of the Philippines at 14.50°N—the west boundary current heading north comes in to Kuroshio, and the Mindanao sea current is the opposite one to it. One part of Mindanao sea current joins to the south current known as "Equatorial Counter Current", and one part flows to Indian Ocean after joining into the Indonesia Sea. When the west boundary current—Kuroshio passes the Luzon Straits toward north, a little part of it enters westward to the South China Sea through the Luzon Straits, and form South China Sea Current System in the South China Sea. At that current system, some waters flow NE-ward to East China Sea through Taiwan Straits, while the other part joins in the Indonesia Sea through the southern straits. Besides this embranchment joining to the Luzon Straits, Kuroshio intrudes eastward to East Sea from Taiwan Island, and go northeastward along the south coast of Japan Island. And its northward trend is suffocated by the southward Oyashio at 40 °N, and after these two currents converging into the eastward North Pacific Sea Current, they flow to the east coast of Pacific. These characters accord with the outcome of the previous model [4, 7, 8]. The current field of 5°S - 5°N Pacific equator is rather mussy, because the Coriolis force(f) near the equator is too small, which is the common defect[4] in all the diagnostic models. In South Pacific, it presents anticlockwise circulation, and only Peru Sea Current turns north-west ward at 20°S when it go northward along the coast of Peru, forming the westward South Equator Current. So it seems that, there's a huge anticlockwise circulation in the southeastern Australia. In the middle layer current field in Pacific (Fig. 3), we can see that the North Equator Current bifurcated at the east coast of Philippines; and the phenomenon of the eastward turning of the northward Kuroshio at about 30°N. Although we can see clearly that the path of Kuroshio in the lower layer current field, at the northern Luzon Straits, its intensity has weakened enormously. So there is no branching of the North Equator Current at the east coast of Philippines in that layer of current field. However, it seems that we can see subtle Kuroshio in the layer depth of more than 2 000 m, to the east of Japan.

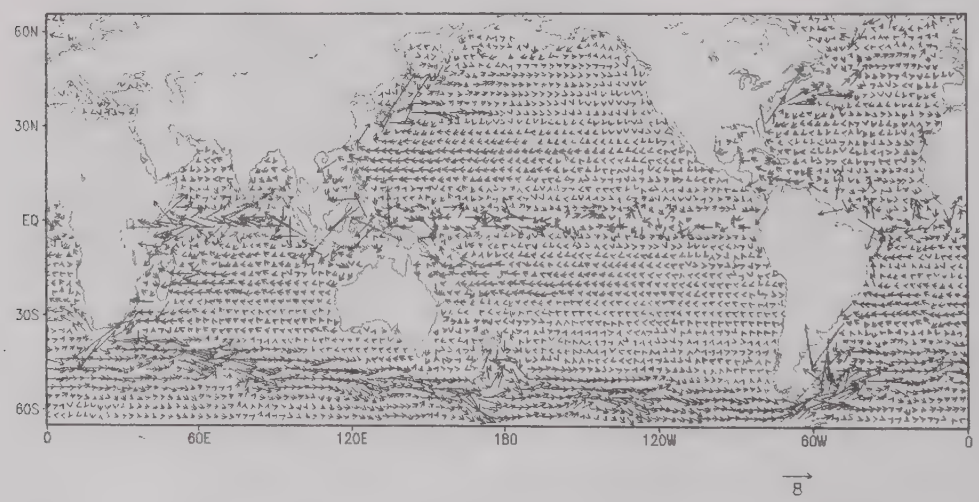

Fig. 3 Global annual mean circulation at the middle layer (200 - 1 000 m) (unit: cm/s)

2.2.2 Atlantic

According to the outcome of this paper, the circulation in the Atlantic is quite complex. In the upper layer (Fig. 2), there are two independent circulation systems in the north and south Atlantic, respectively. There is an obvious equatorial counter current flowing from east to west in the tropic ocean of equator between two current systems. After the north equator current reaches the west coast of Atlantic, most of it flows to the north along the coast of continent, forming the notable border current of west in Atlantic--Gulf Current. On the way to the north, after meeting the ocean current of Labrador Sea Current which flows along the north-east coast of Labrador Peninsula of Canada, it forms to the North Atlantic Ocean Current flowing to the north-east. During the process of flow of the north Atlantic current, some part of ocean current drops off in 40°N and flows to the eastern, and then forms into Canary Current along the east coast, and join to the north equator current back. While except for the Norway Current which reaches Norway flowing from southwest to northeast, the remain North Atlantic Current together with Labrador Current, West Greenland Current, East Greenland Current make up the North Atlantic anticlockwise subpolar current cycle in the middle high latitude waters during the process of flowing. And the other part of the gulf current forms into clockwise subtropics current system. South and North Equator Current also exist in the Atlantic. Similar to the Pacific, its South and North Equator Current are not symmetrical by the equator. And there is a large scale anticlockwise current system in the South Atlantic. East wing is Benguela Current (from south to north), south wing is Antarctic Circumpolar Current (from west to east), west wing Brazil Current (from north to south), and north wing South Equator Current (from east to west). The four current forms a big anticlockwise circulation. Similar to the upper layer current field, the middle layer current field (Fig. 3) presents gulf current, and anticlockwise circulation system of sea basin scale still exists in the South Atlantic. Gulf current can not reach deep layer, which means the current changes direction between 1 000 -2 000 m (Fig. 4). In addition, the structure of bottom layer (Fig. 5) is similar to the one of lower layer.

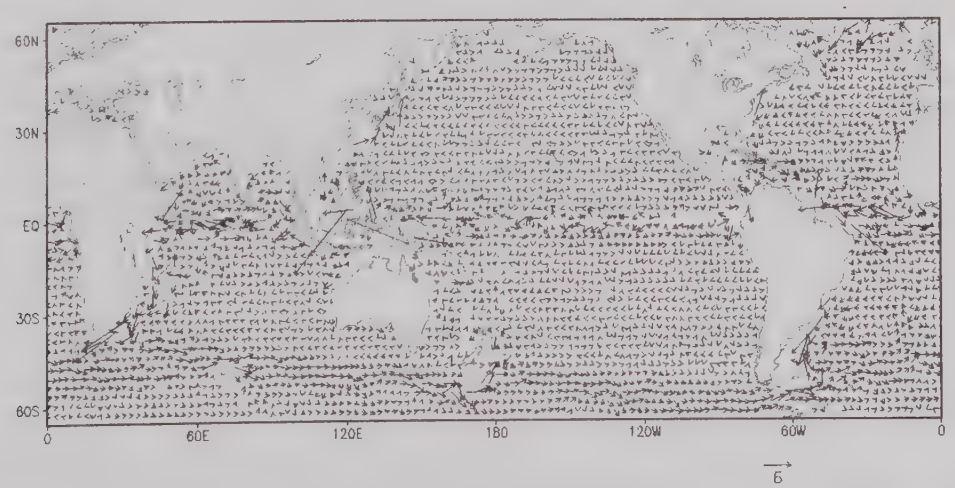

Fig. 4 Global annual mean circulation at the lower layer (1 000 - 2 000 m) (unit: cm/s)

2.2.3 Indian Ocean

The terrain of Indian Ocean is different from Pacific, and Atlantic. North Indian Ocean is influenced by the India Monsoon markedly. Due to its small room, there is no enough sea area for the development of the circulation. However, India Monsoon has little effect on the South Indian Ocean which has a wide sea area. So that the discrepancy of the circulation structure between South and North Indian Ocean is obvious. In the North Indian Ocean, due to the annual mean effect of the monsoon, it's hard to identify the North Indian Ocean current field. There appears a weak clockwise circulation in Arabia Sea; while the current system in South Indian Ocean is more stable. The South Equator Current flow passes the Indian Ocean from east to west, reaching the Madagascar Island. One part passes round this island by the north, crossing the Mozambique Straits, which known as Mozambique warm current; the other part flows straight southward along this island, which known as Madagascar warm current. After these two warm current meeting at the northwest of the Madagascar Island, it flows southward along the east coast of Africa, then it's called Cape Agulhas warm current when it reaches the Cape Agulhas Angle. At 40°S, Cape Agulhas warm current joins in West Wind Drift in South Indian Ocean, flowing to the southwest sea area of Australia. Most of it continues to flow eastward to Pacific, but a little part will go northward along the southwest cost of the land, making up the anticlockwise circulation in the southern Indian Ocean. The middle layer current field (Fig. 3) is similar to the upper layer current field, and the weak clockwise circulation in North Indian Ocean and the anticlockwise circulation in South Indian Ocean still exist. Two circulations exists at the lower layer (Fig. 4) and bottom layer (Fig. 5) as well.

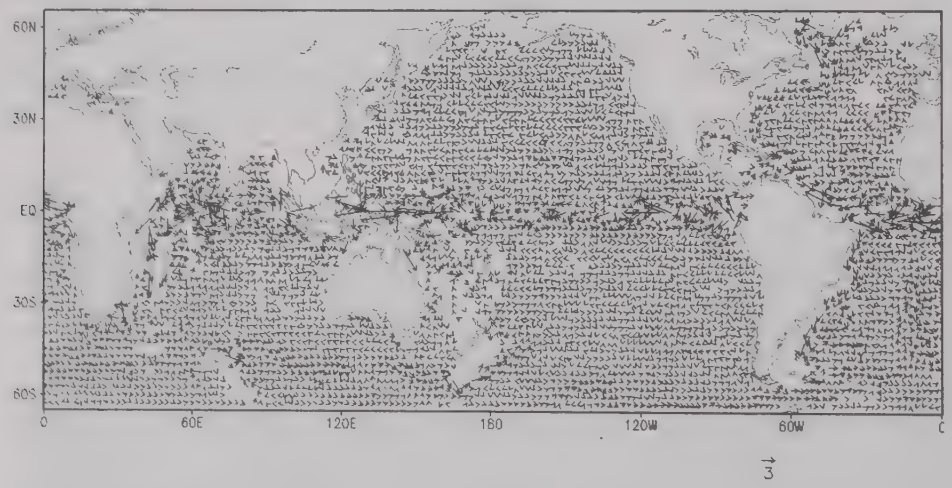

Fig. 5 Global annual mean circulation at the bottom layer (1 000 - 2 000 m) (unit: cm/s)

3 Epilogue

A 2-dimensional global free surface diagnostic model, combined with dynamic calculation, is used to simulate the world ocean circulation. The simulated outcome is similar enough to the simulated and

observed outcome of other models.

a) As to the distribution of the flow function, North and South Equator Current, North Equatorial Countercurrent, Antarctic Circumpolar Current, and the subtropical maelstrom of Antarctic, Pacific, South Indian Ocean, as well as the strengthen west boundary ocean current, such as Gulf current, Kuroshio and Cape Agulhas current etc, can be seen and separated clearly. And they agree well with the previous outcome of observation and simulation. As to the isoclines density of the flow function, west boundary of the ocean are particular thick, while thin at the east boundary, which matches the phenomenon of the westward strengthen of the ocean circulation, such as the famous Kuroshio and Gulf current etc. Furthermore, high value isoclines which are unusual thick exist surrounding the Antarctica, where the Antarctic Circumpolar Current just locates.

b) As to the distribution of the horizontal flow field in each layer, most of the main current systems of each ocean reappear well. For instance, Kuroshio and the Antarctic Circumpolar Current can reach deeply to the bottom layer; but the Gulf current can not reach the bottom layer, which has change direction between 1 000 - 2 000 m.

Acknowledgement

This paper was supported by the Project Funding of the Fund Committee of Science Department (No.40346029), National Natural Science Foundation (40346029), and the offing comprehensive evaluation of our country (908-02-01-03).

Reference

[1] Fujio S. Prognostic simulation of the World Ocean Circulation and its Comparison with Diagnostic simulation [J]. Journal of Oceanography, 1997, 53:283 - 297.

[2] Sarkisyan S. C numerical analysis and prediction [M]. 1980

[3] Fujio S, Imasato N. Diagnostic calculation for circulation and water mass movement in the deep pacific [J]. J.Geophys Res, 1991, 96(c1): 759 - 774.

[4] Fujio S. World Ocean Circulation Diagnostically Derived From Hydro- graphic and Wind Stress Fields 1: The Velocity Field [J]. J Geophys Res, 1992a, 97(c7): 11 163 - 11 176.

[5] Fujio S. World Ocean Circulation Diagnostically Derived From Hydro- graphic and Wind Stress Fields 2: The Water Movement [J]. J.Geophys Res, 1992b, 97(c9): 11 439 - 11 452.

[6] Yuan Y, Su J, Xia S. A diagnostic model of summer circulation on the northwest shelf of the East China Sea [J]. Prog Oceanog, 1987, 17: 163 - 176.

[7] Wei Z. Byung-Ho Choi, Fang G. Water heat and salt transports from diagnostic world ocean and north pacific circulation models [J]. La mer, 2000, 38: 211 - 218.

[8] WEI Zexun, QIAO Fangli, FANG Guohong. Diagnostic Study of the World Ocean Circulation--Current Field and Stream Function [J]. Advances in Marine Science, 2004, 22(1):1 - 15.

[9]. Zhou W, Yang Y, Dong D P. The calculation of the circulation in South China Sea by a diagnostic model [J]. Acta Oceanological Sinica, 2008, 27:31 - 45.

[10] Zhou W. An alternative leapfrog sheme for surface-gravity-wave equations [J]. J Atmos Ocean Tech, 2002a, 19:1 415 - 1 432.

[11] Zhou W A. Proper time integration with split stepping for the explicit free-surface modeling [J]. Adv in Atmos Sci, 2002b:119: 255 - 265.

[12] Imawaki S, Uchida H, Ichikawa H. Satellite a ltimeter monitoring the Kuroshio transport south of Japan [J]. Geo Res Lett, 2001, 28:17 - 28.

[13] Godfrey J S. A Sverdrup model of the depth-integrated flow for the world ocean allowing for island circulations [J]. Geophys AstroPhys Fluid Dyn, 1989,45:89 - 112.

大洋环流的诊断计算

杨阳[1]，周伟东[2]，董丹鹏[2]

（1. 国家海洋局 南海分局工程勘察中心，广东 广州 510300；2. 中国科学院南海海洋研究所热带海洋环境动力学重点实验室，广东 广州 510301）

摘 要：采用二维的全球高分辨率（1/4°×1/4°）的自由表面诊断模型结合动力计算估算全球大洋环流，模拟结果与其他模拟结果非常相似。流函数的分布表明，全球大洋中的主要流系均得到体现，包括大洋环流的西向强化的现象（黑潮、湾流等）。黑潮主轴的流量约 54*Sv*($1Sv=10^6 m^3/s$)，非常接近实测值；各层水平流场分布情况显示，各大洋的一些基本流系都能得到很好的再现。如黑潮和南极绕极流可深达底层。湾流不能到达深层，大约在 1 000 ～ 2 000 m 之间海流即已转向。

关键词：诊断模型；流函数；动力计算；大洋环流

Analysis of a Wenzhou-Hitting Exceptionally Strong Rainstorm Associated with a Typhoon Inverted Trough in September, 1999

ZHENG Feng

1. *Chinese Academy of Meteorological Sciences, Beijing* 100081, *China;*
2. *Nanjing University of Information Science & Technology, Nanjing* 210044, *Jiangsu Province, China;*
3. *Wenzhou Meteorological Bureau, Wenzhou* 325027, *Zhejiang Province, China*

Abstract: Using T106 numerical products, MM5 simulations in conjunction of Q-vector scheme-computed NCEP results, observations and satellite cloud images, study is undertaken for an exceptionally intense rainstorm event afflicting the Wenzhou region of Zhejiang province far away from the tropical storm center happening early on the morning of September 4, 1999 (TS9909 hereinafter). Evidence suggests that, like previously-studied typhoons landing in autumn south of Xiamen to the eastern part of Guangdong, TS9909 has an inverted trough in the central south of the coastal belt of Zhejiang province that produces the rainstorm from the meso convective complex (MCC) on the warm, moist shear inside; the time and order of the magnitude of the rainfall are bound up with the development of the pattern of strong Q-vector divergence gradients during the event for the study area; the NE – SW coastline and the unique topography of the Yandang mountains inside the region are favorable for air lifting are the major contributors to the torrential rains.

Keywords: long-distance-away; typhoon rainstorm; inverted trough MCC; Q-vector divergence gradient

1 Introduction

The main part of typhoon disaster is associated with the rainstorm and the study of such precipitation aids in improving the prediction of typhoon-related weather, for which one of the difficult issues is the research in the rainfall associated with typhoons landing far away. Weather/climate analysis shows that typhoons landing on Zhejiang and Fujian tend to produce rainfall in excess of 100 mm over North to NE China and such rainstorms far away from typhoon cores bear a relation to such physical factors as upper-air jets, unchanged intensity of landing typhoons, westerly troughs, northward extending inverted troughs inside as well as southward incursion of cold air. This type of rainstorms happen owing to activities of meso- and small-scale synoptic systems in the favorable background of large-scale systems and the

Received on June 18, 2008

Corresponding author: zhengfeng121@yahoo.com.cn

strong precipitation is marked by meso characteristics spatially and temporally (Lin et al., 2004; Xu et al., 2004). Besides, the torrential rains are often neglected as a result of their position well to the north and difficulties in prediction by means of conventional techniques (Liu, 1998).

2 Data and methodology

MM5 (version 2) simulations and Q-vector equation-computed NCEP dataset at a 2.5×2.5 resolution are employed to generate the Q-vector divergence pattern.

2.1 Definition of quasi-geostrophic Q vector

Hoskins et al. (1978) derived a new-type quasi-geostrophic ω equation, starting from the quasi static, quasi-geostrophic, adiabatic and frictionless equations of motion on the *f* plane in the P coordinates, with the new equation in the form

$$-A^2\omega = -2\nabla \cdot Q$$

showing that the *f* plane quasi-geostrophic vertical motion depends only on the Q vector divergence. With wavy character available over the ω field, we find ω to be in positive correlation with the divergence so that it can be inferred that for the divergence < 0, ω < 0 denotes rising motion and v.v. Consequently, the quasi-geostrophic ω equation with Q vector divergence as the only forcing term saves a large volume of computations, characterized by explicit physical implication and convenience of calculation (Li, 1997).

2.2 Brief Introduction to the numerical model

The MM5V2 was used and it has horizontal spacing of 54 km, centered at 36°N, 105°E, with 129 and 121 gridpoints zonally and meridionally, respectively, and for the nested mesh it has the grid length of 18 km, with 85 gridpoints in the E - W (N - S) direction covering 21 unequally spaced σ levels in the vertical and the terrain resolution of 10'. The BETLS/MILLER (MRF) scheme was utilized as the cumulus convective parameterization (for planetary boundary layer), with inclusion of long- and shortwave caused radiation . The timestep was 2 mins and the interval of integration spanned 48 hrs, equivalent to a little more than 2 hrs on computer.

3 Typhoon inverted trough in association with exceedingly strong rainstorm

TS9909 begot a heaviest rain event never experienced in the past 100-yr period or so, dominantly hitting part of Wenzhou, Taizhou and Lishui of Zhejiang, with rainfall reaching 392.7 and 235.6 mm recorded in the weather stations at Wenzhou and Yongjia, respectively, as well as the records in excess of 200 mm from 12 hydrological stations distributed over 5 counties between 0800/3 and 0800 BST/4, September. The exceptionally strong precipitation began at 0000 BST, September 4 from the inverted trough wherein meso convective cloud cluster emerged over the Wenzhou area far away from the landing TS9909 zone, which maximized at 0500 - 0800 hr interval, staying almost motionless over the Wenzhou region, leading to the cumulative precipitation of 347 mm in that period, a figure exceeding the highest

record in history and also being the highest ever recorded in the province of Zhejiang, with the amount hardly reported in China. The rainstorm caused landslide and cropland flooding, leading to colossal economic loss and heavy casualties.

Analysis of 11 study cases of 1949 - 1989 yields that, landing on the coastal belt from Xiamen of Fujian to eastern Guangdong in September and October and following tracks directed NW or WNW, the typhoons had strong precipitation mostly in coastal SE Zhejiang far away from their landfall (Fan et al., 1996). Under the effect of the inverted trough in the outer region of typhoons as in the case of TS9909, Wenzhou received rainfall ranging over 100 - 200 mm, with >200 mm in 7 records, of which the figures exceeding 300 mm were found from 2 typhoons on a local basis that were TS9909 and TS8116. They were categorized into a typical class of easterly jets, with precipitation from a tropical cloud cluster inside easterly jets in the outer region of the tempest and the situation is illustrated as follows: 1) the subtropical high stays motionless, whose 120°E ridge line is north of 30°N; 2) the surface and lower levels are on the S - SW side of an E - W oriented high-pressure or transformed high-pressure belt; 3) there is a branch of mid-lower level E - SE jet stream over the waters around Taibei and the Ishigaki island, which are deep enough, moving as fast as 34 m/s; 4) with the northward migrating inverted trough, easterly disturbances in the moist, wet airflow in the north of the typhoon propagate steadily in the SE to NW direction. For such intense rainstorms in the outer region there is a warm shear line formed by southerlies and easterlies that is responsible for the considerable increase in the torrential rains leading to explosive precipitation of >300 mm locally (Zhang et al., 2000). Moreover, strong rainfall would take place from the inverted trough should cold air come (vide supra for source).

4 Weather situation related to the unusually strong rainstorm

The TS9909 was coded at 0500 BST, September 3, moving thereafter in the northwest direction (see Fig. 1). The study rainstorm arose from the TS9909 inverted trough in its north during its journey towards the northwest at a slow pace. At 0800 BST, September 3, a 500-hPa western Pacific subtropical high covered the mid ~ lower Yangtze valley, the eastern Yellow Sea and East China Sea, the Korean peninsula and Japan, centered on the waters to the south of Japan. A vast expanse of low-level easterly jets formed in the eastern Chinese seaboard between the landing typhoon and the subtropical high. After 2 000 BST, day 3 the high intensified, extending west and the high remained strong on the north side, especially the portion of the high to the northeast of the Taiwan province of China that was amplified, extending westward to great extent. The TS9909 traveling northwestward with its inverted trough moved north led to the re-intensified northerly jet streak responsible for increased vapor transport. The flowfield exhibits certain cyclonic bending over the southeastern seaboard as a result of the high's westward extension and the inverted trough migrating northward, resulting in a convergence line – the shear line at the top of the trough that formed on the south side of Wenzhou and stayed in a quasi-stationary manner, which gave rise to the intense precipitation.

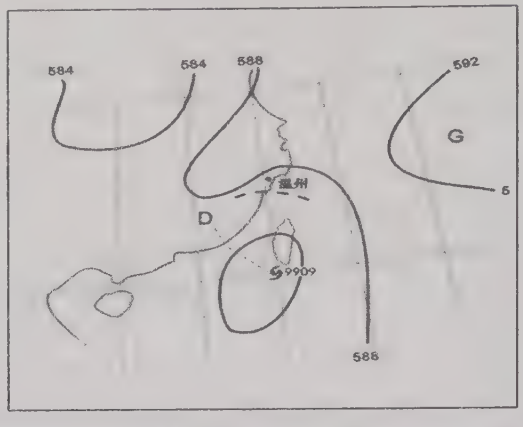

Fig. 1 Synoptic situation for 0800 BST, September 3, 1999, with the 850 hPa warm shear at 2000 BST denoted by dashed line

5 Variation in the cloudtop minimal TBB related to precipitating cloud cluster intensity

The selected was the hourly lowest T_{BB} at the cloudtop from satellite images over the target area from early on the morning to noon hours of September 4. Examination of Fig. 2 yields that T_{BB} displayed a rise – drop pattern, indicative that the meso cloud cluster experienced the weak – strong – weak phases, accompanied by the rainfall quickly intensified as T_{BB} dropped steadily, reaching the maximum of 137.6 mm/hr at 0600 BST with the lowest T_{BB} observed. Subsequently, at 0700 and 0800 BST the black-body temperature was low, corresponding to the precipitation of 97.5 and 87.7 mm/h, respectively, thereby indicating that the strong rainfall bears a correspondence to T_{BB} values.

6 Analysis of related element fields

For weather prediction in the fields of dynamic meteorology and numerical simulation, the focus lies on meso vapor flux convergence, as given by

$$\nabla \cdot q\vec{V} = \vec{V} \cdot \nabla q + q\nabla \cdot \vec{V}$$

The first term on the right of the equation denotes the requirement of sufficient vapor supply and the second denotes that of dynamic rising force from convergence, both being indispensable.

Comprehensive study was undertaken of the two terms by using products of T106 physical fields at 2000 BST, September 3 prior to the rainstorm.

6.1 Role of vertical motion in the rainfall happening

From the figures we see that convection is vigorous all over the fallout zone, with intense rising at middle-lower levels, and the averaged vertical speed, relative vorticity and divergence in the vertical over the gridpoints closest to the precipitation (Fig. 3) indicates that the rainfall occurs all over the rising extent;

maximal ω is 700 hPa, reaching -3.2×10^{-3} hPa/s; convergence (divergence) emerges below (above) 500 hPa, with the strongest convergence of -3.8×10^{-5}/s at 850 hPa; ξ is positive throughout the extent, maximizing at 7.0×10^{-5}/s at 700 hPa, that all the conditions favor the occurrence of the research precipitation.

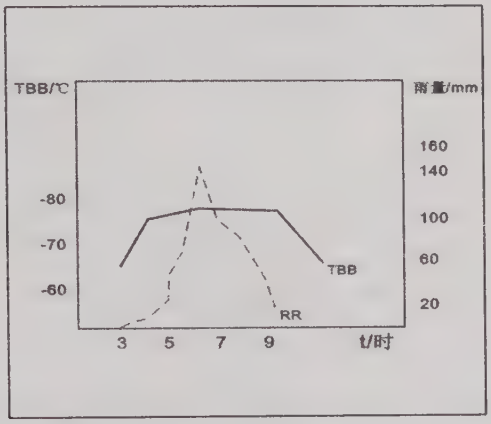

Fig. 2 Variation in the cloud-top T_{BB} (solid line) associated with the intensity of the rainfall on the morning of September 4, 1999

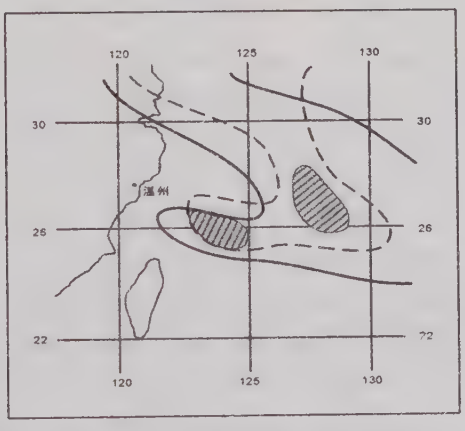

Fig. 3 Divergence and vorticity at 850 hPa and vertical velocities at 700 hPa level, with the high-value area denoted by full (dashed) lines for vorticity ξ (divergence *D*) and by shading for vertical motion ω, and their superimposition zone by slashed lines at 2000 BST, September 3, 1999

6.2 Energetics

The 850-hPa θ_{se} pattern on September 3 shows there to be a high-value energy zone in the southeastern coastal belt of Zhejiang, wherefrom vast amounts of energy are transferred landward on a continuous basis, leading to a remarkable strong-gradient area of θ_{se} around Wenzhou (Fig. 4). The relation between the energy front and typhoon precipitation has been addressed by a lot of researchers, stating that both are positively correlated (Ye and Gu, 1993), implying the stronger the energy front, the heavier the rainfall. The project rainstorm fell just in the strong energy front of θ_{se}, as our analysis shows.

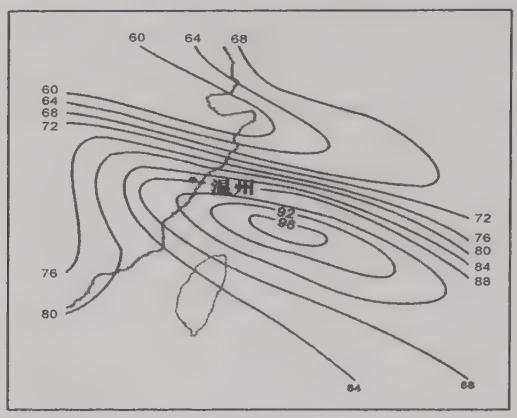

Fig. 4 850 hPa θ_{se}. Otherwise as in Fig. 3

6.3 Vapor

The inverted trough rainstorm related to strong plentiful vapor transport coming largely from Okinawa to the east, thus falling into a category of "dependence on eastern vapor source", with a high-value vapor flux tongue both at 850 and 700 hPa, which peaks at 120 g/hPa cm s around Okinawa to the northeast of the Taiwan Isle.

Additionally, a high-value convergence zone (central value of -200×10^{-5}g cm hPa) of vapor flux divergence in the easterly direction of the Isle. The convergence region corresponded better to easterly jets, suggesting the connection with the low-level disturbance of the easterlies (see Fig. 5).

6.4 Easterly jetstream

Under the joint effects of the landing TS9909 and the subtropical high, there was a vigorous easterly jet stream at lower levels from the southeast Wenzhou to the Taiwan Isle, responsible for the formation and maintenance of the cloud cluster of torrential rains. The low-level easterly did not begin to change into southerly jets gradually till 0800 BST of day 4. The actual situation show that the SE wind high cores are generally 14 - 16 m/s in the middle and lower troposphere, with winds stronger at 850 than at 700 hPa, suggesting that the vapor passage was lower in location, and *in situ* observations also indicate that middle-level (700 hPa) cloud transfer is pronounced, with maximal winds <20 m/s, a situation that favors the occurrence of the heavy rain (Fig. 6).

Over the synoptic-scale low-level jets, there were intense wind centers of meso disturbance, propagating downstream to the upwind side of the heavy-rain cloud cluster to produce significant convergence of mass there, leading to vigorous rising motion that triggered not only the generation of rainstorm cloud cluster but favored its reinforcement as well.

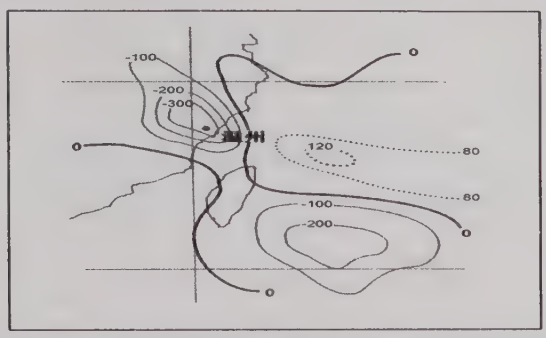

Fig. 5 Divergence of vapor fluxes at 500 (full line) and 850 hPa vapor fluxes (dashed line) at 2000 BST, September 3, 1999

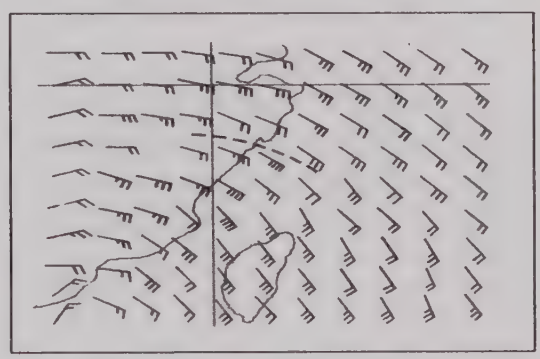

Fig. 6 850 hPa flowfield at the same time as in Fig. 5

Subsequent to 2000 BST, day 3, the subtropical high extended west and the inverted trough moved north, a situation that made the triggering zone around Okinawa traveling westward and the meso disturbance gale zone to the northeast of the Taiwan was amplified, migrating downstream. The above analysis shows that the abundant water supply and powerful dynamic mechanism for triggering available allowed the strong meso-scale convective cloud cluster to develop at rapidity and stay almost motionless over the Wenzhou region, leading finally to the precipitation event so strong that it fell into a kind of heavy rains occurring nearly in a 100-year return period.

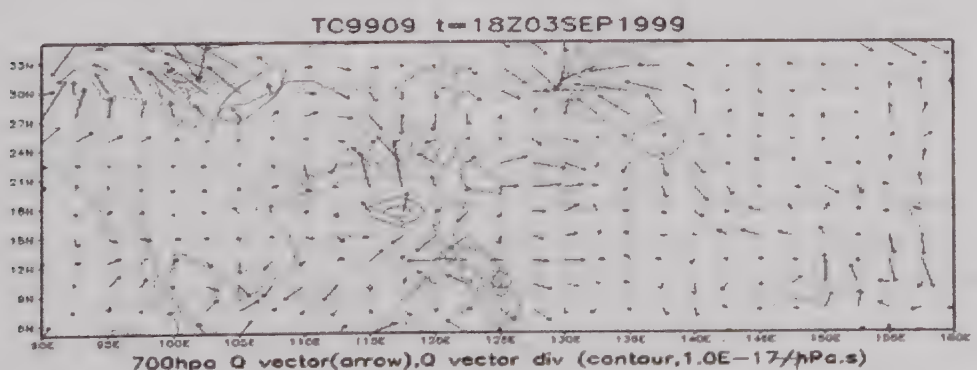

-Fig. 7 Distribution of 700-hPa Q vector divergence at 0200 BST, September 4, 1999

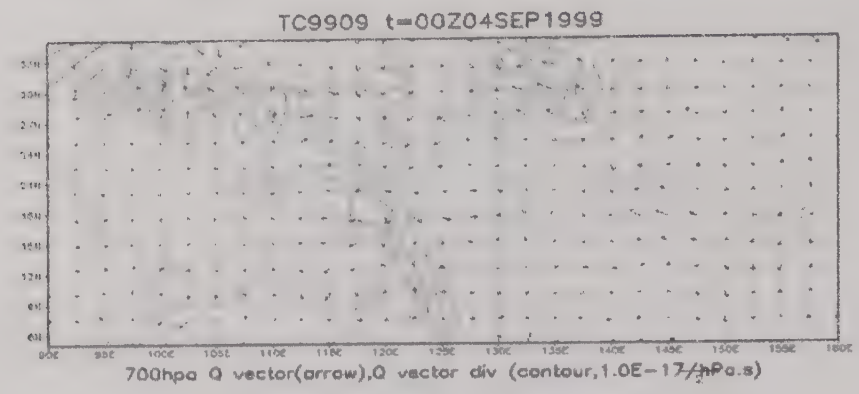

Fig. 8 As in Fig. 7 but for 0800 BST

Fig. 7 shows that a 700 hPa strong convergence zone of the divergence to be in the Zhejiang – Fujian border, with a zone of gradients of the divergence in northern Fujian. As time went on, the convergence zone and gradient area of Q vector divergence moved northward (approximately) along the coastline (Fig. 8), meaning that the Wenzhou region underwent at that time interval the development of strong Q vector divergence and gradients, in good coincidence with the recorded precipitation occurrence time and order of rainfall magnitude.

7 Conclusion

From the foregoing analysis we come to the following conclusions:

1) Strong rainfall hitting southeastern Zhejiang in autumn (September and October) may be caused by far-away typhoons landing south of Xiamen to eastern Guangdong that follow tracks towards the NW or NNW.

2) The warm, wet shear – related meso convective cloud cluster in the typhoon inverted trough has its genesis/dissipation answerable entirely for the evolution of exceptionally torrential rains, and the shear line plays a role in markedly increasing the rainfall, responsible for the explosive development of the event with amount in excess of 300 mm locally.

3) As shown in the element fields, the project precipitation is associated with the zone of instability triggering and high-value vapor flux in the vicinity of Okinawa in conjunction with meso disturbance gale core to the eastly of the Taiwan Isle, and under the joint impacts of the westward-extending subtropical high and north-moving inverted trough (Liu, 1998), these features meet together in the high-value energy gradient region where they develop vigorously and are maintained, resulting finally in the strong precipitation that would happen in a 100-year return period on a statistical basis.

4) From the used MM5V2 and Q-vector calculated NCEP data, we obtain the distribution of Q vector divergences, indicating good correspondence of the time and order of the rainfall with the development of intense Q vector divergence gradient at the time interval over the Wenzhou region.

Acknowledgement

This work is sponsored jointly by the Natural Science Foundation of China (Grant 4040950009; 402050084) and the Project of Planned National Key Basic Research/Development (2004CB418301).

Reference

[1] Fan Yongqiang, Chen Lianshou, Xie Yiyang et al. Operational Experiments with Typhoons and Theoretical Research in Typhoon Synoptic Dynamics [M]. Beijing: China Meteor. Press, 1996, 67 - 69.

[2] Ki Guida. Judgement of rainstorm intensity from the vertical shearing of low-level jets [J]. Zhejiang Meteor. Sci./Tech. 1997,18 (4), 53 - 55.

[3] Lin Ailan, Ding Weiyu, Qi Wanlin et al. Distribution and variation of mesoscale precipitation of tropical cyclones [J]. Meteorology, 2004, 30 (10), 17 - 18.

[4] Liu Huanzhu. The status and outlook of typhoon rainstorm weather forecasting [J]. Meteorology, 1998, 24 (7), 5-9.

[5] Lou Liyin, Huang Kehui, Zhang Yiquan. Analysis and prediction of intense rainfall from the outer-zone of typhoons in autumn [J]. Zhejiang Meteor. Sci and Tech, 2003, 21 (3), 15 - 16.

[6] Xu Xiangchun, Hao Liqing, Weng Xiaofang. Analysis of the track and precipitation of the severe tropical storm KONI coded as 0308 [J]. Meteorology, 2004:30 (11), 17 - 18.

[7] Ye Zhixiang, Gu Fengming. Analysis of frontal physical fields of landing typhoon as well as diagnosis of precipitation related to Typhoons coded as 05, 12 and 18 in 1990 [C]. in Collection by the Sci./Tech. Association of Wenzhou, 1993, 77 - 79.

[8] Zhang Jingzhen, Hou Shumei, Zhang Hongwei, et al. Impacts of interactions among midlatitude systems upon the heavy rain over Shangdong in August of 1998 [J]. Meteorology, 2000, 6 (5), 36 - 39.

温州“9.4”台风倒槽特大暴雨分析

郑 峰

（1. 中国气象科学研究院，北京 100081；2. 南京信息工程大学，江苏 南京 210044；3. 温州市气象局，浙江 温州 325027）

摘 要：运用 T106 数值预报产品、MM5模式结合Q矢量计算NCEP资料、天气实况及卫星云图等非常规资料，对1999年9月4日凌晨在远离9909号热带风暴中心的浙江省温州市引发的特大暴雨进行了探讨。发现秋季在厦门以南至广东东部登陆的台风，在浙中南沿海形成台风倒槽，该倒槽内的暖湿切变线的中尺度对流复合体（Mesoscale Convective Complex，MCC）是引起特大暴雨的重要条件。从计算得出的Q矢量散度分布看，本次特大暴雨降水发生时间和量级与该时段内温州经历的强Q矢量散度梯度发展有密切联系。同时，温州呈东北 — 西南走向的海岸线及境内雁荡山脉有利地形的抬升作用，对本次热带风暴倒槽降水中局地特大暴雨的形成有重要贡献。

关键词：远距离台风暴雨；台风倒槽；中尺度对流复合体（MCC）；Q矢量散度梯度

Horizontal Distribution and Annual Variations of Fecal Coliform Bacteria in Luoyuan Bay

CAI Lei-ming

1. *Fuzhou Marine Environmental Monitoring Station, Fuzhou* 350026, *Fujian Province, China;*

2. *Fuzhou Ocean and Fisheris Technology Center, Fuzhou* 350026, *Fujian Province, China*

Abstract: Fecal Coliform Bacteria (FCB) of marine waters was monitored in Luoyuan Bay from January, 2003 to December, 2005. The results showed that number of FCB in marine water samples ranged from no detection (<2 cfu/100 mL) to 540 cfu/100 mL in Luoyuan Bay. Values of FCB during August to October were significantly higher than those during January to April during three year period. Monthly changes of FCB values at each year period were mainly due to monthly precipitation. In addition, compared with FCB values in difference sample sites, values of FCB in Bay-head were significantly higher than those in middle of bay and Bay-mouth, Luoyuan Bay. However, values of FCB in Bay-mouth were significantly less than those in middle of bay. The ratios to the par of FCB in 2003, 2004, and 2005 years were 100%, 98.0%, and 97.9%, respectively. Therefore, we considered that the pollution of FCB of surface marine water in Luoyuan Bay was not serious.

Keywords: Luoyuan Bay; fecal coliform bacteria; horizontal distribution; annual variations

1 Introduction

Fecal Coliform Bacteria (FCB) and Coliforms group are the most important indicators in hygienic and epidemiology, used to assess the effects of sewage-holding water body [1]. Coliforms group have four Wikipedia including Escherichia, Citrobacter, Enterobacter, and Klebsiella. Citrobacter, Enterobacter, and Klebsiella could come from natural soils, sediments, waters, and feces [2]. However, Escherichia only come from feces, but FCB does not accumulate and persist in natural water bodies. Because Citrobacter, Enterobacter, and Klebsiella could come from nature waters, Coliforms group could not investigate feces pollution [3]. Therefore, FCB acts as a good indicator in WHO, ISO, world water quality automatic monitoring system, and many countries. In China, Coliforms group was changed into FCB in Integrated wastewater discharge Standard (GB 8978-1996) and Environmental quality standards for surface water (GHZB1-1999), showed data of standard. The changes could be effective to assess the effects of sewage-holding water body [5]. Some studies have reported FCB in freshwater body in China, but a few studies in the coast sea. FCB were investigated in Bohai and Yellow Sea coast [6], the coastal area of Liaodong Bay [7, 8], and the seacoast of Zhejiang Province [9]. However, frequency of investigations was very low and periodicity of investigation was not integrity. Because the lifetime of FCB in marine water is

Received on April 9, 2008

Corresponding author: caileiming@21cn.com

1-2 day and very short compared with other bacteria [10], these investigations could not show the pollution of PCB in this sea area. Therefore, integrated and periodic investigation of FCB should be necessarily in sea region.

The Luoyuan Bay locates in eastern Fujian province (26°25′N, 119°43′E), which is surrounded by hills with a large internal sea area and a narrow mouth. Its area is approximately 206.2 km^2. The water body exchanges mainly depend on the tidal current. The Luoyuan Bay is not only a main harbor in Fujian Province, but also an important marine aquaculture base. In recent years, with the increasing of human activities, the marine water in this region was serious polluted. To understand the marine water quality in Luoyuan Bay polluted by sources on land and cultured in cages, the FCB pollution in Luoyuan Bay, the long-term data of FCB were collected during the period from January 2003 to December 2005.

2 Material and method

2.1 Study site and sampling

Fig. 1 showed four sampling sites, including 1#, 2#, 3#, and 4# sites in the Luoyuan Bay. The 1# , 2#, 3#, and 4# site were located in the Luoyuan Bay mouth, the Gangyu marine cage culture area, the middle of Luoyuan Bay, and Luoyuan Bay-head, respectively. For data of sample were continuous and comparison and according to tide changes, twice times per month were sampled from 2003 to 2004, the sampling time was at height term of spring tide. However, one time per month were investigated in 2005.

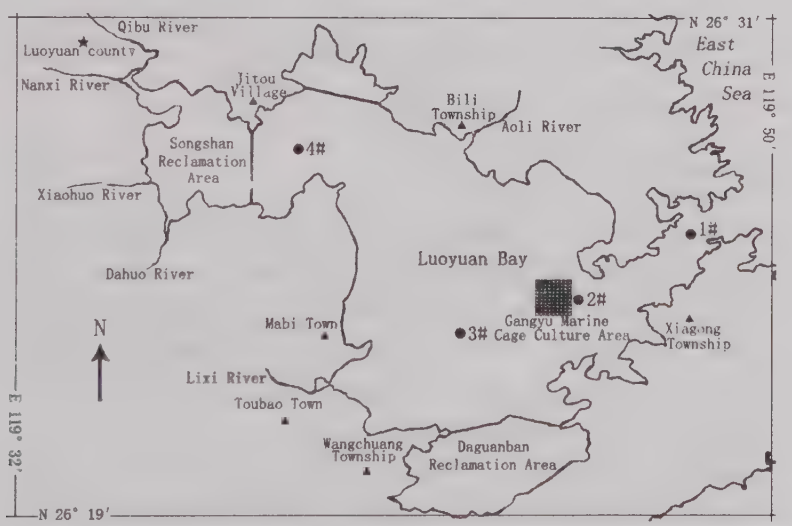

Fig. 1 Sampling sites in Luoyuan Bay

2.2 Methods

100 mL samples were collected below the surface (0.5 m - 1 m) using sterile glass bottles and stored at 4 °C, then delivered to a laboratory for bacterial analyses. The measurement of FCB was based on the

National Standard of PRC (GB17378.7-1998)[11], which was issued by the State Quality and Technical Supervision Administration. The data of FCB per 100 mL for water samples were calculated based on most probable number (MPN).

2.3 Referenced standard

The survey results were evaluated by the Third class (FCB≤200cfu/100mL) of Sea Water Quality Standard (GB 3097-1997).

3 Results

3.1 FCB in the sea samples

During the period of the 3-year investigation, FCB of 248 seawater samples were determined in Luoyuan Bay. The concentration of FCB in Luoyuan Bay ranged from no detection (<2 cfu / 100 mL) to 540 cfu / 100 mL with an average of 16.6 cfu / 100 mL (Tab. 1). The concentrations of FCB in 196 samples were more than the minimum detection limit, and monitored ratios were 79.0%. The concentrations of FCB in 52 samples were less than the minimum detection limit (14 samples at the 1# and 3# site, 15 samples at the 2# site, and 9 samples at the 4# site). The seawater samples with less than 200 cfu / 100 mL FCB were 248, the ratio was 98.8%. The concentrations of FCB in 3 samples were more than 200 cfu / 100 mL, which exceeded the Third class (FCB≤200 cfu / 100 mL) of Sea Water Quality Standard (Tab. 1). The concentrations of FCB at 2# and 3# site on Sept 16, 2004 and at 4# site on Oct 8, 2005 were 350 cfu / 100 mL, 240 cfu / 100 mL, and 540 cfu / 100 mL, respectively.

3.2 The time changes of FCB in seawater samples

3.2.1 The month changes of FCB values

The monthly average concentrations of FCB in seawater samples were from 0.25 to 156.5 cfu / 100 mL in Luoyuan Bay during the period of investigation (Fig. 2). In 2003, the monthly average concentrations of FCB (0.25 to 27 cfu / 100 mL) were relative low. The minimum value was observed in March, while the maximum value in August. In addition, the concentrations of FCB were relative low in July and October. FCB value dropped in July, and peaked in August, then decreased in the winter. In 2004, the monthly average concentrations of FCB were from 3.12 to 81.75 cfu / 100 mL. The maximum value was measured in September, while the minimum value in April. In other month, the concentrations of FCB were from 3.12 to 18.63 cfu / 100 mL. In 2005, the monthly average concentrations of FCB were from 2.5 to 156.5 cfu / 100 mL. The minimum value was determined in January, while the maximum value in October. The monthly average concentration of FCB in October was 156.5 cfu / 100 mL and was the maximum value during the three years period of investigation. In addition, the relative low values were observed in May and July, while the relative high values in November.

The monthly average concentrations of FCB at different sites were showed in Figs. 3 - 6. The

monthly average concentrations of FCB at 1# sites were from no detection to 49 cfu / 100 mL and were relative low during the three years period (Fig. 3). The changes of monthly average values were not significant. In 2003, the monthly average concentrations of FCB at 1# sites were from no detection (<2 cfu / 100 mL) to 28 cfu / 100 mL. The three peaks were observed in April, May and September, respectively. However, the minimum value was observed in March and October. In 2004, the monthly average concentrations of FCB at 1# sites were from no detection to 37 cfu / 100 mL. The minimum value was observed in October, while the maximum value in February. In 2005, the monthly average concentrations of FCB at 1# sites were from no detection to 49 cfu / 100 mL. The minimum value was observed in March, while the maximum value in November.

Tab. 1 FCB in marine waters in Luoyuan Bay

Time	1#	2#	3#	4#	Time	1#	2#	3#	4#
2003.01.06	<2	<2	2	<2	2004.04.06	<2	2	<2	8
2003.01.20	<2	2	2	<2	2004.04.22	2	3	2	8
2003.01.28	5	5	5	33	2004.05.08	5	5	2	7
2003.02.18	2	2	2	11	2004.05.21	8	4	2	11
2003.03.05	<2	<2	<2	<2	2004.06.07	4	2	5	8
2003.03.20	<2	<2	<2	2	2004.06.21	<2	4	2	2
2003.04.04	49	11	5	17	2004.07.05	2	<2	2	11
2003.04.18	5	<2	2	11	2004.07.19	5	14	32	2
2003.05.07	5	5	2	2	2004.08.03	14	40	12	40
2003.05.19	49	49	8	79	2004.08.18	7	5	<2	2
2003.06.02	2	5	<2	<2	2004.09.02	<2	5	11	17
2003.06.16	8	5	17	49	2004.09.16	4	350	27	240
2003.07.02	5	<2	2	2	2004.10.01	<2	79	13	17
2003.07.17	2	<2	<2	2	2004.10.16	<2	2	2	5
2003.07.31	5	<2	2	<2	2004.11.01	<2	5	2	5
2003.08.15	<2	49	<2	11	2004.11.15	2	8	13	5
2003.08.29	8	5	94	49	2004.11.30	3	7	7	11
2003.09.15	7	8	14	11	2004.12.15	5	5	17	17
2003.09.28	49	<2	<2	5	2004.12.29	3	7	11	22
2003.10.13	<2	5	2	2	2005.01.10	2	<2	8	<2
2003.10.27	<2	5	2	5	2005.02.04	2	<2	8	22
2003.11.11	2	2	<2	<2	2005.03.14	<2	5	5	49
2003.11.26	5	31	79	8	2005.04.11	5	5	5	8
2003.12.11	17	22	27	17	2005.05.10	5	49	13	49
2003.12.26	17	5	<2	8	2005.06.09	5	<2	2	8
2004.01.09	70	26	17	17	2005.07.08	4	79	8	14
2004.01.16	4	8	2	5	2005.08.08	4	17	<2	5
2004.02.09	4	2	<2	<2	2005.09.06	13	8	2	2
2004.02.25	2	<2	<2	33	2005.10.08	7	<2	79	540
2004.03.08	2	5	<2	<2	2005.11.04	49	33	49	79
2004.03.23	2	23	2	8	2005.12.02	5	<2	5	15

The monthly average concentrations of FCB at 2# sites were from no detection to 178 cfu / 100 mL during the three years period (Fig. 4). In 2003, the monthly average concentrations of FCB at 2# sites were no detection to 27 cfu / 100 mL. The two peaks were observed in May and August, while the minimum value in March. In 2004, the monthly average concentrations of FCB at 2# sites were no detection to 178 cfu / 100 mL. The three peaks were observed in August, September, and October, while the minimum value in February. In 2005, the monthly average concentrations of FCB at 2# sites were no detection to 79 cfu / 100 mL. The three peaks were observed in May, July, and November, moreover the maximum value in July. In addition, low month average values at 2# sites were observed in January, February, June, October, and December.

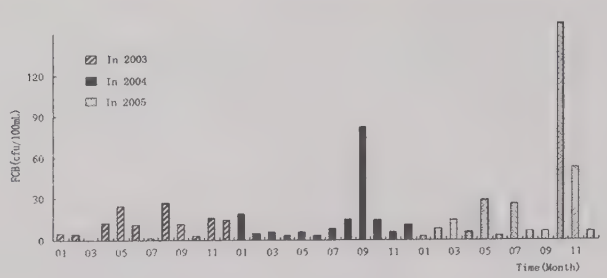

Fig. 2 Monthly changes of FCB values in Luoyuan Bay

The monthly average concentrations of FCB at 3# sites were from no detection to 47cfu / 100 mL during the three years period (Fig. 5). In 2003, the monthly average concentrations of FCB at 3# sites were no detection to 100 cfu / 100 mL. The two peaks were observed in August and November, moreover the maximum value in August. However, the minimum value was observed in March. In 2004, the monthly average concentrations of FCB at 3# sites were no detection to 19 cfu / 100 mL. The changes of monthly average values at 3# sites were not significant in 2004. The minimum value was observed in February, while the maximum value in September. In addition, the month average value in July was relative high. In 2005, the monthly average concentrations of FCB at 3# sites were no detection to 79 cfu / 100 mL. The minimum value was observed in August, while the maximum value in October. In addition, the month average value in November was relatively high.

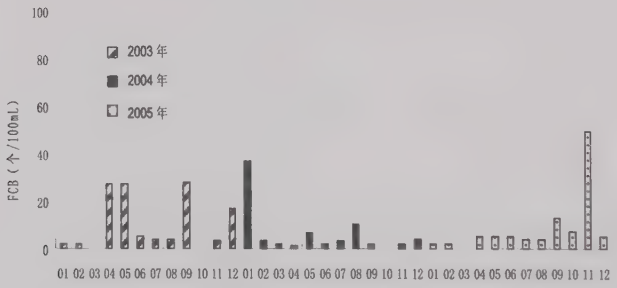

Fig. 3 Monthly changes of FCB values in 1# site

The monthly average concentrations of FCB at 4# sites were from no detection to 540 cfu / 100 mL during the three years period of investigation (Fig. 6). The changes of monthly average values at 4# sites were significant during three years period. In 2003, the monthly average concentrations of FCB at 4# sites were no detection to 40.5 cfu / 100 mL. The two peaks were observed in May and August, moreover the maximum value in May. However, the minimum value was observed in March. In 2004, the monthly average concentrations of FCB at 4# sites were no detection to 128.5 cfu / 100 mL. The maximum value was observed in September, while the minimum value in February. In 2005, the monthly average concentrations of FCB at 4# sites were no detection to 540 cfu / 100 mL. The maximum value was observed in October and the highest values at four sites during the three years period of investigation.

However, the minimum value was observed in January.

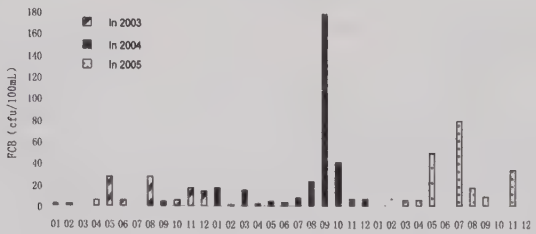

Fig. 4 Monthly changes of FCB values in 2# site

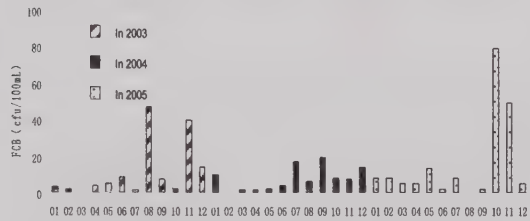

Fig. 5 Monthly changes of FCB values in 3# site

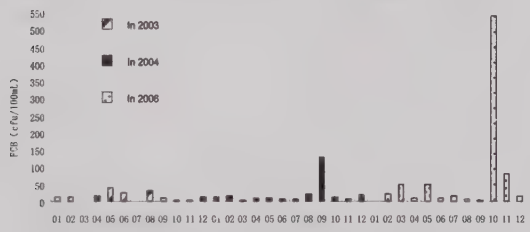

Fig. 6 Monthly changes of FCB values in 4# site

3.2.2 Annual Changes of FCB

The annual average concentrations of FCB at the four sites were shown in Fig. 7 in Luoyuan Bay during the three years period of investigation. The annual average concentration of FCB at 1# sites in 2003 (9.93 cfu / 100 mL) was the highest, while the minimum value (8.42 cfu / 100 mL) in 2004. In addition, the median value (6.1cfu / 100 mL) was observed in 2005. The annual average concentration of FCB at 2# sites have been observed during the three years period of investigation. The results showed that the value in 2004 (25.18 cfu / 100 mL) > that in 2005 (16.33 cfu / 100 mL) > that in 2003 (8.99 cfu / 100 mL). The changes of annual average concentrations of FCB at 3# sites were the value in 2005 (15.33cfu/100mL) > that in 2003 (11.03 cfu / 100 mL) > that in 2004 (7.32 cfu / 100 mL). In addition, the annual average concentrations of FCB at 4# sites were increased with time increasing. The annual average concentrations of FCB at 4# sites in 2003, 2004, and 2005 were 13.44 cfu / 100 mL, 20.58 cfu / 100 mL, and 65.98 cfu / 100 mL, respectively. These results showed that the changes of annual average concentrations of FCB at different sites were different. However, the annual average concentrations of FCB in Luoyuan Bay were increasing with time increasing during the three years period of investigation.

The annual average concentrations of FCB in Luoyuan Bay n 2003, 2004, and 2005 were 10.9 cfu / 100 mL, 15.3 cfu / 100 mL, and 26.5 cfu / 100 mL, respectively.

3.3 Horizontal distribution of FCB

The horizontal distribution of FCB in Luoyuan Bay was shown in Fig. 7. In 2003, the order of the annual average values of FCB was 4# sites higher than 3# sites higher than 1# sites higher than 2# sites. In 2004, the order of the annual average values of FCB was 2# sites higher than 4# sites higher than 3# sites higher than 1# sites. In 2005, the order of the annual average values of FCB was 4# sites higher than 2# sites higher than 3# sites higher than 1# sites. The concentrations and annual average values of FCB in four sites in Luoyuan Bay were shown in Tab. 1 and Fig. 4. At 1# sites, the concentrations of FCB were from no detection to 70 cfu / 100 mL. The minimum value was 8.15 cfu / 100 mL at bay during the three years period of investigation. At 2# sites, the concentrations of FCB were from no detection to 350 cfu / 100 mL. The average value of FCB was 16.83 cfu / 100 mL during the three years period of investigation. At 3# sites, the concentrations of FCB were from no detection to 94 cfu / 100 mL. The average value of FCB was 11.23 cfu / 100 mL during the three years period of investigation. At 4# sites, the concentrations of FCB were from no detection to 540 cfu / 100 mL. The maximum value of FCB was 33.31cfu / 100 mL at bay during the three years period of investigation.

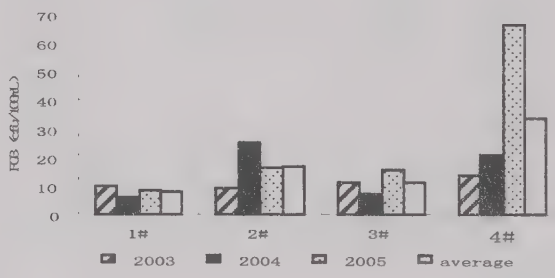

Fig. 7 Horizontal distribution and variation of FCB in Luoyuan Bay

4 Discussion

4.1 The changes of the concentrations of FCB in seawater samples

The values of FCB in seawater samples at 1# and 3# sites were less than that of the Third class in Sea Water Quality Standard (FCB≤200 cfu / 100 mL) (GB 3097-1997) during three years period of investigation. The detection rate of the FCB in seawater samples at four sites during the three years period of investigation was 79.0%. The concentrations of the FCB in 1.2% seawater samples at four sites during the three years period were more than 200 cfu / 100 mL (the Third class in Sea Water Quality Standard). The concentrations of FCB in Luoyuan Bay were compared with those of other sea regions in Tab. 2. The concentrations, detection rates, and excess Standard rates of FCB in Luoyuan Bay were less than those in the Bohai and Yellow Sea coast, Liaodong Bay and the seacoast of Zhejiang Province.

These results showed FCB pollutions in Luoyuan Bay were not serious.

Tab. 2 Comparison of FCB in marine waters in different coastal areas (China)

Sea area	Bohai and Yellow Sea coast [6]	Liaodong Bay [7, 8]	the seacoast of Zhejiang Province [9]		Luoyuan Bay
Year	1997 - 1998	2002	1998		2003 - 2005
Month	May, October, November, December	May, August, October	May, June, September, October		Every month
Level	Surface layer	Surface layer	Surface layer	bottom layer	Surface layer
Sample number	16	13	60	60	248
FCB / cfu / 100 mL	<4~ > 4800	<2~ > 2400	2 - 540	2 - 540	<2 - 540
rates of detection	93.7%	84.6%	100%	100%	79.0%
exceed Standard rates	43.7%	46.2%	9.78%	8.35%	1.2%

4.2 Relation of the concentrations of FCB and precipitation

The results of investigation showed that there was a relationship between time changes of FCB in Luoyuan Bay and changes of precipitation. May in Fujian Province is rain season. In addition, typhoon and other factors effects raining, therefore another raining season in Fujian Province is from July to September[12]. The runoffs in Luoyuan Bay were increasing because there are rains in May and from July to September. Therefore the concentrations of FCB are increasing with the runoffs in rivers increasing. The peaks of the concentrations of FCB were observed in May and from July to September, which were rain season. In May, 2003 and 2005, there were two peaks of the concentrations of FCB in Luoyuan Bay (Tab. 1 and Fig. 3). The values of FCB in 2003 and 2005 were 24.9 cfu / 100 mL and 29 cfu / 100 mL, respectively. However, the precipitation in Fujian Province in 2004 was 295.36 mm, and it was significantly decreasing, so the concentrations of FCB in May, 2004 in Luoyuan Bay were 5.5 cfu / 100 mL and less than those in other years. The precipitations in August, 2003, September, 2004, and July, 2005 were significantly increasing, therefore the peaks of the concentrations of FCB in Luoyuan Bay were observed in those times. In addition, on September 7-10 and 14-17, 2004, there were two continuous storm periods in the seacoast of Fujian Province. The average concentration of FCB was 8.3 cfu / 100 mL September 2, 2004 ago. However, the average concentration of FCB was 155.3 cfu / 100 mL after September 16, 2004. Because Longwang typhoon cause the increasing of precipitation and flood disaster in October, 2005, therefore the month average concentrations of FCB significantly increased and there was a highest peak in March, 2005. In addition, the low concentrations of FCB in Luoyuan Bay were observed in March, July, and October, 2003, in April, June, 2004, and in June, 2005 because the precipitations were very low.

The time changes of the concentrations of FCB at four sites in Luoyuan Bay were determined in Fig. 3, 4, 5, and 6. According to the relationship between month changes of FCB and changes of precipitations, we found that the month changes of FCB at 1# sites were very small. Because 1# site was located far from the land, so the effect of precipitation was low. Moreover, the month changes of FCB affect by the changes of precipitations. In addition, effects in changes of FCB at 4# sites were very serious. The maximum values of FCB at 4# sites were observed when the maximum precipitations occurred. The main pollution source of FCB is discharge of land-based pollutants into sea, whereas, discharging into sea is also the main treatment method of land-based pollutants. Therefore, the major effect factor of FCB in

Luoyuan Bay was precipitation.

4.3 Annual average changes of FCB

The annual average concentrations of FCB in Luoyuan Bay undergo a time-dependent increase from 2003 to 2005. The annual average concentration of FCB in Luoyuan Bay in 2004 was 1.40 times of that in 2005. The annual average concentration of FCB in Luoyuan Bay in 2005 was 1.73 times of that in 2004. The concentrations of FCB in September, 2004 and October, November, 2005 in Luoyuan Bay significantly increased when the precipitations significantly increased. The average values of FCB in the three months were 81.75 cfu / 100 mL, 156.5 cfu / 100 mL, and 52.5 cfu / 100 mL, respectively. These would cause the increasing of annual average concentrations of FCB. Therefore, significant increasing of annual average concentrations of FCB in 2004 and 2005 in Luoyuan Bay mainly due to the significant increasing of precipitations.

The annual average changes of FCB at four sites were shown in Fig. 7. The annual average changes of FCB at 1# and 3# sites were not significant. The annual average concentrations of FCB in 2003 and 2004 at 2# sites near to cage culture region were 8.99 cfu / 100 mL and 25.18 cfu / 100 mL, respectively. There was an increasing range of 180.1%. The annual average concentrations of FCB in 2003 and 2004 at 4# sites near to sewage drainage outlets of Songshan reclamation region were 13.44 cfu / 100 mL and 20.58 cfu / 100 mL, respectively. It was an increasing range of 53.1%. These results suggested that cage culture and sewage discharge into sea significantly increased pollution of seawater in Luoyuan Bay. Because activities of cage culture in 2005 significantly less than those in 2004, the concentration of FCB at 2# sites decreased in 2005. However, the concentration of FCB at other three sites in 2005 significantly increased by 2.97 times than those in 2004. These results suggested that land-based pollutants such as sewage drainage outlets of Songshan reclamation region caused the significantly increasing of sea water pollution in Luoyuan Bay. Therefore, the another major effect factor of the significant increasing of annual average values of FCB in Luoyuan Bay in 2004 and 2005 was the increasing of cage culture and land-based pollutants.

4.4 Horizontal Distribution of FCB

The effect factors of the horizontal distribution of FCB in seawater included tides, variation of coastal terrain, tidal flow direction, terrestrial pollution, distribution of coastal population, and human marine activities et al. The concentration of FCB at 1# site was the minimum of inner bay because terrestrial pollution was less and water flow exchanges were greater at this site. At 3# site, the concentration of FCB was relative small and only higher than that at 1# site. The 3# site locates at central waters of the Luoyuan Bay. There are Bili Town of Luoyuan County in north and Guanban and Mabi Town of Lianjiang County in south and west. Because the distance between 3# site and land is very far, the terrestrial pollution was less. At 4# site, it is located at abdominal sea region in Luoyuan Bay. Because the distance between the sea area and bay mouth is very far and water flow exchanges were not smooth, whereas, there was the biggest sewage drainage outlets of terrestrial pollution (sewage drainage outlets of Songshan

reclamation region). In addition, sewage and agricultural wastewater from Luoyuan County entry into Luoyuan Bay by Qibu Stream, Nanxi Stream, Xiaohuo Stream, and Dahuoxi Stream trough Songshan reclamation region. These pollutions caused the significant increasing of FCB at abdominal sea region in Luoyuan Bay. According to this investigation, the effect factors of the horizontal distribution of FCB included the distance of sea to land, pollutant discharge of marine cage culture, and discharge of land-based pollutants into sea. However, the major effect factor of the horizontal distribution of FCB was discharge of land-based pollutants into sea by river.

5 Conclusion

5.1 Pollution of FCB in seawater

The concentrations of FCB in Luoyuan Bay were from no detection (<2 cfu / 100 mL) to 540 cfu / 100 mL during the three year period. The annual average concentration of FCB at four sites was 16.6 cfu / 100 mL with a standard-reaching rate of 98.7%. These results showed that the pollution effects of domestic sewage on sea water in Luoyuan Bay were light and there was an good quality condition of sea water in Luoyuan Bay.

5.2 The Time Changes of FCB in seawater

The month average values of FCB in Luoyuan Bay were from no detection (<2 cfu / 100 mL) to 156.5 cfu / 100 mL during the three year period. The month changes of FCB in different month were significant. The maximum average value of FCB was 625 times of the minimum. The main effect factor of month average changes of FCB was different precipitation in different months. The annual average concentrations of FCB in Luoyuan Bay undergo a time-dependent increase during the investigation period. The major effect factor of the significant increasing of annual average values of FCB in Luoyuan Bay was the increasing of cage culture and land-based pollutants.

5.3 Horizontal Distribution of FCB

According to the investigated results, the concentration of FCB at bay mouth in Luoyuan Bay (1# site) was less than that at central sea area in Luoyuan Bay (3# site) and less than that at inner bay with marine cage culture in Luoyuan Bay (2# site) and less than that at abdominal sea area in Luoyuan Bay (4# site). According to this investigation, the effect factors of the horizontal distribution of FCB included the distance of sea to land, pollutant discharge of marine cage culture, and discharge of land-based pollutants into sea. However, the major effect factor of the horizontal distribution of FCB was discharge of land-based pollutants into sea by river.

Reference

[1] Jiang Xinxin. Uses Fecal Coliform Bacteria appraisal sea water bathing place water quality rank and the source of

pollution research [J]. Science and Technology of West China, 2005. 21: 25 - 26.

[2] Li Su-yu. Environment microorganism classification and examination technology [M]. Beijing: Chemical and Industral Publishing House, 2005.284-285.

[3] Yu Qing-fu. Moden Sanitary Microbiology [M]. Beijing: People's Medical Publishing House, 1995. 28 - 78.

[4] APHA, AWWA, WPCF. Standard methods for the examination of water and wastewater [M]. 15th ed.Baltimore, Maryland: Port City Press, 1985. 748 - 756.

[5] Wan Deng-bang, Qiu Chang-qiang, Ma Ning, et al. Assessment of urban water bodies centaimination using pollution indication bacteria [J]. Acta Hydrobiologica Sinica, 1994.18(4):341 - 347.

[6] He Jie, Lin Feng-ao, Bian Zheng-he, et al. Fecal coliform bacteria in shellfish and habiat in Bohai and Yellow Sea coast [J]. Marine Environmental Science, 2002. 21 (2): 42 - 46.

[7] Lin Feng-ao, Yu Zhan-guo, Liang Yu-bo, et al. The fecal coliform and total bacteria in shellfish in the coastal environment of Liaodong Bay [J]. Marine Environmental Science, 2004. 23 (3): 43 - 45.

[8] Fan Jing-feng, Song Li-chao, Zhang Xi-chang, et al. Distribution of hepatitis a virus and fecal coliform in the coastal area of Liaodong Bay [J]. Marine Environmental Science, 2004. 23(4): 35 - 37.

[9] Du Ai-fang. Bacterial analysis in the water samples from the seacoast of Zhejiang Province [J]. Journal of Zhejiang University (Agriculture & Life Sciences), 2003.(5): 523 - 528.

[10] Lessard E J, Siebuth J M. Survival of natural sewage populations of enteric bacteria in diffusion and batch chambers in the marine environment [J]. Appl. Environ. Microbiol. 1983. 45: 950 - 959.

[11] GB 17378.7 – 1998. The specification for marine monitoring Part7: Ecological survey of offshore pollution and biological monitoring [S]. Chinese Standard Publishing House, 1998. 59 - 65.

[12] Fujian Province meteorological bureau, Fujian Province meteorological observatory. Fujian Province climate bulletin in 2004. [EB] 2005.

罗源湾海水中粪大肠菌群的分布和年际变化

蔡雷鸣

（1. 福州市海洋环境监测站，福建 福州 350026；2. 福州市海洋与渔业技术中心，福建 福州 350026）

摘 要：本文于 2003 年 1 月到 2005 年 12 月对罗源湾海区表层海水中的粪大肠菌群数量和分布进行了调查监测。监测结果表明：罗源湾表层海水中粪大肠菌群的数量在<2 ～ 540 个/100 mL 之间，3 年中月平均高值出现在 8 到 10 月份，低值出现在 1 到 4 月份，几年平均值呈逐年递增。原因分析发现，影响湾内海水中 FCB 的月平均值数量变化的最主要因素是降水量。另外通过多点采样结果比较，发现罗源湾表层海水中 FCB 的空间分布呈现为：湾内腹海区>湾中间海区>湾口海区。通过国家海水水质标准（GB 3097 - 1997）对本次的调查监测结果进行评价，从 2003 年到 2005 年罗源湾海区海水中粪大肠菌群的达标率分别为 100%，98.0% 和 97.9%，表明罗源湾海区表层海水的 FCB 污染相对较轻。

关键词：罗源湾；粪大肠菌群；空间分布；时间变化

Three 5'-flanking Regions of *crt*O Encoding β-carotene Oxygenase in *Haematococcus pluvialis*

GAO Zheng-quan[1], MENG Chun-xiao[1], YE Nai-hao[2]*

1. School of Life Sciences, Shandong University of Technology, Zibo 255049, *Shandong, China*

2. Yellow Sea Fishery Research Institute, Qingdao 266071, *Shandong, China*

Abstract: Three separate 5'-flanking regions (1.1 kb, 1.9 kb and 2.2 kb) of *crt*O were cloned through walking upstream. Results of sequence analysis show that three 5'-flanking regions of *crt*O might have some similar putative *cis*-acting elements such as ABA (abscisic acid)-responsive element (ABRE), C-repeat/dehydration responsive element (C-repeat/DRE), light-responsive element (G-box, GAG-motif, I-box and ATC-motif), wound-responsive element (WUN-motif), auxin-responsive element (TGA-element), MeJA-responsive element (TGACG-element) and MYB binding site (MBS), except for typical TATA box or CCAAT box. These findings might mean diversiform regulatory patterns of *crt*O being in astaxanthin biosynthesis of *Haematococcus pluvialis*.

Keywords: astaxanthin; *cis*-acting elements: *crt*O; 5'-flanking region; *Haematococcus pluvialis*

Introduction

The ketocaronoid astaxanthin (3, 3'-dihydroxy-β, β-carotene-4, 4'-dione) is of great commercial interest due to its high price (approximately US $ 2 500 / kg). There is growing commercial interest in the biotechnological production of astaxanthin because of its antioxidative properties and the increasing amounts needed as supplement in the aquaculture of salmonoids and other seafood [1]. Under extreme environmental conditions, the unicellular green algae *Haematococcus piuvialis* accumulates secondary carotenoids, mainly astaxanthin esters, in cytoplasmic lipid vesicles up to 4% of its dry mass. It is therefore one of the preferred microorganisms for the biotechnological production of these antioxidative compounds [2].

The pathways of astaxanthin biosynthesis in *H. pluvialis* were elucidated by inhibitor studies [3], and most of the involved genes are cloned [4, 5]. The cellular localization and regulation of the enzyme β-carotene oxygenase in *H. pluvialis* that catalyzes the introduction of keto functions at position C-4 of the β-ionone ring of β-carotene and zeaxanthin were reported in previous studies [6]. Harker *et al.* (1997) also reported that *crt*O can function in cyanobacteria in conjunction with the intrinsic carotenoid enzymes to produce astaxanthin [7]. Recently, a 700 bp 5'-flanking region of *bkt* (encoding β-carotene ketolase) was cloned through walking upstream and a promoter-like region (-630/-308 bp) without typical TATA box and

Received on March 24, 2008

*Corresponding author: mengchunxiao@126.com

CCAAT box was characterized in *H. pluvialis* [8]. Moreover, a 919 bp 5'-flanking region of carotenoid hydroxylase gene including a promoter-like region (-378/-22 bp) without typical TATA box and CCAAT box was characterized in *H. pluvialis* based on the same method above [9]. However, much is still unknown about regulatory 5'-regions of *crt*O in astaxanthin biosynthesis from *H. pluvialis*. This research reported the cloning of three separate 5'-flanking regions (1.1 kb, 1.9 kb and 2.2 kb) of *crt*O in *H. pluvialis*.

1 Marterials and methods

Haematococcus pluvialis (strain 712) were grown in a liquid medium under a light density of 25 μmol photon m^{-2} s^{-1} (12h: 12h) at 25 °C [10]. A Universal GenomeWalker (Clontech, California, USA) kit was used to isolate 5'-flanking region of *crt*O gene. According to manufacturer's instructions, total genomic DNA was digested with four kinds of restriction endonucleases (*Dra* Ⅰ, *Eco*RⅤ, *Pvu*Ⅱ, *Stu* Ⅰ) respectively, then ligated with a GenomeWalker adaptor before used as each template for nested PCR. The adaptor primer AP1 (5'-GTAATACGACTCACTATAGGGC-3') provided by this kit and a gene-specific primer GSP1 (5'-GACTCGCGGGTTCAAGGCAGTGCAGACT-3') designed based on the data from GenBank No.X86782 were used in the primary PCR amplification. Moreover, the other nested adaptor primer AP2 (5'-ACTATAGGGCACGCGTGGT-3') and a nested gene-specific primer GSP2 (5'-GCAGGTGTTGACTTGCGCGCGCTGACTT-3') designed based on the same data as above were used in the secondary PCR amplification. The PCR product was cloned into TA vectors and sequenced by custom service of CA Sarray Co., Ltd. (Shanghai, China). Moreover, software ClustalX (1.81)[11] and Internet tool (http://bioinformatics.psb.ugent.be/webtools/plantcare/html/) [12] were used to perform sequence analysis including prediction of possible *cis*-acting elements.

2 Results and discussion

Using genome-walking method, three different fragments (No.AY820773, No.AY820774 and No.AY820775) were proved to be the part of the 5'-flanking regions of *crt*O according to the results of ClustalX (1.81) (Fig. 1). Computer analysis using *PlantCARE* for potential regulatory elements revealed that except for typical TATA box or CCAAT box, they might have some similar regulatory elements such as ABA (abscisic acid)-responsive element (ABRE), C-repeat/dehydration responsive element (C-repeat/DRE), light-responsive element (G-box, GAG-motif, I-box and ATC-motif), wound-responsive element (WUN-motif), auxin-responsive element (TGA-element), MeJA-responsive element (TGACG-element), and MYB binding site involved in light responsiveness (MBS). Nevertheless, the 1.9 kb 5'-region had its specific regulatory elements other than that of the 1.1 kb 5'-region such as elicitor-responsive element (EIRE), heat-shock element (HSE), and *cis*-acting element involved in cell cycle regulation (MSA-like), and the 2.2 kb 5'-region had its specific regulatory elements other than that of the 1.1 kb 5'-region such as elicitor-responsive element (EIRE), *cis*-acting element involved in salicylic acid responsiveness (TCA-element) and *cis*-acting element involved in cell cycle regulation (MSA-like). Further, C-repeat/DRE, ABRE, ERE, HSE, WUN-motif, GC-motif, MBS and TCA-element have also been

reported to be involved in stress-inductive gene expression of high plants [13 - 20]. Therefore, we conclude that there might be three separate 5′-UTRs with diverse regulatory patterns to regulate transcription of *crt*O in *H. pluvialis*.

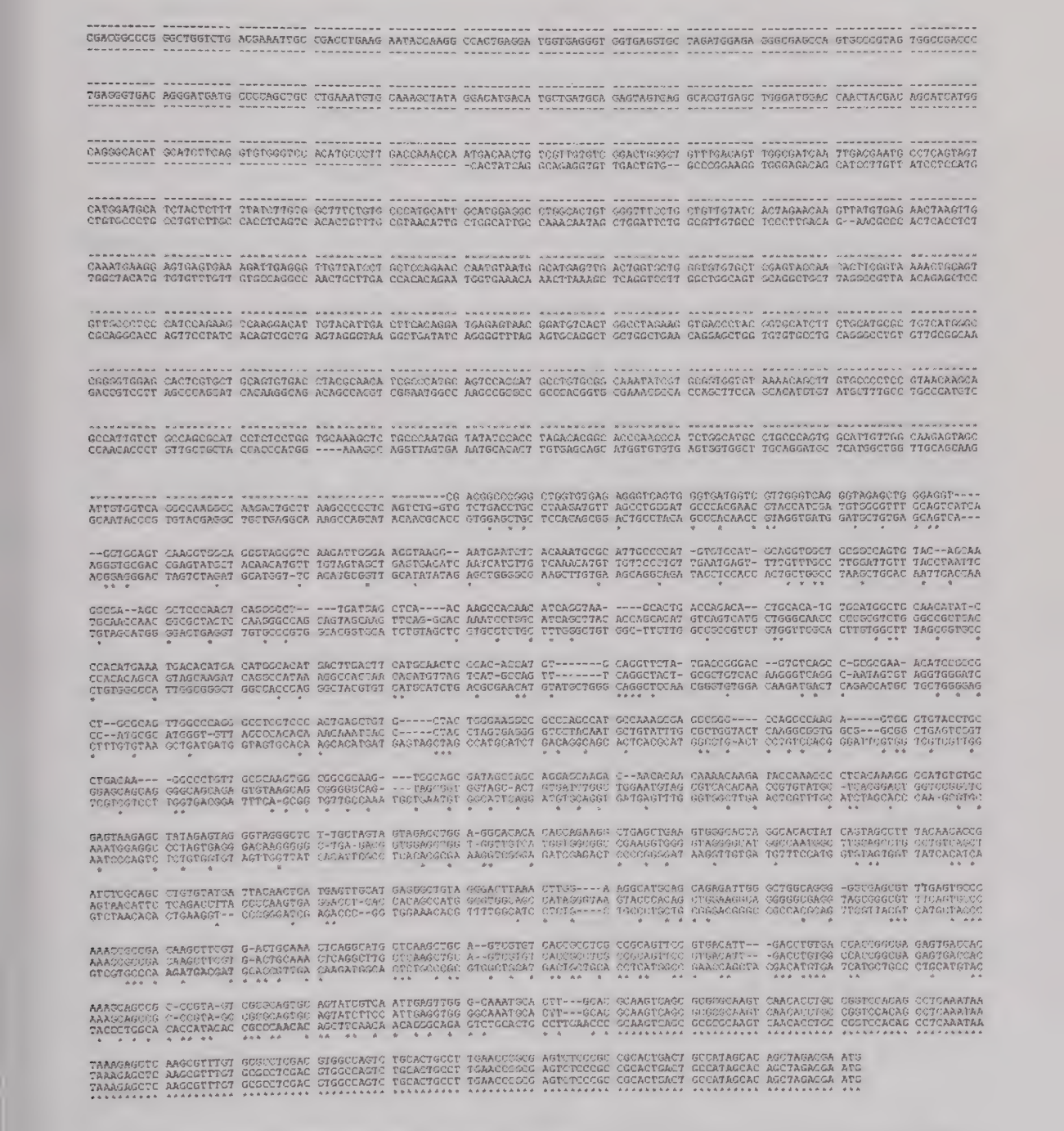

Fig. 1 Alignment of three separate 5′-flanking regions (1.1 kb, 1.9 kb and 2.2 kb) of *crt*O in *H. pluvialis*

(The information about ATG start codon is derived from the data in Genbank No. X86782.)

Two enzymes are involved in the biosynthesis of astaxanthin from β-carotene, β-carotene C-4 oxygenase (ketolase) and β-ring hydroxylase. β-carotene C-4 oxygenase mRNA levels have been shown to exhibit kinetics of induction during the first 4 days, but thereafter they declined by 50% of the maximum [21]. This behavior was different from the enzyme PDS that showed a parallel change in the amounts of mRNA and of the protein. Thus, besides regulation at the mRNA level, post-translational mechanisms seem to be involved in CRTO induction [6]. Moreover, two similar cDNAs were cloned from two different strains of *H. pluvialis* by Lotan and Hirschberg (1995) and Kajiwara *et al.* (1995) [22, 23]. In our previous studies, two separate 5'-flanking regions (1.5 kb and 2 kb) of β-ketolase gene were cloned through walking upstream in *H. pluvialis* [24]. Moreover, two separate 5'-flanking regions of IPP isomerase gene were cloned through walking upstream (no.AY786410 and no.AY786411). Furthermore, several human genes, e.g. human aldolase A, human estrogen receptor-α and human guanine nucleotide exchange factor (SGEF) had been reported to contain alternative promoters [25-27]. All these encode multiple mRNA species that differ in their 5'-UTRs. There are other reports suggesting the involvement of more than one promoter the transcription of the cathepsin B gene in mammalian cells [28, 29]. However, present study is the first one to demonstrate multiformity of 5'-UTRs in *crt*O transcription from *H. pluvialis*.

However, determining the precise contribution of a particular regulatory element to an expression profile is often complicated by the presence of multiple elements of different types in a given promoter. In conjunction with reporter gene assays, further studies are necessary to explore the interactions between these elements and their relevant environmental factors.

Acknowledgement

The research were supported by the National Natural Science Foundation (40706050; 40706048), Natural Science Foundation of Shandong University of Technology (4040306017) and Start-up Foundation for Ph.D of Shandong University of Technology (4041-405017; 4041-405016), National Key Technology R&D program(11200602), Foundation of State Commonweal Institute (2060402/2).

Reference

[1] Lotan R T, Cysewski G R. Commercial potential for *Haematococcus* microalgae as a subject: natural source of astaxanthin [J]. Trends Biotech, 2000, 18: 160 - 167.

[2] Boussiba S. Carotenogenesis in the green alga *Haematococcus pluvialis*: cellular physiology and stress response [J]. Physiol Plant, 2000, 108: 111 - 117.

[3] Harker M, Young A J. Inhibition of astaxanthin synthesis in the green alga, *Haematococcus pluvialis* [J]. Eur J Phycol, 1995, 30: 179 - 187.

[4] Sun Z, Francis X, Cunningham J, et al. Differential expression of two isopentenyl pyrophosphate isomerases and enhanced carotenoid accumulation in a unicellular chlorophyte [J]. Proc Natl Acad Sci USA, 1998, 95: 11 482 - 11 488.

[5] Linden H. Carotenoid hydroxylase from Haematococcus pluvialis: cDNA sequence, regulation and functional complementation [J]. Biochim Biophys Acta 1999, 1446: 203 - 212

[6] Grünewald K, Hirschberg J, Hagen C. Ketocarotenoid biosynthesis outside of plastids in the unicellular green alga *Haematococcus pluvialis* [J]. J Biol Chem 2001, 276: 6023-6029.

[7] Harker M, Hirschberg J. Biosynthesis of ketocarotenoids in transgenic cyanobacteria expressing the algal gene for β-C-4-oxygenase, *crtO* [J]. FEBS Lett, 1997, 404:129 - 134.

[8] Meng C X, Teng C Y, Jiang P, et al. Cloning and characterization of beta-carotene ketolase gene promoter in *Haematococcus pluvialis* [J]. Acta Biochem Biophys Sin, 2005, 37: 270 - 275.

[9] Meng C X, Wei W, Su Z L, et al. Characterization of carotenoid hydroxylase gene promoter in *Haematococcus pluvialis* [J]. Indian J Biochem Biophys, 2006b, 43: 284 - 288.

[10] Boussiba S, Vonshak A. Astaxanthin accumulation in the green alga *Haematococcus pluvialis* [J]. Plant Cell Physiol, 1991, 32: 1077-1082.

[11] Thompson J D, Higgins D G, Gibson T J. CLUSTAL W: improving the sensitivity of progressive multiple sequence alignment through sequence weighting, position-specific gap penalties and weight matrix choice [J]. Nucleic Acids Res, 1994, 22: 4 673 - 4 680.

[12] Lescot M, Dehais P, Thijs G, et al. PlantCARE: a database of plant *cis*-acting regulatory elements and a portal to tools for in silico analysis of promoter sequences [J]. Nucleic Acids Res, 2002, 30: 325 - 327.

[13] Barke S S, Wilhelm K S, Thomashow M F. The 5'-region of *Arabidopsis thaliana cor15a* has *cis*-acting elements that confer cold-, drought- and ABA-regulated gene expression [J]. Plant Mol Biol, 1994, 24: 701 - 713.

[14] Uno Y, Furihata T, Abe H, et al. *Arabidopsis* basic leucing zipper transcription factors involved in an abscisic acid-dependent signal transduction pathway under drought and high-salinity conditions [J]. Proc Natl Acad Sci USA, 2000, 97: 11 632 - 11 637.

[15] Ohem-Takagi M, Shinshi H. Ethylene-inducible DNA binding proteins that interact with an ethylene-responsive element [J]. Plant Cell, 1995, 7: 173 - 182.

[16] Newton E M, Knauf U, Green M, et al. The regulatory domain of human heat shock factor 1 is sufficient to sense heat stress [J]. Mol Cell Biol, 1996, 16: 839 - 846.

[17] Ni M, Cui D, Gelvin S B. Sequence-specific interactions of wound-inducible nuclear factors with mannopine synthase 2' promoter wound-responsive elements [J]. Plant Mol Biol, 1996, 30:77 - 96.

[18] Manjunath S, Saches M M. Molecular characterization and promoter analysis of the maize cytosolic glyceraldehyde 3-phosphate dehydrogenase gene family and its expression during anoxia [J]. Plant Mol Biol, 1997, 33: 97 - 112.

[19] Sugimoto K, Takeda S, Hirochik A H. MYB-related transcription factor NtMYB2 induced by wounding and elicitors is a regulator of the tobacco retrotransposin *Ttol* and defense-related genes [J]. Plant Cell, 2000, 12: 2 511 - 2 528.

[20] Goldsbrough A P, Albrecht H, Stratford R. Salicylic acid-inducible binding of a tobacco nuclear protein to a 10 bp sequence which is highly conserved amongst stress-inducible genes [J]. Plant J, 1993, 3: 563 - 571.

[21] Grünewald K, Eckert M, Hirschberg J, et al. Phytoene desaturase is localized exclusively in the chloroplast and up-regulated at the mRNA level during accumulation of secondary carotenoids in *Haematococcus pluvialis* (*Volvicales, chlorophyceae*) [J]. Plant Physiol, 2000, 122: 1 261 - 1 268.

[22] Lotan R T, Hirschberg J. Cloning and expression in *Escherichia coli* of the ketocarotenoid canthaxanthin in *Haematococcus pluvialis* [J]. FEBS Lett, 1995, 364: 125 - 128.

[23] Kajiwara S, Kakizono T, Saito T, et al. Isolation and functional identification of a novel cDNA for astaxantin biosynthesis from *Haematococcus pluvialis*, and astaxanthin synthesis in *Escherichia coli* [J]. Plant Mol Biol, 1995, 29: 343 - 352.

[24] Meng C X, Liang C W, Jiang P, et al. There are two 5'-flanking regions of *bkt* encoding beta-carotene ketolase in the *Haematococcus pluvialis* [J]. Phycologia, 2006b, 45: 218 - 224.

[25] Qi H, Fournier A, Grenier J, et al. Isolation of the novel human guanine nucleotide exchange factor Src homology 3 domain-containing guanine nucleotide exchange factor (SGEF) and of C-terminal SEGF, an N-terminally truncated form of SGEF, the expression of which is regulated by androgen in prostrate cancer cells [J]. Endocrinology, 2003, 144: 1 742 -1 752.

[26] Schuur E R, McPherson L A, Yang G P, et al. Genomic structure of the promoters of the human estrogen receptor-α gene demonstrate changes in chromatin structure induced by AP2γ [J]. J Biol Chem, 2001, 276: 15 519 - 15 526.

[27] Stauffer J K, Colbert M C, Ciejek-Baez E. Nonconservative utilization of Aldolase A alternative promoters [J]. J Biol Chem, 1990, 265: 11 773 - 11 782.

[28] Berquin I M, Sloane B F. Cathepsin B expression in human tumors [J]. Adv Exp Med Biol, 1996, 389: 281 - 294.

[29] Rhaissi H, Berchet D, Ferrara M. Multiple leader sequences for mouse cathepsin B mRNA [J]. Biochimie, 1993, 75: 899 - 904.

雨生红球藻中 *crt*O 基因存在 3 个 5'上游侧翼序列

高政权[1]，孟春晓[1]，叶乃好[2]

（1. 山东理工大学生命科学学院，山东 淄博，255049；2. 中国水产科学院黄海水产研究所，山东 青岛，266071）

摘 要：在本研究中，我们首次通过基因组上游第一次步移克隆到了雨生红球藻中 *crt*O 基因的 3 个不同大小的 5'上游侧翼序列 1.1 kb，1.9 kb 和 2.2 kb。利用生物信息学方法分别预测并比较了这 3 个不同大小的 5'上游侧翼序列，结果发现，三者具有与高等植物相类似的顺式作用元件，如脱落酸反应元件（ABRE）、干燥或低温反应元件（DRE/C-repeat）、几种光反应元件（G-box, GAG-motif，I-box and ATC-motif）、热激反应元件（HSE）、机械伤害反应元件（WUN-motif）、生长素反应元件（TGA-element）、茉莉酸甲酯反应元件（TGACG-element）和反式作用因子 MYB 蛋白的结合位点（MBS and MRE）等等，但是三者并不具有典型的 TATA 框和 CCAAT 框。上述研究预示了雨生红球藻虾青素合成中 *crt*O 基因调控方式的多样化。

关键词：虾青素；顺式作用元件；5'上游侧翼学列；雨生红球藻；*crt*O

Genetic Analysis of Five *Porphyra* Species by Isozyme Markers

SHEN Song-dong[1*], LI Yan-yan[1], XU Pu[2], ZHANG Mei-ru[3], YUAN Zhao-lan[1], WANG Jian-wei[1], ZHU Jian-yi[2]

1. *Life Sciences College, Suzhou University, Suzhou* 215123, *Jiangsu Province, China;*

2. *Department of Biology and Foodstuff Engineering, Changshu Institute of Technology, Suzhou* 215500, *Jiangsu Province, China;*

3. *Marine Fisheries Institute of Jiangsu, Nantong* 226007, *Jiangsu Province, China*

Abstract: Vertical polyamide gel electrophoresis was used to investigate isozyme polymorphisms among different isolates (including wild and cultivated) of *Porphyra katadai*, *Porphyra oligospermatangia*, *Porphyra yezoensis*, *Porphyra haitanensis*, and a hybridize species (*Porphyra yezoensis* × *Porphyra haitanensis*) sampled from China. Whereafter, the analyses of probable minimum loci numbers, observed alleles sum, genetic diversity, and unweighted pair-group arithmetic average (UPGMA) cluster were carried out. After initial activity and resolution testing of bands of 23 enzymes, 6 of them (MDH, ME, LDH, GDH, IDH and G-6-PDH) were proved to be appropriate for analysis of the full sample set. The probable minimum numbers of loci and alleles analyses showed that the five species of *Porphyra* had an extraordinary consistent result in ME loci and alleles. However, *P. katadai* and *P. oligospermatangia* differed from other three species of *Porphyra* in LDH and GDH loci and alleles. *P. katadai* was independent in the analyses of MDH and *P. oligospermatangia* and *P. haitanensis* differed from other three species in IDH analyses. Moreover, *P. yezoensis* and *P. haitanensis* were apart from other three species in G-6-PDH analysis. Taking one with another, *P. katadai* was relatively separated in the probable minimum numbers of loci and alleles analyses. The results indicated that the genetic variation among the five *Porphyra* species was limited with a genetic identity of 0.7550. The hybridize species (*P. yezoensis* × *P. haitanensis*) seemed to be high homologue with *P. oligospermatangia*, unexpectedly got relatively lower average genetic identities with both *P. yezoensis* and *P. haitanensis*. The 4 strains of *P. yezoensis* were relatively divergent with an average genetic identity of 0.7428, and *P. katadai* presented the most differentiated, compared with other species, which consistented with the result summarized in the probable minimum numbers of loci and alleles analyses.

Keywords: *Porphyra*; isozyme; allele; gene locus; genetic variety

Received on September 24, 2008

*Corresponding author: shensongdong@suda.edu.cn

1 Introduction

The red alga *Porphyra*, which was the popular food in China, Japan and Korea centuries ago, recently had been incorporated in diet around the world because of its abundant nutrition such as protein, polysaccharide, vitamins, and minerals [1]. Besides, it had also been used in traditional Chinese medicine as drug and in industrial application. *Porphyra*, distributing worldwidely, had a long evolutionary history [2]. There were more than 130 *Porphyra* species [3], more than half of which were described inhabiting in the North Pacific. Current understanding of the genus suggested that the habitats of most species were regionally confined, and no species was known to be common in both northern and southern hemispheres [4].

Isozymes, which catalyzed the same reaction and differentiated in makeup, physical and chemical characteristics, are the direct product of the transcription and translation of genes. They reflect the information of the DNA sequences which encode the enzyme proteins [5]. In organism evolution process, isozymes are supplied for the various needs of the cell metabolism. On genetics, when a group of special enzymes is subjected to a set of genes, it can adapt to the various environment better. When one of the genes becomes futile by gene mutation, other genes can still produce the isozymes which provide similar functions. It is a good mechanism that can reduce the disadvantages brought by gene mutation [6]. As a bio-chemical marker, the isozyme has been widely applied in both theory researches and actually applied field, such as germplasm identification, gene linkage analysis, evolution theories, environmental physiology, interbreeding research, and population inheritance structural analysis [7-10]. The technique of separating isozymes by electrophoresis has become the cardinal research means for the biochemical genetics, and the polyacrylamide gel electrophoresis has been used mostly nowadays.

The objective of this study was to examine the genetic properties and relationships of *Porphyra* species which located in China tideland by using isozyme markers. Compared with direct or indirect sequencing of DNA, isozyme electrophoresis still remains the fastest and most efficient method to study genetic variation in a large number of genes. Thus, analysis of isozymes adds another genetic dimension to study the relationships among *Porphyra* species.

2 Materials and methods

2.1 Materials

Eight free conchocelis of *Porphyra* (Tab. 1) were studied in this paper, including *Porphyra katadai*, *Porphyra oligospermatangia*, *Porphyra haitanensis*, four strains of *Porphyra yezoensis*(0008, 9965, 9509 and 2035), and a hybridize species of *Porphyra yezoensis* × *Porphyra haitanensis*. All of them were supplied by the National Germplasm Resources of *Porphyra*, Ministry of Agriculture and their Geographical origins were marked in Fig. 1.

Tab. 1 List of *Porphyra* isolates used in this study

Species	Isolate code	Cultivated /Wild	Geographical origin	Coll.Date
Porphyra yezoensis-0008	*PY*a	Cultivated	Nantong, China	2001
Porphyra yezoensis-9965	*PY*b	Cultivated	Nantong, China	1999
Porphyra yezoensis-9509	*PY*c	Cultivated	Nantong, China	1995
Porphyra yezoensis-2035	*PY*d	Wild	Qingdao, China	1999
Porphyra yezoensis × *Porphyra haitanensis*	*PYH*	Cultivated	Nantong, China	1993
Porphyra katadai	*PK*	Wild	Qingdao, China	2001
Porphyra oligospermatangia	*PO*	Wild	Qingdao, China	1994
Porphyra haitanensis	*PH*	Cultivated	Lianjiang, China	1993

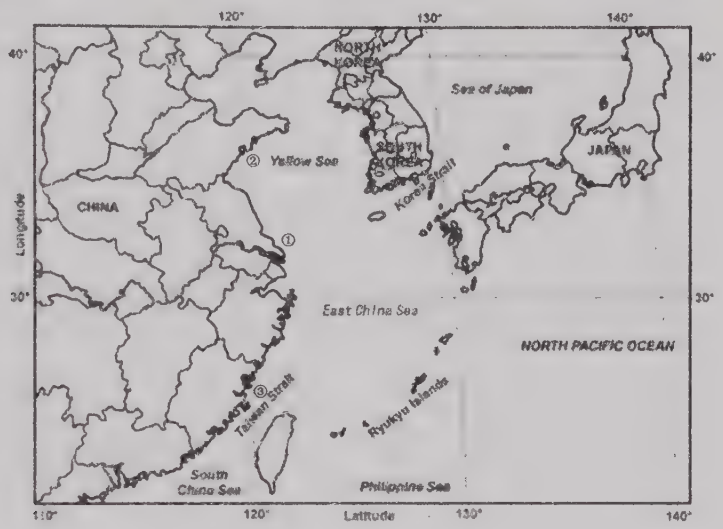

Fig. 1 Map of East China Sea

a) Nantong of Jiangsu Province, China; b) Qingdao of Shandong Province, China; c) Lianjiang of Fujian Province, China

2.2 Methods

2.2.1 Protein extraction

The free conchocelis of *Porphyra* were blotted up with absorbent paper after abluted by distilled water. This research took each sample (0.4 g) in a precooled mortar with extraction buffer (1M Tris-HCl [pH 6.8], W/V=1:3) and the right quartz sands, then grinded in ice bath for 10 - 15 mins. The homogenate was then centrifuged at 10 000 r/min for 30 mins at 4 °C. The supernatant was collected from the tube without disturbing the upper layer lipid, and was dispensed into another microtube. The microtubes were stored at - 20 °C until needed for electrophoresis.

2.2.2 Electrophoresis and coloration

Vertical polyamide electrophoresis was conducted, with 5%concentrating gel and 7.5% separating gel. A spot of bromophenol blue was added into the extracts as indicator before blotting. The electrophoresis was progressed at a initial voltage 100V for 1h, and then adjusted the voltage to 150V progressed 3h to 4h. When the bromophenol blue moved a distance up to 2 cm, turn off the

electrophoresis. The whole electrophoresis process was at 0 °C to 4 °C. All samples were extracted and electrophoresed thrice respectively.

Coloration was conducted according to Wang [11]. Enzyme systems test in this study were listed in Tab. 2. Electrophoretograms were noted by DC after bands showed clearly.

Tab. 2 Enzyme systems tested in this study and their Enzyme Comission (E.C.) numbers

Isozyme	E.C. No.	Activity	Loci scored	Buffer system / s
Aconitase, ACN	4.2.1.3	–	–	–
Adenylate kinase, AK	2.7.4.3	+		TG 8.5
Alcohol dehydrogenase, ADH	1.1.1.1	–	–	–
Aldehyde oxidase, AO	1.2.3.1	–	–	–
Fumarate hydratase, FUM	4.2.1.2	+		TG 8.5
Glucose-6-phosphate dehydrogenase, G6PDH	1.1.1.49	–	–	–
Glutamate dehydrogenase (NAD), GDH	1.4.1.2	–	–	–
Glutamate dehydrogenase (NADP), GDH	1.4.1.4	+		TG 8.5
Glucose-6-phosphate isomerase, GPI	5.3.1.9	+		TG 8.5, TGC 7.5
Glycerol-3-phosphate dehydrogenase, GPDH	1.1.18	–		–
Hexokinase, HEX	2.7.1.1	–	–	–
Isocitrate dehydrogenase (NADP), IDH	1.1.1.42	+		CAAPM 7.0
Lactate dehydrogenase, LDH	1.1.1.27.	+		RID
Malate dehydrogenase, MDH	1.1.1.37	+		CAAPM 7.0; TGC 7.5
Malic enzyme, ME	1.1.1.40	–	–	–
Peptidase A (Gly-Leu), PEP A	3.4.11/13	+		TG 8.5
Peptidase B (Leu-Gly-Gly), PEP B	3.4.11/13	+		TG 8.5
Peptidase D (Phe-Pro), PEP D	3.4.13.9	+		TG 8.5
Phosphoglucomutase, PGM	5.4.2.2	+		TG 8.5
6-Phosphogluconate dehydrogenase, 6PGDH	1.1.1.44	+		CAAPM 7.0
Peroxidase, PRX	1.11.1.7	–	–	–
Shikimate dehydrogenase, SKDH	1.1.1.25	–	–	–
Succinate dehydrogenase, SUD	1.3.99.1	–	–	–

2.2.3 Data analysis

The relative mobility (R_f value) was calculated by the formula: $R_f = A_i/B$ ("A_i" represented the distance that i_{th} band of isolate "A" moved; "B" represented the distance that the indicator moved). The probable minimum loci and alleles numbers analyses of each enzyme for every species were progressed by the genetic model which we established. Genetic distance and identity value were calculated by Nei's methods [12]. The species and strains relationships were constructed by the unweighted pair-group arithmetic average (UPGMA) cluster analysis [13].

3 Results and analysis

3.1 Atlas description and the relative mobility

After testing the enzyme systems (Tab. 2), we finally chose 6 isozymes to apply, which were MDH, ME, LDH, GDH, IDH and G-6-PDH. We finally got 58 enzyme bands in total, 17 of MDH, 11 of ME, 10 of LDH, 9 of GDH, 11 of IDH and 10 of G-6-PDH. In the eight *Porphyra* isolates, these isozymes had both the common and private loci (Fig. 2).

Malic enzyme is a tetramer enzyme. The ME test of the eight *Porphyra* isolates showed eleven loci (Fig. 2a), of which the R_f value were 0.477, 0.486, 0.491, 0.543, 0.571, 0.600, 0.614, 0.663, 0.728, 0.737

and 0.843. There were two common bands where R_f value were 0.663 and 0.843 respectively, which maybe represent the ME characteristic bands of *Porphyra*.

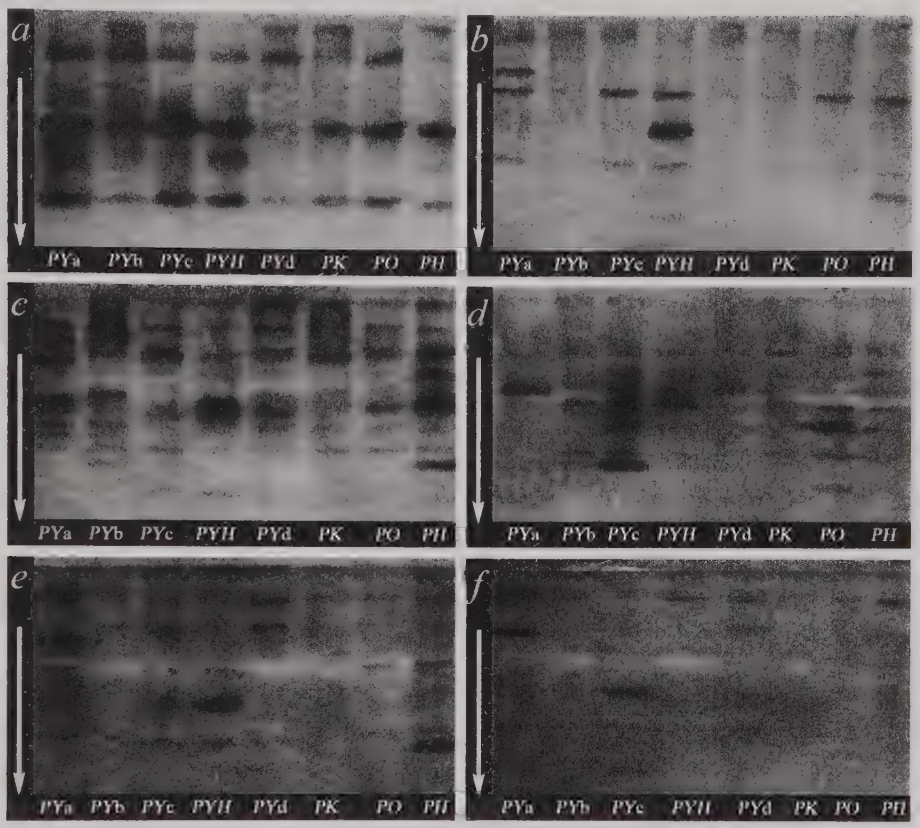

Fig. 2 Electrophoretic patterns of ME (a), LDH (b), MDH (c), IDH (d), GDH (e) and G-6-PDH (f) in each of the investigated isolates: PYa, PYb, PYc, PYd, PYH, PK, PO and PH. The arrows indicated the directions from cathode to anode in electrophoresis

Lactate dehydrogenase is a tetramer enzyme. The LDH test of the eight *Porphyra* isolates showed 10 loci (Fig. 2b), of which the R_f value were 0.400, 0.416, 0.428, 0.486, 0.497, 0.514, 0.623, 0.714, 0.771 and 0.828. There were two common bands where R_f value were 0.514 and 0.714 respectively. At the point where R_f value was 0.623, the *PY*d isolates had a distinct saturated band, which differentiate it from other isolates.

Malate dehydrogenase is a dimeric enzyme. The MDH test of the eight *Porphyra* isolates showed the most complex situation in this study (Fig. 2c), and 17 bands distributed to two regions obviously. First region contained eight bands which got R_f values as 0.317, 0.347, 0.361, 0.372, 0.403, 0.417, 0.439 and 0.458 respectively, and there were two common bands in first region where R_f value were 0.361 and 0.439 respectively. Second region contained nine bands which got R_f values as 0.522, 0.542, 0.567, 0.597, 0.639, 0.667, 0.694, 0.742 and 0.817 respectively, and there were also two common bands in second region where R_f value were 0.639 and 0.667 respectively.

Isocitrate dehydrogenase is a dimeric enzyme. The MDH test of the 8 *Porphyra* isolates showed the enzyme bands distributed to two regions (Fig. 2d). First region contained 6 bands which got R_f values as 0.419, 0.435, 0.468, 0.503, 0.522 and 0.574 respectively, and second region contained five bands which got R_f values as 0.613, 0.677, 0.758, 0.800 and 0.861 respectively. The band locations of the *Porphyra* isolates were different from each other, presenting plenty of genetic varieties.

The Glutamate dehydrogenase test of the eight *Porphyra* isolates showed two regions of bands (Fig. 2e), both with varieties. First region contained four bands which got R_f values as 0.425, 0.450, 0.512 and 0.550 respectively, and second region contained five bands which got R_f values as 0.625, 0.638, 0.700, 0.800 and 0.850 respectively. There were two common bands where R_f value were 0.425 and 0.800 respectively, which maybe represent the ME character of *Porphyra*.

Glucose-6-phosphate dehudrogenase is a dimeric polymer enzyme. The G-6-PDH test of the eitht *Porphyra* isolates showed two regions of bands (Fig. 2f), both of which contained five bands. The R_f values of all the ten bands were 0.426, 0.436, 0.449, 0.516, 0.532, 0.601, 0.617, 0.702, 0.787 and 0.905 respectively. Among them, the 3rd and 9th were common bands, which maybe represent the ME character of *Porphyra*.

3.2 Gene loci and alleles analysis

Many diversities in both dimeric enzyme banding patterns (MDH, IDH, G-6-PDH) and tetramer enzyme banding patterns (ME, LDH, GDH) were detected in this study. There were substantial differences in the numbers of bands as well as different migration distances between both the intra and inter taxa of the isolates we surveyed. For instance, in the IDH survey (Fig. 2d), *PY*b isolate had the same phenotype with hybrid *PYH* isolate, but it was distinctly different from *PY*c sample which was conspecific in taxonomy. The complex phenotypes were presented (Fig. 2). On account of the shortage of methods and techniques, making a tentative interpretation of banding patterns was more difficult in diploids than haploids [14], especially considering the possible production of multiple bands by single allele [15.16]. We did not explore and explain the unambiguous genetic mode of *Porphyra*, instead, we intended to establish genetic models to expatiate on the probable minimum loci and alleles numbers of this five species of *Porphyra* in this study and research the genetic relationships by these indices.

The genetic models which we established accorded with five main postulates: (1) All the five species of *Porphyra* which we surveyed were diplontic; (2) two haploid genomes of a diploid genome had the same loci of a special gene; (3) every enzyme could be constituted with subunits produced by the same and different loci respectively; (4) enzymes with different composes of subunits never got the same migration distance; (5) the modification of protein after translation affected the relative mobility (R_f value) barely[17].

According to the five main postulates enumerated above, a schematic illustration which we explained the complex genotypes of *Porphyra* was established (Fig. 3). In this illustration, six models of dimeric enzymes (MDH, IDH, G-6-PDH) were narrated to explain the genetic information, and three

models of tetramer enzymes were also narrated. Every model contained four main informations: genotypes, total kinds of alleles, minimum sum of loci and maximum sum of phenotypes. In the information, the maximum sum of phenotypes was the key index. When it was confirmed, other information was accordingly confirmed. So we could inspect the probable minimum numbers of loci and alleles of each isolate by their banding sum and positions. For example, in the ME test, *P. yezoensis* got eleven bindings, which were collated to our genetic models (Fig. 3). It consisted with the model three of tetramer enzyme, so the probable minimum numbers of ME loci and alleles of *P. yezoensis* were two and three respectively. The two indices of five species of *Porphyra* were confirmed by the same method (Tab. 3). However, some special conditions must be explained here. Fig. 4 was the produce scanning graph of ME of all isolates, from which we found three common kurtosis (marketed *a*, *b* and *c*). Their relative mobility (R_f value) were 0.477, 0.663 and 0.843 respectively, judged by electrophoresis graph, and we believed that they represented the homozygote bands. In the ME test, *P. oligospermatangia* got three bands, which should consisted with the model one of tetramer enzyme and the probable minimum numbers of ME loci and alleles should be one and two respectively. In addition, we found the relative mobility (R_f value) of its three bands were 0.477, 0.663 and 0.843 respectively, the same with the three most probable homozygote bands of other species of *Porphyra*, so we believed that the three bands of *P. oligospermatangia* were the homozygote bindings. And the ME test of *P. oligospermatangia* also should consist with the model three of tetramer enzyme and its probable minimum numbers of ME loci and alleles should be two and three respectively.

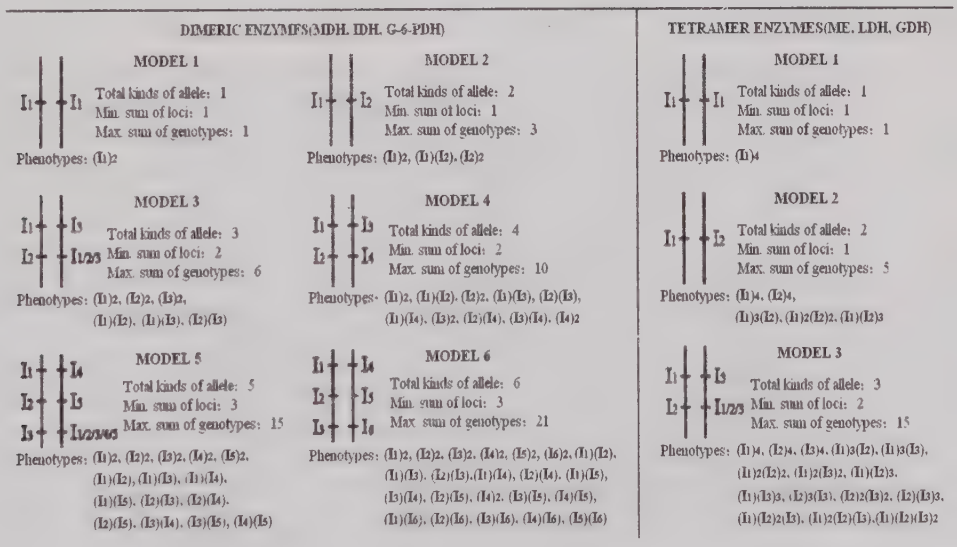

Fig. 3 Schematic representation of the relationship of loci, allele, and genotypes. "Ii" represent the allele which produced the subunits of enzymes

The probable minimum numbers of loci and alleles analyses showed that all the five species of *Porphyra* had an extraordinary accordant result in ME loci and alleles. *P. katadai* and *P. oligospermatangia* differed from other three species in LDH and GDH loci and alleles, while *P. katadai* was unaided in the

probable minimum loci numbers and observed alleles sum analyses of MDH. *P. oligospermatangia* and *P. haitanensis* differed from other three species in IDH analyses, and *P. yezoensis* and *P. haitanensis* were apart from other three species in G-6-PDH analysis. Taking one with another, *P. katadai* was most detached in the probable minimum numbers of loci and alleles analyses.

Tab. 3 Summary of probable minimum loci number of ME, LDH, MDH, IDH, GDH and G-6-PDH, number of observed alleles for four species and one hybrid specie of *Porphyra*

Isozymes which to code	Number of subunits		Species *P. yezoensis*	*P. katadai*	*P. oligosper -matangia*	*P. haitane -nsis*	*P. yezoensis* × *haitanensis*
		nL	2	2 (1)	2 (1)	2 (1)	2
ME	4	*nA*	3	3 (2)	3 (2)	3 (2)	3
		nL	2	1	1	2	2 (1)
LDH	4	*nA*	3	2	2	3	3 (2)
		nL	3	2	3	3	3
MDH	2	*nA*	6	4	5	5 (6)	6
		nL	2	2	3	3	2
IDH	2	*nA*	4	4	5	5	4
		nL	2 (1)	1	1	2	2
GDH	4 (6, 8)	*nA*	3 (2)	2	2	3	3
		nL	2	2 (1)	2	2	2
G-6-PDH	2	*nA*	4	3 (2)	3	4 (3)	3 (4)

nL= loci number, *nA*= number of observed alleles; Parentheses show probable values

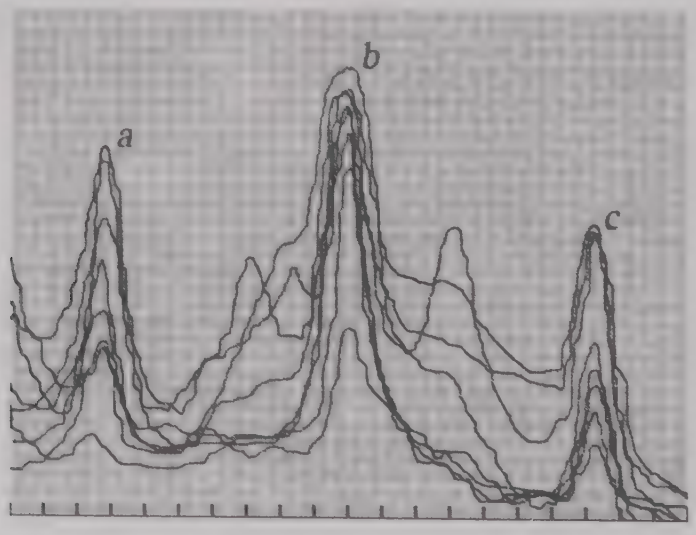

Fig. 4 Produce scanning graph of ME of all isolates

3.3 Genetic diversity analysis

After testing the enzyme systems, we found that the four species of *Porphyra* (isolate code: *PYH*, *PK*,

PO and *PH*) and four strains of *P. yezoensis* (isolate code: *PY*a, *PY*b, *PY*c and *PY*d) in the study presented extremely consistent phenotypes in their interior. It was due to the long-term artificial culturing and selection, so the genetic distance inside isolates were ignored in this study.

The genetic identities and distances of all the 8 isolates were listed (Table 4). *PYH* and *PO* had the maximum homologue, getting genetic identity as 0.8937. *PY*a and *PO*, *PY*a and *PH*, *PY*c and *PK* seemed to be maximum irrelated, had the same genetic distance as 0.3333.

Four strains of *P. yezoensis* were significantly divergent with an average genetic identity of 0.7428, which was similar to the mean genetic identities of *PY*a, *PY*b, *PY*c and *PY*d with other four species (*PYH*, *PK*, *PO* and *PH*).

PY×H, which was a hybridize species crossed by *P. yezoensis* and *P. haitanensis*, got a mean genetic identity with four strains of *P. yezoensis*as 0.7679, and a genetic identity with *PH* as 0.7826, which was lower than its genetic identity with *PO*.

The mean genetic identity of isolates (*PY*a, *PY*b, *PY*c and *PYH*) sampled from Nantong was 0.7612, and that of *PY*d, *PK* and *PO* sampled from Qingdao was 0.7686. The mean genetic identity between isolates sampled from Nantong and Qingdao was 0.7468, and between isolates sampled from Nantong and Lianjiang was 0.7543. While between isolates sampled from Qingdao and Lianjiang it was 0.8136.

To study the effect of artificial feeding and selection, we calculated the average genetic identities of two clusters of isolates, and grouped according to cultivated and wild species. The mean genetic identity of isolates which were cultivated (*PY*a, *PY*b, *PY*c, *PYH* and *PH*) was 0.7584, and that of the wild (*PY*d, *PK* and *PO*) was 0.7686.

Tab. 4 Pairwise comparison of Nei's (1978) unbiased genetic identities (upper diagonal) and genetic distances (lower diagonal) of 8 *Porphyra* isolates

	PYa	*PYb*	*PYc*	*PYd*	*P(Y×H)*	*PK*	*PO*	PH
PYa	—	0.7692	0.7632	0.7042	0.7500	0.7059	0.6667	0.6667
PYb	0.2308	—	0.7632	0.7323	0.7500	0.7059	0.7536	0.7733
PYc	0.2368	0.2368	—	0.7246	0.7714	0.6667	0.7462	0.7945
PYd	0.2958	0.2676	0.2754	—	0.8000	0.7213	0.8387	0.8235
P(Y×H)	0.2500	0.2500	0.2286	0.2000	—	0.7097	0.8937	0.7826
PK	0.2941	0.2941	0.3333	0.2787	0.2903	—	0.7458	0.7384
PO	0.3333	0.2464	0.2537	0.1613	0.1063	0.2542	—	0.8788
PH	0.3333	0.2267	0.2055	0.1765	0.2173	0.2615	0.1212	—

The unweighted pair-group arithmetic average (UPGMA) cluster analysis [13], using Nei's [12] genetic distance as the scale, depicted a complex phenomena of the eight isolates (Fig 5). The most distinct character observed from the UPGMA dendogram was the lack of similarity between the four strains of *P. yezoensis*. Though *PY*a, *PY*b and *PY*c formed a distinct cluster, with a mean genetic distance of 0.2348 which was quite higher than that of *PYH*, *PO* and *PH*, and *PY*d . It was apparently deviated from other strains. Another distinct phenomenon was that the hybridize species *PYH* did not cluster with any strain of *P. yezoensis* or *PH*, instead, it formed a most substantial cluster with *PO*. Finally, *PK* presented most differentiated, branching away all other seven isolates, and this result was consistent with which

summarized in the probable minimum numbers loci and alleles analyses.

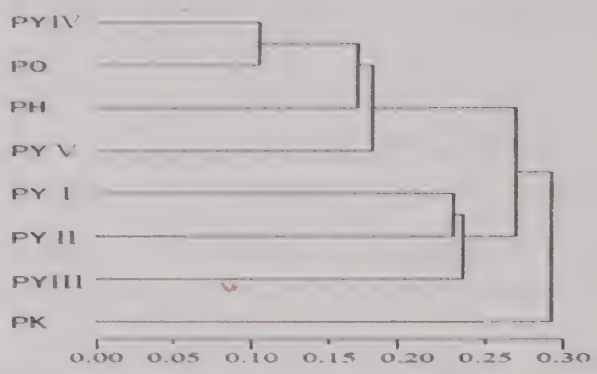

Fig. 5 UPGMA dendogram with scale based on Nei's genetic distance for *Porphyra* populations using Isolate code given in Tab. 1

3 Discussion

3.1 Community inherence

The results of isozyme analysis in the present study indicated that genetic variations in five species of *Porphyra* were limited as the genetic identity was 0.7550, which was in the range (0.3-0.8) of congeneric species [20]. In view of the data from isozyme analyses, there was no reason to put the specific taxonomic status of the five species in question.

Hofstra [21] considered the generally low level of intra- and inter-population genetic diversity in aquatic macrophytes, which could be explained to the effects of different reproductive strategies and habitats. In Hofsta's theory, aquatic plants were under less pressure than terrestrial plants. Laushman [22] focused on population genetics of clonally reproducing aquatic angiosperms, and pointed out that aquatic species (in contrast to terrestrial species) had the greater ability to spread more rapidly by fragmentation, resulting in lower levels of genetic variation and sexual reproduction of facultative asexual species. *Porphyra* reproduced both by asexual and sexual manner. The lack of genetic variation among the five species of *Porphyra* might indicate a high level of asexual propagation among them. Because of the higher level of sexual reproduction and the feasibility of hybridize, combined with the relatively broad distribution of these species, the genetic properties of *Porphyra* dispersed into each of them averagely and a high genetic identity of them was expectable. The quite accordant minimum probable loci and alleles of ME, LDH, MDH, IDH, GDH and G-6-PDH of the five species of *Porphyra* incarnated the high level of homozygosis.

Compared with wild breeds, artificial culturing breeds got more complex when analyzed the genetic properties. In the present study, we calculated the average genetic identities of two groups of isolates, and all of the samples grouped by cultivated and wild. The mean genetic identity of cultivated isolates was 0.7584, and that of the wild isolates was higher than that of the cultivated as 0.7686. This result was

consistent with the prospective situation that the mean genetic identity of wild isolates was higher than cultivated.

In the genetic diversity tests, the hybridize species of *P. yezoensis* × *P. haitanensis* got a high mean genetic identity with *P. oligospermatangia*, and unexpectedly got relatively low mean genetic identities with both *P. yezoensis* and *P. haitanensis*. However, in the comparison of the minimum probable loci and alleles numbers of ME, LDH, MDH, IDH, GDH and G-6-PDH, it was much more consistent with *P. yezoensis* and *P. haitanensis* than with *P. oligospermatangia*. This result seemed to be disordered and quite contrary with anticipate. However, after exploring the electrophoretic patterns, it was explicable. The banding sum of each enzyme test of *P. yezoensis* × *P. haitanensis* was almost equal with that of *P. yezoensis* and *P. haitanensis*, but their relative mobilities were different evidently. The situation between hybridize species and *P. oligospermatangia* was the distinct difference of banding sums and high percentage of the same relative mobility values. Therefore, we guessed that the *P. yezoensis* and *P. haitanensis* had more similar genetic properties of enzyme systems than *P. oligospermatangia*, while in the evolution process, *P. oligospermatangia* was fresher than *P. yezoensis* and *P. haitanensis*. A broader test of enzyme systems or other indices of genetics was needed to confirm this suppose.

3.2 Genetic inherence

The genetic identity among the four strains of *P. yezoensis* (0.7428) was relatively low among species in our study, and had a good agreement with the values reported for such marine algal species as *Eucheuma isiforme* and *Eucheuma nudum* [23], *Chondrus crispus* [24] and *Chaetomorpha linum* [25].

Besides the factor of reproductive manner as depicted above, artificial intervention was another important influence of genetic identity, especially considering that *P. yezoensis* was the most broad cultivated species in China. Pellegrin [26] considered that the level of genetic variation in one species was relevant to the present or future environmental adaptation of that species. High levels of genetic variation might infer greater potential of the adaptation of one species in a changing environment. However, the situation of the four strains of *P. yezoensis* studied could be absolutely contrary. The relatively high level of variation within *P. yezoensis* studied might have origins brought by artificial intervention. The original seedlings of *P. yezoensis* for culture were collected from the wild. At the same time, *P. yezoensis* could cover a wide range of habitats, so the variation between the breeds of *P. yezoensis* cultivated in different part of the world, even in China, ineluctably existed. Because of the manner of culture, the breeds of *P. yezoensis* were stable in different places. Combined with the jarless ecological situations for cultivated breeds, environmental pressure was excluded and the original variation was kept. However, it didn't draw this conclusion with certainty until more similar situations had been examined. If, in a more comprehensive inquiry, the same situation indeed appeared in some other species of *Porphyra*, the hybridize behavior of *Porphyra* and genetic properties could be confirmed.

3.3 Regional inherence

Two similarities were apparent among isolates of the same species or congener independently from

geographic origins. Such uniformity among plant pathogen isolates from different geographic origins has been frequently noted [27-31]. The value was the quite high genetic identity (0.775 0) among the five species of *Porphyra*, not appearing particularly dissimilitude among them as presented in the most differentiated species *PK*, getting a branch of 0.2903. It suggested that the genetic diversity of *Porphyra* species was relatively limited and the phenotypes probably represented a felicitous situation. However, these were some phenomena to study the genetic diversity of different geographic origins.

From the UPGMA dendogram, we could find a distinct cluster of three strains of *P. yezoensis* (*PY*a, *PY*b and *PY*c), of which the mean genetic distance was 0.234 8, while, another strain of *P. yezoensis* (*PY*d) branched away from this cluster. Comparing with the geographic origins, we could explain this phenomenon partially. Due to the *PY*a, *PY*b and *PY*c isolates were all sampled from the same region (Nantong), and *PY*d isolate was sampled from another region (Qingdao). The genetic diversity of the isolates was incarnated here. A better understanding of the geographic patterns of distribution and differentiation of *P. yezoensis* needed a broader survey including populations in other parts, particularly considering *P. yezoensis* occurred in a continuous distribution along the coast.

Contrasting to the *P. yezoensis* situation, the comparisons of the mean genetic identities of all five isolates were studied, and grouped by the different geographic origins. It showed another phenomenon. If it matched the prospective conclusion, according to their geographic distribution, the genetic identity between Qingdao and Lianjiang should be minimum, but it did not occur in this study. Although *P. haitanensis* species was brought from Qingdao primitively, it vegetated better in Lianjiang sea area than in Qingdao as it better adapted the subtropical climate. Despite of the lack of the *P. haitanensis* species settled in Qingdao, the direct comparison of genetic identity with the *P. haitanensis* species sampled in Lianjiang could not be applied. Other species settled in Qingdao could share some genetic propertied with *P. haitanensis* in the manner as we discussed aboved. These common genetic properties transplanted to Lianjiang region by replantation. It might be explained in part that the remarkable observation of distributed populations consisting of a single putative heterozygous genotype in other species of alga.

Acknowledgement

This work was sponsored jointly by the Natural Science Foundation of China (No. 40206019) and Agricultural Innovation Project of Nantong (No. L4017).

Reference

[1] Noda H J. Health benefits and nutritional properties of nori [J]. J Appl Phycol, 1993, 5: 255 - 258.

[2] Ragan M A, Bird C J, Rice E L, et al. A molecular phylogeny of the marine red algae (Rhodophyta) based on the nuclear small-subunit rRNA gene [J]. Proc Natl Acad Sci USA, 1994, 9: 7 276 - 7 280.

[3] Yoshida T. The history and future prospects of systematics of Bangiaceae, Rhodophyta [J]. Natl His Res, Special Issue, 1997, 3: 14.

[4] Yoshida T, Notoya, Kikuchi N, et al. Catalogue of species of *Porphyra* in the world with special reference to the type locality and bibliography [J]. Natl His Res, Special Issue, 1997, 3: 5 - 18.

[5] Gao M. Methods of plant isozyme gene locations [J]. J Ocean Univer Qingdao, 1994, 24(2): 195 - 202.

[6] Zou C J, Sheng X F, Han W Q, et al. Isozyme analysis technology and its application in plant research [J]. Chin J Ecol, 2003, 22(6): 63 - 69.

[7] Zhou Z G and Hu Y J. Application of isoenzyme in phycology [J]. J Shanghai Fish Univer, 2001, 10(3): 264 - 268.

[8] Wang D Q, Li T W, Su X R, et al. Factors affecting isozymes [J]. Fish Sci, 2004, 23(5): 45 - 46.

[9] Wang S M, Tan F J and Hu L P. Genetic diversity assessment of adzuki bean germplasm resources based on isozyme analysis. Agric Sci China, 2002, 35(11): 1 311 - 1 318.

[10] Fujita Y, Tanak M Y, Hara M, et al. Enzyme polymorphism and population structure of the haploid laver *Porphyra yezoensis* [J]. Nippon Suisan Gakkai, 1987, 53(3): 357 - 362.

[11] Wang Z R. Plant allozyme analysis [M]. Beijing: Science Press, 1996.

[12] Nei M. Estimation of average heterozygosity and genetic distance from a small number of individuals [J]. Genetics, 1978, 89: 583 - 590.

[13] Ferguson A. Biochemical Systematics and Evolution. Glasgow: Blackie, 1980, 366.

[14] Weeden N F, Gottlieb L D. Distinguishing allozymes and isozymes of phosphoglucoisomerases by electrophoretic comparisons of pollen and somatic tissues [J]. Biochem Genet, 1979, 17: 287 - 296.

[15] Berg B M, Van D, Wijsman H J W. Genetics of the peroxydase isozymes in Petunia [J]. Theor Appl Genet, 1981, 60: 71 - 76.

[16] Bachmann K, Chambers K L, Price H J. A second marker enzyme in the genetics of pappus part numbers in *Microseris* hybrid B 87 (Asteraceae, Lactuceae) [J]. Pl Syst Evol, 1984, 145: 243 - 258.

[17] Heyduk E, Heyduk T. Mapping protein domains involved in macromolecular interactions: a novel protein footprinting approach [J]. Biochemistry, 1994, 33: 9 643 - 9 650.

[18] Oudemans P, Coffey M D. Isozyme comparison within and among worldwide sources of three morphologically distinct species of *Phytophthora* [J]. Mycol Res, 1991, 95: 19 - 30.

[19] Hellmann R, Christ B J. Isozyme variation of physiologic races of *Ustilago hordei* [J]. Hytopathology, 1991, 81: 1 536 - 1 540.

[20] Avise F J. Genetic differentiation during speciation. In: Ayala F J ed. Molecular Evolution. Sinauer Associates,Sunderland, Massachusetts. 1976, 106 - 122.

[21] Hofstra D E, Adam K D, Clayton J S. Isozyme variation in New Zealand populations of *Myriophyllum* and *Potamogeton* species [J]. Aquatic Botany, 1995, 52: 121 - 131.

[22] Laushman R H. Population genetics of hydrophilous angiosperms. In: Phisbrick C T and Les D S, eds. Evolution of Aquatic Angiosperms [J]. Aquat Bot, 1993, 44, 147 -1 58.

[23] Cheney D P and Babbel G R. Biosystematic studies of the red algal genus *Euchema*. I. Electrophoretic variation among Florida populations [J]. Mar Biol, 1978, 47: 251 - 264.

[24] Cheney D P and Mathieson A C. Population differentiation in the seaweed *Chondrus crispus*: preliminary results [J]. Isozyme Bull, 1979, 12: 57.

[25] Blair S M, Mathieson A C and Cheney D P. Morphological and electrophoretic investigations of selected species of *Chaetomorpha* (Chlorophyta: Cladophorales) [J]. Phycologia, 1982, 21: 164 - 172.

[26] Pellegrin D, Hauber D P. Isozyme variation among populations of the clonal species *Phragmites australis* (Cav.) Trin. Ex Steudel [J]. Aquatic Botany, 1999, 63: 241 - 259.

[27] Burdon J J, Marshall D R, Luig N H, et al. Isozyme studies on the origin and evolution of *Puccinia graminis* f. sp. *tritici* in Australia [J]. Aust J Biol Sci, 1982, 35: 31 - 238.

[28] Leung H, Williams P H. Enzyme polymorphism and genetic differentiation among geographic isolates of the rice blast fungus [J]. Phytopathology, 1986, 76: 778 - 783.

[29] Bosland P W, Williams P H. An evaluation of *Fusarium oxysporum* from crucifers based on pathogenicity, isozyme polymorphism, vegetative compatibility and geographic origin [J]. Can J Microbiol, 1987, 65:2 067-2073.

[32] Kirby G C. Variation in *Ustilago bullata* on *Agropyron scabrum* in Australia and New Zealand [J]. Aust Plant Pathol, 1987, 16: 10 - 12.

[31] Linde D C, Groth J V, Roelfs A P. Comparison of isozyme and virulence diversity patterns in the bean rust fungus *Uromyces appendiculatus* [J]. Phytopathology, 1990, 80: 141 - 147.

五种紫菜同工酶标记的遗传分析

沈颂东[1]，李艳燕[1]，许 璞[2]，张美如[3]，袁昭兰[1]，王建伟[1]，朱建一[2]

（1. 苏州大学生命科学院，江苏 苏州 215123；2. 常熟理工食品工程与生物系，江苏 苏州 215500；
3. 江苏省海产渔业研究所，江苏 南通 226007）

摘 要：用垂直凝胶电泳来研究采自中国的（条斑紫菜×坛紫菜）杂交种、坛紫菜、条斑紫菜、少精紫菜、半叶紫菜的同工酶多态性。然后分析最小可能位点数和观察同位基因数、遗传差异性和采用平均连接聚类法。选取 23 种酶带中的六个酶(MDH，ME，LDH，GDH，IDH 和 G-6-PDH)进行分析。最小可能等位基因位点数显示五种紫菜在 ME 等位基因位点都只有一个。LDH 和 GDH 等位基因位点半叶紫菜和少精紫菜和另外的三种紫菜不同，而在分析 MDH 时半叶紫菜比较独特。在 IDH 位点分析时少精紫菜和坛紫菜和其他三种不同，而条斑紫菜和坛紫菜和其他三种不同在 G-6-PDH 位点不一致。总的来看，最小可能等位基因位点数分析半叶紫菜是最分离的。遗传多样性结果分析表明当遗传相似度为 0.755 0 时，五种紫菜中的遗传变异研究受到限制。条斑紫菜和坛紫菜的杂交种非常接近少精紫菜。当遗传相似度达到 0.893 7 时，出乎意料的是条斑紫菜和坛紫菜遗传同一性很低。条斑紫菜 4 个株系的平均遗传相似度仅为 0.742 8，差异比较大。在所有紫菜中半叶紫菜是最分化的分支，它与最小可能等位基因位点数分析一致。

关键词：紫菜；同工酶；等位基因；基因位点；遗传多样性

Phylogenetic Relationships between Purple and Tea-green Individuals of the Blue Swimming Crab *Portunus trituberculatus* by PCR-SSCP Analysis

CHI Da-li [1, 2], GAO Huan [1], SHEN Song-dong [2], YAN Bin-lun [1*]

1. *Jiangsu Key Laboratory of Marine Biotechnology, Huaihai Institute of Technology, Lianyungang,* 222005, *Jiangsu Province, China;*

2. *School of Life Sciences, Suzhou University, Suzhou* 215123, *Jiangsu Province, China*

Abstract: As an important commercial species, the blue swimming crabs with different body-colors were discovered along the coast of East China in recent years. Both purple and tea-green crabs have similar, even the same physical characteristics except for the carapace color. In order to identify the relationships between them, we amplified and compared two conserved mitochondrial gene fragments of color-different crab individuals through PCR-SSCP and DNA sequencing analyses. The results showed that there was no distinct variation of DNA bands of both the *COI* and *16srRNA* genes detected in polyacrylamide gels through SSCP analysis between purple and tea-green crab samples, and the following sequence analysis of color-different crab individuals presented 99.81% and 99.91% nucleotide sequence identity of the *COI* and *16srRNA* genes respectively, which indicated that there was no species or subspecies differentiation between them. In addition, the purple individuals were more conserved in DNA sequence in comparison with that of the tea-green ones.

Keywords: *16srRNA*; body-color; *COI*; PCR; *Portunus trituberculatus*; SSCP

1 Introduction

The blue swimming crab, *Portunus trituberculatus* (Crustacea: Decapoda: Brachyura), is an important fishery species with great economic value in world portunid crabs, and inhabits at the coastal seafloor with mud or sands, being widely distributed along the coast of China. Japan and Korea lie off the Pacific Ocean [1].

Given the commercial and ecological importance of the blue swimming crab, it has been artificially propagated and widely stocked as one of the most common edible crabs in the eastern part of China, and the researches on *P. trituberculatus* have been developing well from the 1950s including embryonic development, population structure, ultrastructure description and karyotype analysis et al. [2] The few studies on molecular biology of *P. trituberculatus* published to date are based on protein polymorphisms (allozyme data), phylogenetic identification, and analysis of the complete mitochondrial genome sequence

Received on April 24, 2009

*Corresponding author: yanbinlun@yahoo.com.cn

and so on. Yamauchi et al.[3] reported the first example of a complete nucleotide sequence of the mitochondrial genome determined by using a long PCR technique and primer walking strategy, and specified the location of genes in the mitochondrial genome of the blue swimming crab. Till now, the genetic markers- random amplified polymorphic DNA (RAPD) and amplified fragment length polymorphism (AFLP) have been applied on *P. trituberculatus* to identify the genetic structure, with the results showing conformed to conventional taxonomy[4,5]. These studies determined the applicability of genetic markers used for population structure analysis of *P. trituberculatus*. However, there is a surprising scarcity of information on the topic of body-color difference of this species.

Generally, the common carapace (especially for the cephalothorax) color of *P. trituberculatus* is tea-green; while some crab individuals whose carapaces and appendages are purple in natural existence through the whole span of their lives have been discovered in their natural habitats (Lianyungang, China) in recent years. Both purple individuals and tea-green ones have similar, even the same physical characteristics except for the carapace color, and the carapace color has no direct relationship with the sexual difference of the blue swimming crabs, meaning that the body-color is not a sex-linked character. Besides, the ratio of number of purple crabs to that of all wild captured ones is about 9% according to our preliminary statistical researches.

Because of maternal inheritance, a fast evolutionary rate (especially in the non-coding control region) compared to that of the nuclear DNA, and a lack of intermolecular genetic recombination, mitochondrial DNAs (mtDNAs) have been extensively used for studying population structure, phylo-geography, and phylogenetic relationships at various taxonomic levels[6]. Till now, the subunit I of cytochrome *c* oxidase (*COI*) and *16srRNA* genes located on the mitochondrial genome have been effectively used for studying identification of phylogenetic relationships in crustacean biology [3]. And the *16srRNA* gene was more conserved in DNA sequences than the *COI* gene[7], which indicated the *COI* gene was appropriate for genetic diversity analysis for intraspecies, and the *16srRNA* gene for interspecies.

Fig. 1 Agarose gel electrophoresis of mitochondrial *COI* gene fragments

(Lanes 1 - 10 are PCR products of *COI* gene fragments. M represents the 2000 bp DNA ladders and CK represents the control without genomic DNA in the PCR reactions.)

Single strand conformation polymorphism (SSCP) analysis is one of the simplest and perhaps one of the most sensitive methods for the detection of mutations based on PCR technology [8]. This technique

is based on the relationship between the electrophoretic mobility of a single-stranded DNA (ssDNA) in non-denaturing polyacrylamide gels and its folded conformation, which in turn reflects the nucleotide sequence [9]. Due to its technical simplicity, SSCP is widely used in various investigations, ranging from the clinical diagnosis of human hereditary diseases to the characterization of microbial communities [10]. And the SSCP technique has been proved successful for the identification of fishery products [11]. We determined here the phylogenetic relationships between purple and tea-green crab individuals of *P. trituberculatus* by comparing the mitochondrial *COI* and *16srRNA* genes, which were identified with SSCP technique and DNA sequencing analyses.

2 Materials and methods

2.1 Samples and DNA extraction

Both purple and tea-green crab individuals were obtained from the same aquaculture pond in Ganyu County, Lianyungang, China and maintained in water recycle systems for laboratory breeding experiments in the summer and autumn of 2007. The ambulatory muscle tissues from twenty tea-green crabs (ten female ones) and twenty purple ones (ten female ones) were excised and preserved at -70 ℃ in a ultra refrigerator. The genomic DNA was extracted using conventional phenol-chloroform extraction methods with some modifications as follows: 100 mg of muscular tissue was taken from the appendage and homogenized in 475 μL of DNA extraction buffer (10 mM Tris-HCl, pH 7.6; 100 mM EDTA) in an Eppendorf Tube, after which 25 μL of 10% SDS and 4 μL of 20 mg/mL proteinase K were added for lysis. The lysates were incubated at 55 °C for 4 hours or so, after which the mixture was extracted twice with phenol and chloroform, and was precipitated by adding 1/25 volumes of 5 M NaCl and two volumes of ethanol. Finally, the DNA samples were collected by brief centrifugation and washed twice with 70% ethanol, then air-dried at room temperature (RT), and dissolved in 30 μL of TE buffer (10 mM Tris-HCl, pH 7.6; 100 mM EDTA).

The DNA samples were electrophoresed for confirmation on a 0.8% agarose gel (OXOID™, England) stained with GoldView for band characterization via ultraviolet transillumination, and the concentration of DNA samples was assessed with a Gene Quant *Pro* (Amersham Biosciences™, England) spectrophotometer for absorption at 260 nm.

2.2 Amplification of the mitochondrial *COI* and *16srRNA* genes

In the experiment, the mitochondrial *COI* and *16srRNA* genes were used for studying the identification of phylogenetic relationships between purple and tea-green crab individuals. The fragments of mitochondrial *COI* and *16srRNA* genes were amplified using specific primer pairs COI-H/COI-L (5'-taaacttcagggtgaccaaaaaatca-3', 5'-ggtcaacaaatcataaagatattgg-3') and 16S-AR/ 16S-BR (5'-cgcctgtttatcaaaaacat-3', 5'-ccggtctgaactcagatcacgt-3') respectively [10], which were synthesized by Sangon company (Shanghai).

PCR reactions were carried out in a Multicolor Real-Time PCR Detection System (Gene cycler™,

Bio-Rad, USA) with 35 cycles of 25 μL reaction volume containing 12.3 μL sterile distilled H_2O, 2.5 μL 10× PCR buffer (10 mM Tris-HCl, pH 9.0; 50 mM KCl and 0.1% Triton X-100), 2 μL dNTPs (10 μM), 2 μL 25 mM $MgCl_2$, 0.2 μL *Taq* polymerase (5 U/μL), 2 μL of each primer (10 μM), and 2 μL template DNA (genomic DNA, 300 ng/μL). Samples without genomic DNA were included in each amplification run as controls.

The thermal cycle profile was as follows: denaturing at 94 °C for 45 s, annealing at 48 °C for 60 s, and extension at 72 °C for 60 s. And the PCR products were electrophoresed for confirmation on a 1.0% agarose gel stained with GoldView for band characterization via ultraviolet transillumination after amplification.

2.3 Single strand conformation polymorphism (SSCP) analysis

SSCP analysis was carried out essentially as described previously[10,12,13] with some modifications as follows: the non-denaturing polyacrylamide gel was prepared from 3.4 mL of 30% acrylamide solution (acrylamide/bisacrylamide, 29:1), 4 mL of a 5×TBE buffer (446 mM Tris-base and 10 mM EDTA), 13 mL deionized water, 125 μL of 10% ammonium persulfate, and 10 μL *N,N,N',N'*-tetramethylethylenediamine (TEMED). After the gel mixture was prepared and poured in 170×160×0.4 mm^3 dimension glass-plates, it was allowed to polymerize for at least 1 h at RT. During that time, 4 μL of the PCR products mixed with 4 μL loading buffer (98% formamide, 10 mM EDTA, 0.25% bromophenol blue and 0.25% xylene cyanol) were denatured for 7 min at 95 °C, then the mixture samples were cooled down immediately in an ice bath, and loaded on a 5% non-denaturing polyacrylamide gel. Electrophoresis was performed at a constant voltage of 120 V using 1×TBE buffer as a running solution for about 6 h at 4 - 16 °C.

After electrophoresis, silver-staining-procedure was used to visualize the bands. Briefly, fix the gel with 1 L of 10% acetate acid for 20 min and then wash with 150 mL of deionized water for 3 times (2 min/time). Stain the gel with 1 L of 0.1% $AgNO_3$ containing 30 μL of 37% formaldehyde for 30 min. Reveal the gel with 20 mL of 1.5% Na_2CO_3 containing 300 μL of 37% formaldehyde and 200 μL of 2 mg/mL $Na_2S_2O_3$ for 4-6 min until DNA bands appeared clearly, and finally, stop silver stain with 1 L of 10% acetate acid.

2.4 Sequencing of PCR products and analyses

The most direct means of obtaining information from PCR products is by sequencing, which is time consuming and technically demanding but will produce a relatively large amount of information, requiring good data handling capacity[11]. The PCR products that showed a different mobility shift pattern in the SSCP analysis were purified and subjected to sequencing by Sangon company (Shanghai) in both directions with the same primer pairs as used in the amplification reactions. The sequences were analyzed using the computer software DNAMAN™ (Version 6.0.40, Lynnon BioSoft, America).

Pairwise comparisons were made of the level of sequence differences (D) using the formula D=1-(M/L), where M is the number of alignment positions at which two sequences have a base in common, and L is the total number of alignment positions over which the two sequences are compared [13].

3 Results and discussion

3.1 Applicability of using genomic DNA as templates to amplify conserved mitochondrial genes

In the experiment, we extracted the genomic DNA and took it as template for the amplification of the specific genes on the mtDNA. The concentration of genomic DNA extracted from both tea-green and purple crabs reached as high as 1200 ng/μL, and the average concentration was about 500 ng/μL. The *COI* and *16srRNA* genes amplified by PCR presented clear and distinct bands through 1.0% agarose gel electrophoresis (Fig. 1 & Fig. 2). The fragment lengths of *COI* and *16srRNA* genes were about 658 and 566 bp respectively[10], and the bands presented in the agarose gel showed identical DNA fragment lengths with the conventional results, and in return, it served good verifications that the genomic DNA functioned well in the PCR analysis for the two conserved mitochondrial genes.

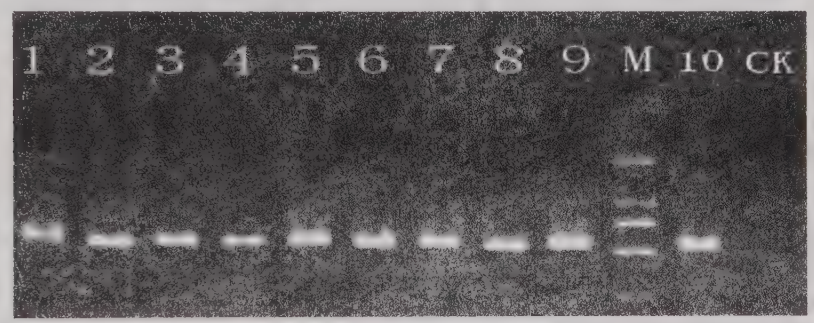

Fig. 2 Agarose gel electrophoresis of mitochondrial *16srRNA* gene fragments

(Lanes 1 - 9 and 10 are PCR products of *16srRNA* gene fragments. M represents the 2000 bp DNA ladders and CK represents the control without genomic DNA in the PCR reactions.)

3.2 Sequence analysis and annotation

In the experiment, there was no distinct variation of DNA bands of both the *COI* and *16srRNA* genes detected in polyacrylamide gels through SSCP analysis between tea-green and purple samples of the blue swimming crab (Fig. 3 & Fig. 4). Four PCR samples from color-different crab individuals were sequenced and analyzed using the computer software DNAMAN™.

The overall A+T content of the sequenced *COI* gene was about 63.0% (A=36.6%; C=16.4%; G=20.5%; T=26.4%), and the overall A+T content of the sequenced *16srRNA* gene was about 69.7% (A=34.5%; C=12.4%; G=18.0%; T=35.2%), which was similar to that of the blue swimming crab mitochondrial DNA (70.2%)[3]. And the *COI* and *16srRNA* gene sequences of purple and tea-green crab individuals of *P. trituberculatus* showed 99.81% and 99.91% nucleotide sequence identity respectively.

It is clear that there is no nucleotide change in the *COI* gene among the purple crab individuals, while more nucleotide changes exist in the tea-green ones, meaning that the purple crab individuals are

more conserved in DNA sequence in comparison with the tea-green ones (Fig. 5).

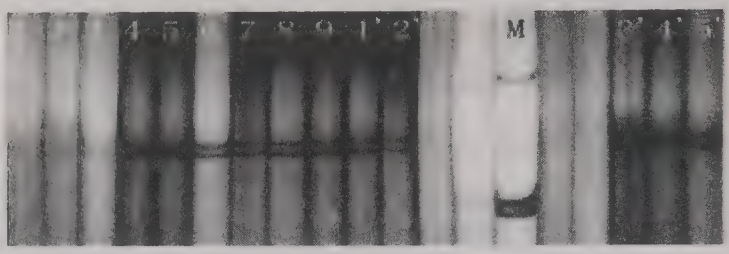

Fig. 3 DNA band patterns of SSCP analysis for the blue swimming crab *COI* gene

(Lanes 1-6 represent *COI* gene fragments from tea-green crabs and others from purple ones. M represents the DNA marker, of which the bands are 750 and 500 bp respectively.)

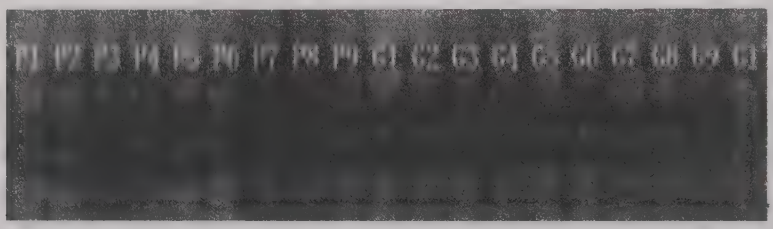

Fig. 4 DNA band patterns of SSCP analysis for the blue swimming crab *16srRNA* gene

(Lanes P1-P9 represent *16srRNA* gene fragments from purple crabs and Lanes G1-G9 and G1' represent *16srRNA* gene fragments from tea-green ones.)

Through the multiple sequence alignment of *16srRNA* gene fragments of color-different crab individuals, only one nucleotide showed variable in the sequence, and the variation of the nucleotide appeared in both purple and tea-green crab individuals (Fig. 6). The difference between *16srRNA* gene fragments of color-different crab individuals lies in the different number of single nucleotide (T) repeats, of which one is seven and the other is eight, saying that *16srRNA* gene is highly conserved and capable of being used in taxonomy analysis especially for some relatively distinct species.

3.3 Comparison of nucleotide sequence and composition of *COI* gene between *P. trituberculatus* and *C. sapidus* (Crustacea: Decapoda: Brachyura)

The mitochondrial gene arrangement of *P. trituberculatus* is identical with the blue crab *Callinectes sapidus* [14], which is reported distributing along the Chesapeake Bay, the largest estuary in the United States lying off the Atlantic Ocean. In this paper, we compared the *COI* gene sequence of *P. trituberculatus* and *C. sapidus* using software DNAMAN™. The two sequences showed 84.35% nucleotide sequence identity (GenBank accession no. NC_005037 and NC_006281), and 98.83% sequence identity at the amino acid level (GenBank accession No. NP_872442 and YP_086829). While the two portunid species, *P. trituberculatus* and *C. sapidus*, distributing in two different oceans separately, but with identical mitochondrial gene arrangement and close *COI* gene nucleotide and amino acid sequence identity, those indicated the close phylogenetic relationships between the two color-different brachyuran species. It is

expected that the two portunid crabs seemly belonging to different genera in the same family may come from the same genus, even the same species due to some reasons such as continental drift [15] et al.

```
G1: GAAGAGATGTTGGTAAAGAACGGGGTCTCCACCCCCGGCAGGGTCGAAGAATGAAGTATTTAAATTACGATCTGT 75
G2: ---------------------------------------------------------------------------
P1: ---------------------------------------------------------------------------
P2: ---------------------------------------------------------------------------

G1: GAGAAGTATAGTAATAGCTCCTGCCAGAACAGGGAGAGATAAAAGAAGAAGAATTGCAGTAATAAATACGGATCA 150
G2: ----------------------------------------------------------c--c-----
P1: ----------------------------------------------------------c-----
P2: ----------------------------------------------------------c-----

G1: TACAAATAGTGGTATTTGGTCTATTCTTATACCAAAAGATCGTATATTAATAACAGTGGTTATAAAATTTACTGC 225
G2: ---------------------------------------------------------------------------
P1: ---------------------------------------------------------------------------
P2: ---------------------------------------------------------------------------

G1: ACCTAAAATAGATGAAACTCCTGCTAAATGAAGAGAAAAAATTCCTAAGTCTACTGATGCACCGGCATGGGCAAT 300
G2: ---------------------------------------------------------------------------
P1: ---------------------------------------------------------------------------
P2: ---------------------------------------------------------------------------

G1: TGCGGCAGAAAGAGGAGGATATACAGTTCATCCAGTACCTACACCTCTTTCTACTATACCTCTTATAAGAAGAAG 375
G2: ---------------------------------------------------------------------------
P1: ---------------------------------------------------------------------------
P2: ---------------------------------------------------------------------------

G1: AGTTAATGAGGGAGGAAGAAGTCAGAATCTTATGTTATTTATACGGGGGAAGGCTATATCAGGAGCTCCTAATAT 450
G2: ---------a-----------------------------------------------------------
P1: ---------a-----------------------------------------------------------
P2: ---------a-----------------------------------------------------------

G1: TAGGGGTACTAATCAATTACCGAATCCTCCAATTATGATTGGTATAACTATAAAGAAAATCATGACGAAAGCATG 525
G2: ------c---------------------------------------------------------------
P1: ---------------------------------------------------------------------------
P2: ---------------------------------------------------------------------------

G1: AGCTGTCACTACAACATTGTAAATTTGGTCGTTGCCAATAAGAGTACCGGGTTGTCCTAATTCAGCACGAATAAT 600
G2: ------------------a--------------------------------------------------
P1: ---------------------------------------------------------------------------
P2: ---------------------------------------------------------------------------

G1: TAGACTAAGTGAAGTTCCTACTATTCCTGATCATGCTCCAAAAATAAAATATAATGTA 658
G2: -----------------------------------------------------
P1: -----------------------------------------------------
P2: -----------------------------------------------------
```

Fig. 5 Multiple sequence alignment of *COI* gene fragments of both tea-green (G) and purple (P) samples of the blue swimming crab

4 Conclusion

Most of the recent advances in understanding the phylogeny of animal taxa are based on the analysis of mitochondrial DNA (mtDNA) sequence. The alignment of nucleotide sequences of mtDNA genes for ribosomal RNAs and subunit I of cytochrome c oxidase (*COI*) and nuclear genes for ribosomal RNAs are the method of choice in many molecular phylogenetic analyze [16]. And the two conserved mitochondrial genes (*COI* and *16srRNA*) showing the same SSCP profiles shared identical or nearly identical nucleotide sequence between purple and tea-green crabs through multiple alignments using software DNAMAN™.

Since there was no distinct variation of DNA bands of both the *COI* and *16srRNA* genes detected in polyacrylamide gels through SSCP analysis between tea-green and purple samples of the blue swimming crab, and the following sequence analysis presented 99.81% and 99.91% nucleotide sequence identity of the *COI* and *16srRNA* genes respectively. It indicated that there was no species or subspecies differentiation between them. And the purple individuals were more conserved in DNA sequence in comparison with that of the tea-green ones. More details about mechanism of color differentiation in the blue swimming crab *P. trituberculatus* are now under investigation.

Fig. 6 Multiple sequence alignment of *16srRNA* gene fragments of both tea-green (G) and purple (P) samples of the blue swimming crab

Acknowledgement

This work was supported by the grant of the Key Project in the National Science & Technology Pillar Program in the Eleventh Five-year Plan Period (2006BAD09A01).

Reference

[1] Hamasaki K, Fukunaga K, Kitada S. Batch fecundity of the swimming crab *Portunus trituberculatus* (Brachyura: Portunidae) [J]. Aquaculture, 2006, 253(1-4): 359 - 365.

[2] Chi D L, Yan B L, Gao H, et al. Advances of molecular biological research on the swimming crab, *Portunus trituberculatus* [J]. Journal of Aquaculture, 2008, 29(4): 11 - 15.

[3] Yamauchi M M, Miya M U, Nishida M. Complete mitochondrial DNA sequence of the swimming crab, *Portunus trituberculatus* (Crustacea: Decapoda: Brachyura) [J]. Gene, 2003, 311: 129 - 135.

[4] Jin S, Zhao Q S, Wang C L, et al. RAPD Genetic Markers in Six Species of Marine Crab [J]. Zoological Research, 2004, 25(2): 172 - 176.

[5] Liu S, Xue S X, Sun J S. Genetic diversity of *Portunus trituberculatus* revealed by AFLP analysis [J]. Oceanologia et Limnologia Sinica, 2008, 39(2): 153 - 156.

[6] Avise J C. Phylogeography [M]. Harvard Univ Press, London, 2000, p. 447.

[7] Guo T H, Kong X Y, Chen S Q, et al. A study of the sequence of mitochondrial *16srRNA* and *COI* gene fragments of *Portunus trituberculatus* [J]. Journal of Ocean University of China, 2004, 34(1): 22 - 28.

[8] Hayashi K. PCR-SSCP: A method for detection of mutations [J]. Genetic Analysis-Bimolecular Engineering, 1992, 9(3): 73 - 79.

[9] Orita M, Suzuki Y, Sekiya T, et al. Rapid and sensitive detection of point mutations and genetic polymorphisms using polymerase chain reaction [J]. Genomics, 1989, 5(4): 874 - 879.

[10] Šeruga M, Krajačić M, Škorić D. The use of SSCP analysis in the assessment of phytoplasma gene variability [J]. Journal of Microbiological. Methods, 2008, 73(1): 69 - 72.

[11] Asensio L. PCR-based methods for fish and fishery products authentication [J]. Trends in Food Science & Technology, 2007, 18(11): 558 - 566.

[12] Li A X, Wu X Y, Ding X J, et al. PCR-SSCP as a molecular tool for the identification of Benedeniinae (Monogenea: Capsalidae) from marine fish [J]. Molecular and Cellular Probes, 2005, 19(1): 35 - 39.

[13] Zhu X Q, Beveridge I, Berger L, et al. Single-strand conformation polymorphism-based analysis reveals genetic variation within *Spirometra erinacei* (Cestoda: Pseudophyllidea) from Australia [J]. Molecular and Cellular Probes, 2002, 16(2): 159 - 165.

[14] Place A R, Feng X J, Steven C R, et al. Genetic markers in blue crabs (*Callinectes sapidus*) II: Complete mitochondrial genome sequence and characterization of genetic variation [J]. Journal of Experimental Marine Biology and Ecology, 2005, 319(1-2): 15 - 27.

[15] Elliston J. Alfred Wegener: The Father of Continental Drift [J]. Earth-Science Review, 1988, 25(1): 76-79.

[16] Bandyopadhyay P K, Stevenson B J, Cady M T, et al. Complete mitochondrial DNA sequence of a Conoidean gastropod, *Lophiotoma* (*Xenuroturris*) *cerithiformis*: Gene order and gastropod phylogeny [J]. Toxicon, 2006, 48(1): 29 - 43.

两种体色三疣梭子蟹亲缘关系的 PCR-SSCP 分析

迟大利[1,2]，高 焕[1]，沈颂东[2]，阎斌伦[1]

（1. 淮海工学院 江苏省海洋生物技术重点建设实验室，江苏 连云港 222005；2. 苏州大学 生命科学学院，江苏 苏州 215123）

摘 要：三疣梭子蟹作为重要的海洋经济动物，其常见体色为茶绿色。近年来在我国东部沿海海域海捕三疣梭子蟹中开始出现体色为紫色的一类梭子蟹，除体色不同外，二者表型特征并无显著差异。为确定两种体色三疣梭子蟹之间的关系，本文对两种体色三疣梭子蟹不同个体的线粒体 *COI* 和 *16srRNA* 基因进行了比较分析以判定体色的差异是否由于种属的差异引起的。通过对以上两个基因部分序列的 SSCP 和相关序列测定分析，发现在紫色和茶绿色群体中这两个线粒体保守序列基因的 SSCP 电泳条带图谱相似，序列分析表明 *COI* 和 *16srRNA* 基因在两种体色三疣梭子蟹群体中的核苷酸序列相似度分别为 99.81%和 99.91%。以上结果表明，紫色三疣梭子蟹并未发生亚种的分化，即紫色和茶绿色群体属于同一个种。此外，紫色梭子蟹群体的线粒体 DNA 序列在进化关系上较茶绿色群体更为保守。

关键词：*16srRNA*；体色；*COI*；PCR；三疣梭子蟹；SSCP

Constructing Marine Ecological Civilization of Qingdao

SUN Yun-tan [1, 2*], YU Xiao [2]

1. *Ocean University of China, Qingdao* 266003, *Shandong Province, China;*

2. *Qingdao Ocean and Fishery Bureau, Qingdao* 266071, *Shandong Province, China*

Abstracts: Ocean is a distinctive and prior resource in Qingdao. This paper makes summary and analysis of the practice of constructing marine ecological civilization in Qingdao and offers suggestions for the future development of the city. With the implementation of the city's strategy of "Protecting the bay and developing the city on the bay", the suggestions focus on between management & utilization, so as to establish the harmony between the optimal utilization of marine resource and marine ecological environment protection, and to consistently promote marine ecological civilization

Key word: marine management; ecological civilization; suggestions

Introduction

Qingdao is a central, economical port and tourism city in the east coast of China. The city's population is 7 600 000, with an area of 10 600 km^2, and its coastal line is 730.64 km, with 49 bays and 69 islands along the coast. The jurisdiction area is 13,800 square km^2, which is 1.3 times of its land area. The ocean is the feature and predominance of Qingdao, and it's an important basical resources for economic and social development.

With implementing the strategy of "Protect the Bay & Develop the Bay" and the condition of sustained and rapid economic growth and continued expansion of the scale of urban conditions , the overall strengthening of the marine ecological civilization construction, the optimal use of marine resources, protection of the marine environment unity , Urban development is not only the basic requirements for the implementation of the strategy, and Qingdao is also building a prosperous and civilized and harmonious modern international city, a necessary condition for the goal.

1 Adhere to the concept of harmonious ocean, coordinate marine ecological protection and utilization

Qingdao always paid high attention to marine work, and regards marine economy as a feature economy. The development strategy "protect the bay & develop the bay" was confirmed this year, which advanced the ocean work to the unprecedented position.The main industrial output of marine economy of the city reached 113 billion yuan in 2007, and the increased value of marine industry reached 49.32 billion,

Received on July 16, 2009

*Corresponding author: sunyuntan@126.com

accounting for 13.02% of the city's GDP.

In the process of boosting the marine economy development, we always insist on "harmonious development" strategy, deal with exploitation and protection appropriately, carry out the duty of ocean integrated management pressingly, enhance the marine ecology environmental protection completely. The ocean environmental quality is stable as a whole, and we achieve the balanced development between oceanic exploitation and protection. Qingdao city in 2006, two years in a row in 2007 was awarded the "a top award of national marine management".

Early in June this year particularly, our city suffered from the Enteromorpha natural disasters, and it has a serious impact on holding the Olympic Sailing race and the marine ecosystem.

Under the guidance of the State Oceanic Administration, our rapid response and effective disposal of the successful completion of this large-scale, sudden natural disasters, marine emergency disposal, the Olympic sailing race was held successfully as scheduled, and we were honored by the CPC Central Committee and the State Council.

1.1 Gradually improve the system of marine laws and regulations

This city always adheres to the principle of legislation, in accordance with the law regulate the development and utilization of marine order. The development of a "sea of Qingdao use regulations", "the city of Qingdao Marine Fisheries Management Regulations" and "coastal Planning and Management of Qingdao City ", and other local laws and government regulations ,in total seven, are about to introduce the development of the "city of Qingdao to protect uninhabited islands and the use of regulations." Qingdao works out a marine function zoning system which gives priority to marine function zoning of Qingdao city. An ocean law system has been formed from the basic of state laws related to ocean, and district regulations and correlative management systems. We have exact laws for regulating ocean exploitations and utilizations basically, and it's a stable basis of well managing and protecting the ocean and the resources.

1.2 Strictly regulate the use of the management of the waters

Conscientiously implementing the "Law on the management of the use of the sea", and promoting the use of the sea lie with the management system of marine function zoning system and the system of compensation for the use of the waters.

Insisting on checking on strictly, demonstrating scientifically, we established some matched systems such as application , show, demonstration, confirm of ocean area using; and evaluation of ocean environmental impacts; and invitation public bidding, auction, value evaluation of access of ocean areas.

Adhering to the principle of "three no's approval"; implementing one-vote veto in ocean environmental impact evaluation and the system of evaluation of coastal and ocean engineering.

A comprehensive sea standardizing the use of examination and approval procedures for many years

to achieve the new project on the sea with a permit, the use of the sea Permit annual rate, deposit rate for the use of the waters of the "three 100%".

At the same time, with implementing the whole city's strategy -"protect the bay & develop the bay", according to the city's industrial layout and different features of different sea resources endowment, insist on using the sea areas and coastline scientifically and intensively, enforce the national policy of sea area classification and ranks strictly, collocating the maritime resources scientifically, to do a good job to use the sea areas, examination and approval services.

It is necessary to boost the marine resources exploitation engineering mainly about ocean area using, reclaiming land from the sea, utilization of sea water; a large passel of national and provincial key infrastructures related to the sea such as great scale oil refining, bridge spanning the sea have settled down in this city. Sea areas using for the city reach 380,000 are, those which ensure the healthy ocean economy development.

1.3 Strengthen marine environmental protection

Establish and improve the city and district levels of the marine environment monitoring system, insist on monitoring the alongshore area environment, bathing beach environment in swimming period and the key aquiculture area environment, issue "Communique of marine environment quality of Qingdao" termly. 660 000 000 yuan investment in the implementation of the sea before the first-line sewage renovation project on the city's 42 sewage into the sea to carry out real-time dynamic monitoring, to reduce the emission of pollutants in urban mass.

Because of work on the Olympic Games Regatta, Qingdao invested more than 3 000 million for the field Olympic sailing race hydrology, water quality monitoring and forecasting system. Qingdao invested more than 1 800 million for the Olympic sailing venue and its neighboring sea area of red tide prevention and control projects. Qingdao input 35 000 000 yuan in the construction of the first national maritime surveillance to monitor the use of dynamic management system, forming a front-line focus of the sea and the marine environment, the ability to monitor real-time monitoring. Qingdao laid out 5 000 million in the implementation of the coast Comprehensive Improvement Project, and the removal of all the region abalone aquaculture facilities. The face of natural waters and marine ecological environment have been restored.

1.4 Highlight the focus of integrated sea regulation

The layout of the status quo of Qingdao City for marine environmental protection and economic development, docking in Qingdao, "the protection of the Central Bay, the development over the Bay" strategic , focus on the implementation of the comprehensive improvement of ecological protection in Jiaozhou Bay project, in accordance with the goal of "two control and one management ".Qingdao invested 17 110 000 yuan into the preparation of the "Central Jiaozhou Bay near the coastline for the protection and use of the regulatory plan," "Jiaozhou Bay waters offshore wind surge planning" .

At Jiaozhou Bay, a sewage treatment plant expansion projects was implemented with 35 000 000 yuan of investment to start, "Pak Nai," project management, to suspend the reclamation project approval, so that the ecological environment of Jiaozhou Bay was improved.

At the same time, the establishment of marine nature reserves seen as an effective way to improve the marine environment and the protection of the marine ecosystem were carried out, and we also build a provincial nature reserve Grand Island, the Island Mountain Nature Reserve, provincial and Qingdao amphioxus municipal aquatic wildlife nature reserve, with a total area of protected areas to achieve more than 110 square kilometers.

1.5 Strengthen law enforcement to monitor the ocean.

In accordance with " governing the sea by law, guarding the sea by law", adhere to the scientific allocation of resources of law enforcement, reasonable arrangements for the activities of law enforcement, to crack down on destruction of marine resources and ecological environment, Qingdao has carried out the "Blue Arrow" marine law enforcement Action. This action last for three consecutive years.

Strengthening the regional focus of the inspections, such as the Jiaozhou Bay, the former first sea, marine engineering major, major sewage outfall, Pirates of the cases of sand-prone areas, the law should be strictly investigated on the illegal sea sand poaching, pollution of the sea, and other acts of destruction of marine resources.

In recent 5 years, marine law enforcement team has investigated and dealt with nearly 200 cases of damage to marine ecological resources, the fine collection of fishery resources and compensation more than 1 000 yuan, so we effectively crack down on illegal use of the sea, marine resources, environmental destruction, so as to maintain good order in the use of the oceans.

In the term to strengthen the protection of the marine ecosystem and the marine ecological civilization construction work, we have made some achievements, but with the rapid development of marine economy, our city is facing some contradictions and problems that can not be ignored.

(a) We need to improve the understanding of the ocean. Social and people lack for understanding of the ocean, environmental protection a priority, and enriching the people in the priority development of the marine practice really can not.

(b) The development of the marine mode is still relatively extensive. The increasing shortage of land resources, the increasing reclaimant to the ocean become more and more obviously, the use of the sea has become a new hot spots and focus, the use of marine resources become more and more contradictory, Marine Management is under increasing pressure.

(c) The coastal ecological environment under great pressure. Marine disasters and emergencies increase in the coastal waters, and biodiversity index declines, the main estuary into the sea and adjacent waters of the ecosystem are sub-healthy or unhealthy in a long term.

(d) Weak marine infrastructure. Marine disaster prevention and mitigation system needs further improvement ,and the marine disaster monitoring, early warning, forecasting ability need to improve, the management teams, equipments and management approaches need to be strengthening.

2 Under the guidance of balanced development concept , speed up the Qingdao Ocean ecological civilization

Now and in the future, should be a comprehensive analysis of urban development in the understanding of the oceans in an important position, in-depth implement the scientific concept of development, Qingdao focus on "protect the Bay and develop the bay" strategy, firmly establish the marine ecology and harmonious development of the marine Ideas, and enhance environmental protection as a priority, the people rich sense as priorities, and promote the civilization of the marine eco-urban construction.

2.1 With the goal of building strong Ocean City, implement the strategy of "protect the bay, develop the bay"

Ocean is the biggest advantage of the development of the city to provide follow-up of the energy space, the future development of our city is a strategic material foundation. To adhere to the marine economy of urban development as an important strategic objectives, give full play to the advantages of marine resources and scientific research, to develop the marine economy, to do all that "sea". To identify the marine economic development and industrialization of the main direction of focus, bigger and stronger marine transport ports, coastal tourism, marine, and other high-tech industries, and strive to build itself into a technology leader in Qingdao, a reasonable structure, significant benefits, environmental quality of the national marine economy Strong City.

According to the national macro-control requirements and the different characteristics of the sea resources endowment, to encourage the development of a clear, restrictions on the Prohibition of the Development and the development of the industry, the introduction of the development of industrial policy and optimize the layout of the marine industry. Organizations to carry out marine resources survey, evaluation and assessment of the marine environment, ecology, resources and disaster situation and the trend for the development of marine development strategy to provide a basis.

At the same time, to be carried out through various forms of propaganda and education, all-round promotion of marine laws of nature, value and status of the strategic role and guide the public awareness of the oceans, marine concern to protect the sea rising public awareness of the modern ocean, and enhance the marine The concept of land.

2.2 With scientific planning of marine resources ad the basis, promote the scientifically intensive use of the sea

Waters, coastal zones, coastal and land, is a valuable non-renewable resources, must adhere to

both the development and protection of the ecological efficiency with both, in accordance with the "reasonable layout, high-intensive, scientific norms" principle, truly in accordance with the law governing the sea, Science by the sea, to achieve sustainable use. Should be strictly implemented marine function zoning, "the city of Qingdao marine function zoning," as a guide decision-making and ocean development activities in the fundamental basis for strict compliance with the laws of nature, according to the regeneration of marine resources and the marine environment carrying capacity, to set the scientific waters.

In the marine industry development and use of the sea in the process of building projects adhere to the scientific proof, strict examination and approval, we can make the scale of the development of marine economy, speed and capacity to adapt resources and the environment, economic, ecological and efficiency, strengthen all-round, coordinated and sustainable development.

On the basis of marine function zoning, "coastal city of Qingdao on the Protection and Use Planning" begin to prepare. The industrial layout and planning of convergence will be divided into coastal waters prohibited zones, restrictions on development, optimize on development and key development zones four Regional category. The proposed use of the shoreline control targets will guide our city's coastal waters appropriate for sustainable use of resources.

To learn from international experience and improve graphic design , insist on the protection of natural coastline, control of artificial coastline, promote artificial Island, block groups, such less impact on the marine environment of the reclaimed land, which will promote the efficient use of resources.

2.3 strictly control pollution of the marine environment, strengthen supervision and management

Strictly implement of the marine environment impact assessment system, deny any illegal industry. Various types of marine engineering, marine engineering projects carried out in accordance with the law of marine environmental impact assessment, implementation and management of the entire process.

Government should establish the target responsibility system for marine environmental protection, strictly focused on the sea waters of the total pollutant emission control targets, with the permission system of marine development projects "at the same time," which will control emissions of pollutants to the ocean.

Promote the integrated management of land and sea, investigated and dealt with land-based sources of pollution in accordance with the law , to speed up urban sewage treatment plant technology upgrading and expansion project, undertaken great efforts to improve the environment in sea River Park, River ink, the Dagu River into the sea, focused on solving the Gulf Fushan, Mission Island catchment areas, to strengthen the supervision and management of enterprises that put pollution straight into the sea to effectively reduce the emission of pollutants which into the sea. According to the principle of "Who protect is who exploit it, who benefit is who compensate" , speed up the establishment of the marine eco-compensation mechanism.

2.4 Focus on integrated management of the region, carry out marine resources and ecological restoration work

Do a good job to comprehensive treatment project in Jiaozhou Bay, to promote the protection of resources and orderly development. Focused on the preparation of the protection and use of planning , to carry out the regulation and control of Jiaozhou Bay shoreline changes, and promote removing companies that with land-based sources of pollution, to strictly control the coastline and waters occupied by construction projects, speed up dealing with sediment pollution and other key regional in the eastern part of Jiaozhou Bay, improve the ecological environment in Jiaozhou Bay.

Do a good job of the marine nature reserve construction, strengthen the Nature Reserve Management for amphioxus in Grand Island, Mountain Island, and improve the construction of nature reserves, to live up to funds become available, the staff in place, responsibility, management in place.

To increase fishery resources restoration efforts, in the past three years, on the basis of implementing fishery resources restoration plan, we made plans on Grand Island, Mountain Island, Bamboo Island, and other waters fork scientifically, put in protective artificial reefs to enhance fish Seafood proliferation Reef-building, to continue to expand the proliferation of species and size of the release, building maritime ecological demonstration zone to improve the marine ecology and coastal resource protection.

2.5 Improve the marine ecology of civilization support system, enhance capacity of protection of marine environment

For the actual situation in Qingdao, some Systems must be carried out to guide the practical work, like "Uninhabited Islands city of Qingdao regulations", "city of Qingdao Marine Environment Protection Ordinance" and "Qingdao City, the proliferation of fishing regulations" and so on.

Good planning and construction of coastal city of Qingdao dynamic monitoring system to monitor and improve the marine ecology of the modern management capabilities. Improve marine environmental monitoring, disaster warning system, the establishment of oil pollution incidents and pollution emergency plan to deal with and enhance the marine disaster early warning forecasting, emergency and rapid response capacity to deal with.

To speed up building the city's marine environment monitoring network, establish Qingdao urban marine environment monitoring and forecasting centers and the marine environment monitoring station on cantonal level, and continuously improve the overall level of marine environmental protection and support capabilities. To take marine environmental protection goals into the coastal urban environmental protection responsibility, the marine environmental protection and ecological construction funds should be included in the government budget at the same level, and establish a special fund.

In short, we will fully implement the marine-related work of the strategic plan of State Oceanic

Administration , to fully implement the balanced development concept, vigorously implement the "protect the Bay & develop the bay" strategy to strengthen integrated marine management, to improve the effectiveness of marine environmental protection and promoting the civilization and the establishment of the marine ecosystem, serve "Ocean City" construction completely, for the construction of a sea as the main characteristics of a prosperous and civilized and harmonious modern international city to make new contribution.

关于青岛市海洋生态文明建设的思考

孙云潭[1,2]，于 晓[2]

（1. 中国海洋大学水产学院，山东 青岛，266003；2. 青岛市海洋与渔业局，山东 青岛，266071）

摘 要： 海洋是青岛的特色和优势。本文总结和分析了青岛海洋生态文明建设的做法，并对未来一个时期城市发展，特别是实施“环湾保护，拥湾发展”城市战略过程中，如何处理好海洋资源开发与保护、管理和利用的关系，实现优化海洋资源利用、保护海洋生态环境相统一，不断推进海洋生态文明建设提出了建议和思路。

关键词： 海洋管理；生态文明；建议

海 洋 通 报（英文版）

HAIYANG TONGBAO

2010 年 5 月　第 12 卷　第 1 期

目　次

东海黑潮温盐与中国东部气温和降水的相互关系 …… 吴志彦 等 (09)

全球变暖背景下对太平洋环流（1960－1999）的模拟 ……蔡　怡 等 (15)

东海大堤对湛江湾水动力环境影响的研究 ……李希彬 等 (29)

大洋环流的诊断计算 …… 杨　阳 等 (38)

温州“9.4”台风倒槽特大暴雨分析……郑　峰 (47)

罗源湾海水中粪大肠菌群的分布和年际变化……蔡雷鸣 (58)

雨生红球藻中 *ctr*O 基因存在 3 个 5′上游侧翼序列 …… 高政权 等 (64)

五种紫菜同工酶标记的遗传分析 …… 沈颂东 等 (78)

两种体色三疣梭子蟹亲缘关系的 PCR－SSCP 分析 ……迟大利 等 (88)

关于青岛市海洋生态文明建设的思考 …… 孙云潭 等 (96)

Marine Science Bulletin

Marine Science Bulletin publishes papers on marine science and technology including physical oceanography, chemical oceanography, marine biology, marine geology, environmental oceanography, estuarine & coastal sciences, marine technology, digital ocean, coastal zone management, ocean engineering, marine economics, etc., and aims to promote international academic exchange.

Editor-in-Chief: XU Sheng (徐　胜)
Associate Editor-in-Chief: HE Guang-shun (何广顺)　LU Ming-sheng (卢明生)
Executive Editor: YANG Rui (杨　瑞)　QIU Wen-jing (邱文静)　LI Xue (李　雪)
ZHANG Xiao-xian (张潇娴)　YUAN Ze-yi (袁泽轶)
English proofed by: WANG Qi (王　琦)

Semi-annually (started in 1999, sum 23)
Publication date: May. 15th and Oct. 15th

Marine Science Bulletin **(Vol. 12, No. 1, May 2010)**

Responsible Institution:
State Oceanic Administration of China
Sponsored by:
National Marine Data and Information Service
Edited by:
Office of Marine Science Bulletin (English edition)
Printed by:
Printery of National Marine Date and Information Service

Published by:
Office of Marine Science Bulletin (English edition)
E-mail: msb@mail.nmdis.gov.cn
Tel: (022) 24011287
Address: 93 Liuwei Rd., Hedong District, Tianjin 300171, China

---

ISSN1000-9620
CN12-1271/N

Price: $ 30.00 / ￥18.00 Per year